Experimental Investigation of the Ternary Mg-Zn-Zr System

Xin Zhang

A Thesis
in
The Department
of
Mechanical and Industrial Engineering

Presented in Partial Fulfillment of the Requirements
for the Degree of Master of Applied Science (Mechanical Engineering) at
Concordia University
Montreal, Quebec, Canada

CONCORDIA UNIVERSITY

School of Graduate Studies

This is to certify that the thesis prepared

By: **Xin Zhang**

Entitled: **Experimental Investigation of the Ternary Mg-Zn-Zr System**

and submitted in partial fulfillment of the requirements for the degree of

Master of Applied Science (Mechanical Engineering)

Complies with the regulations of the University and meets the accepted standards with respect to originality and quality.

Signed by the final Examining Committee:

_____ Chair

Dr. Ivan Contreras

_____ Examiner

Dr. Martin Pugh

_____ Examiner

Dr. Saifur Rahaman

_____ Supervisor

Dr. Mamoun Medraj

Approved by

Chair of Department or Graduate Program Director

Date:

Abstract

Experimental Investigation of the Ternary Mg-Zn-Zr System

Xin Zhang

The Mg-Zn-Zr ternary system was experimentally investigated at 450^{o}C using six diffusion couples and 16 key alloys. Four new ternary compounds, namely as IM1, IM2, IM3 and IM4 were detected. The compositions, homogeneity ranges and the XRD patterns of these compounds were identified in this system using Scanning Electron Microscopy coupled with Energy-dispersive X-ray spectroscopy and X-ray Diffraction techniques. The homogeneity ranges of IM1, IM2, IM3 and IM4 are $Mg_{(23-26)}Zn_{66}Zr_{(8-11)}$, $Mg_{(15-16)}Zn_{66}Zr_{(18-19),}$ $Mg_{(10-11)}Zn_{66}Zr_{(23-24),}$ and $Mg_{(9-13)}Zn_{(79-87)}Zr_{(5-8)}$ respectively. IM1 compound is determined to have the same prototype as $MgZn_2$ phase with the hexagonal structure and $P6_3/mmc$ space group. The binary compounds do not have extended solid solubility into the ternary system. The XRD patterns of IM2, IM3 and IM4 were obtained from key alloys study. The liquid area in the Mg-Zn-Zr ternary system at 450^{o}C was verified by several key alloys. Although large regions of liquid exist in the binary phase diagrams at 450 ^{o}C, the single phase liquid region extended only around 1 at.% into the ternary phase diagram. Two and three-phase regions that contain liquid are up to around 10 at.% Zr. Based on the current experimental results of diffusion couples and equilibrated key alloys, the isothermal section of the Mg-Zn-Zr ternary system at 450^{o}C has been constructed.

Studying this system was challenging due to the large difference in melting points of its components. In order to overcome this problem, Zn-Zr master alloys were prepared to obtain homogenous key samples and to solve the problem of elements evaporation. In addition, two step annealing methods were used to study the microstructure changes of the key alloys.

Acknowledgements

I would like to express my sincere gratitude to my thesis supervisor, Professor Mamoun Medraj, for his constant encouragement, suggestions and cooperation in my research work and study at Concordia University. Conducting this research would not have been possible without his coherent instructions and support. I am especially grateful for the trust and the freedom he gave me during the master.

I wish also to thank the TMG group members for their continuous support and help. I would like to give my special thanks to Yinan Zhang and Dr. Dmytro Kevorkov, because Yinan helped and guided me constantly since I joined the TMG group and Dmytro provided me with many valuable suggestions in terms of experiments and thesis writing. In addition, I sincerely thank Dr. Ahmad for guiding me to use the lab equipment. I would like to extend my thanks to all my friends no matter where they are right now, I am grateful for their friendships. I deeply appreciate my parents' supports, understanding and encouragement over the years. I am not able to stand at this point of my life without their love and support.

Last but not least, special thanks to the natural sciences and engineering research council (NSERC) for the financial support.

Contents

List of Figures

List of Tables

Chapter 1

Introduction

Due to light weight, high specific strength and superior castability, the use of Mg alloys has been increasing in automotive and aerospace industries [1, 2]. Also, Mg alloys are attractive to electronic industries, thanks to the advantages of electromagnetic frequency interference shielding capabilities, good heat dissipation and excellent die castability [1]. In addition, Mg alloys, such as Mg-Al-Zn, Mg-Ca-Zn, Mg-Al-Mn, Mg-Y-RE and Mg-Zn-Zr, are promising candidates for biomedical materials due to their good mechanical properties, biocompatibilities and corrosion resistance [3, 4, 5].

Currently, casting, especially high-pressure die casting is the main process to manufacture Mg sheets and alloys. Pressure die casting Mg alloys have many advantages such as high productivity, high precision, good quality surface, fine cast structure, and energy saving. Nonetheless, the die casting Mg alloys are also restricted by these disadvantages like poor creep resistance, non-heat treatable and unsuitable for welding [1]. Compared to casting Mg alloys, the applications of wrought Mg alloys are limited. This is because there are a few slip systems in the hexagonal crystal structure of Mg, thus the deformation is not easy to initiate. However, wrought technologies have attracted considerable attention in terms of making high toughness and ductile Mg alloys [6]. Besides, wrought Mg alloys show better weldability than cast Mg alloys. Consequently, both cast and wrought technologies have advantages and disadvantages, and their products can be used in different applications.

To date, many series of Mg alloys have been developed and Mg-Zn-Zr (ZK series) based alloys are one of the most important commercial Mg alloys. Zn is one of the major alloying elements added in Mg alloys to improve castability, yield strength, as well as creep resistance [7, 8, 9, 10,

11]. Zn also refines the grain size of the Mg alloys because of the constitutional undercooling effect [12]. Zr is helpful to obtain fine grain size alloys that ensure good room temperature mechanical properties and corrosion resistance [13]. Firstly, Zr is an excellent grain refiner for Mg alloys [14, 15] because Zr has close lattice parameters to Mg, which means Zr is easy to form heterogeneous nucleation for Mg grains [16, 17]. Mg alloys containing Zr have better mechanical properties than pure Mg since grain refinement of Zr can significantly improve the ductility at room temperature by introducing cross slips to non-basal planes [18]. Furthermore, better mechanical and corrosion properties can be obtained when adding Zn and Zr in Mg alloys simultaneously [19].

Apart from structural applications, Gu et. al. [20] recently reported that the Mg-Zn-Zr alloys are promising for biodegradable implants applications because these alloys have slower corrosion rates compared with other Mg alloys such as Mg-Ca and Mg-Zn-Y alloys. In addition, Mg, Zn and Zr are non-toxic elements for the human body. Mg exists in the human body as fourth most prevalent cation and is found in bone tissue naturally [21]. Zn is an essential element for the human body (estimated 15 mg/day) [22] and has physiologically important influence in bone formation [23]. A small quantity of Zr in the human body (<250 mg) shows good biocompatibility and low toxicities [24]. Therefore, Mg-Zn-Zr alloys have great potential to be biomedical materials.

1.1 Motivation

Mg-Zn-Zr system plays an important role in commercial Mg alloys. ZK60 (Mg-6Zn-0.7Zr wt%) alloy is widely used in industry due to relatively high strength properties and improved plasticity [25]. Additionally, both in vitro immersion and cell attachment tests show that this alloy has a great potential as biodegradable implants [20]. ZK51 (Mg-4.6Zn-0.75Zr wt%) alloy has excellent room temperature strength and ductility, enabling it to be used in military and aerospace industries [26]. Besides, ZK61, ZK31 and ZK40 alloys were reported to have good plasticity and

are used for different purposes [27, 28, 29]. In summary, Mg-Zn-Zr alloys are significantly important and promising. Therefore, establishing the equilibrium phase relationships in the Mg-Zn-Zr ternary system is proposed in the present research.

1.2 Objectives

The phase diagram for the Mg-Zn-Zr ternary system is extremely significant due to the strong relationship between the composition, constituent phases of the alloys and the mechanical and bio-corrosion properties. The aim of the current research is to investigate the Mg-Zn-Zr ternary system experimentally by means of diffusion couples and equilibrated key alloys. The specified objectives of this study are:

- To study the phase equilibria of the various phases in the Mg-Zn-Zr ternary system.
- To determine the formation of the ternary compounds, and their crystal structures.
- To study the solubility limits of the ternary and the binary compounds.
- To construct the isothermal section of the Mg-Zn-Zr ternary phase diagram at 450°C experimentally.

Chapter 2

Literature review

In this chapter, the literature review of the Mg-Zn, Mg-Zr and Zn-Zr binary systems and the Mg-Zn-Zr ternary system will be presented. For each system, experimental investigations and thermodynamic modeling results are covered, analysed and summarized. The chapter also summarizes the presence of the binary and ternary intermetallic compounds and other research aspects.

2.1 Mg-Zn system

The Mg-Zn system was investigated both experimentally and thermodynamically over the years [30-40]. Back to 1904, Boudouard [30] firstly determined the liquidus curve for the whole composition range of the Mg-Zn system. Later, the liquidus curve was investigated by Grube [31], Bruni et al. [32] and Chadwick [33], and their results agreed well with each other. Chadwick [33] also investigated the solid solubility of Zn in Mg. However, the results are not accurate due to the presence of impurities in Zn. Afterward, Grube et al. [34] and Park et al. [35] investigated the Mg-solidus curve. The maximum solid solubility of Zn in Mg was measured as 2.5 at.% at 340^{o}C by Park et al. [35]. The maximum solubility of Mg in Zn determined by Hume-Rothery [36] is 0.3 at.% at 400^{o}C. In terms of intermediate phases, Grube et al. [34] reported the $MgZn_2$ binary compound first. Chadwick [33] discovered $MgZn_5$ which was replaced by Mg_2Zn_{11} later based on the more reliable XRD analysis by Samson [37]. The MgZn phase was reported by Hume-Rothery and Rounsefell [36], and it was replaced by the $Mg_{12}Zn_{13}$ compound which was reported by Chadwick [33]. Mg_2Zn_3 and Mg_7Zn_3 were first reported by Takei [38] and the compound Mg_7Zn_3 was later replaced by $Mg_{51}Zn_{20}$ through more reliable XRD analysis by Higashi et al. [39].

The newest thermodynamic phase diagram of Mg-Zn system was recently evaluated by Ghosh et al. [40]. The calculated phase diagram is shown in Figure 2.1, and it shows good agreement with experimental data reported by several research groups. Two eutectic reactions: $L \leftrightarrow Mg_{51}Zn_{20} + Mg_{12}Zn_{13}$ (341°C) and $L \leftrightarrow Mg_2Zn_{11} + Mg$ (368°C), take place at 28.7 at.% and 92.2 at.% of Zn, respectively. One eutectoid reaction of $Mg_{51}Zn_{20} \leftrightarrow Mg + Mg_{12}Zn_{13}$ takes place at 321°C. There are four peritectic reactions: $L + Mg \leftrightarrow Mg_{51}Zn_{20}$ (342°C), $L + Mg_2Zn_3 \leftrightarrow Mg_{12}Zn_{13}$ (347°C), $L + (MgZn_2) \leftrightarrow Mg_2Zn_3$ (410°C), and $L + (MgZn_2) \leftrightarrow Mg_2Zn_{11}$ (380°C). Five intermediate phases, $Mg_{51}Zn_{20}$, $Mg_{12}Zn_{13}$, Mg_2Zn_3, $MgZn_2$ and Mg_2Zn_{11}, are in the phase diagram. In addition, the metastable phase of $Mg_{51}Zn_{20}$ only exists in a short temperature range between 321°C to 345°C.

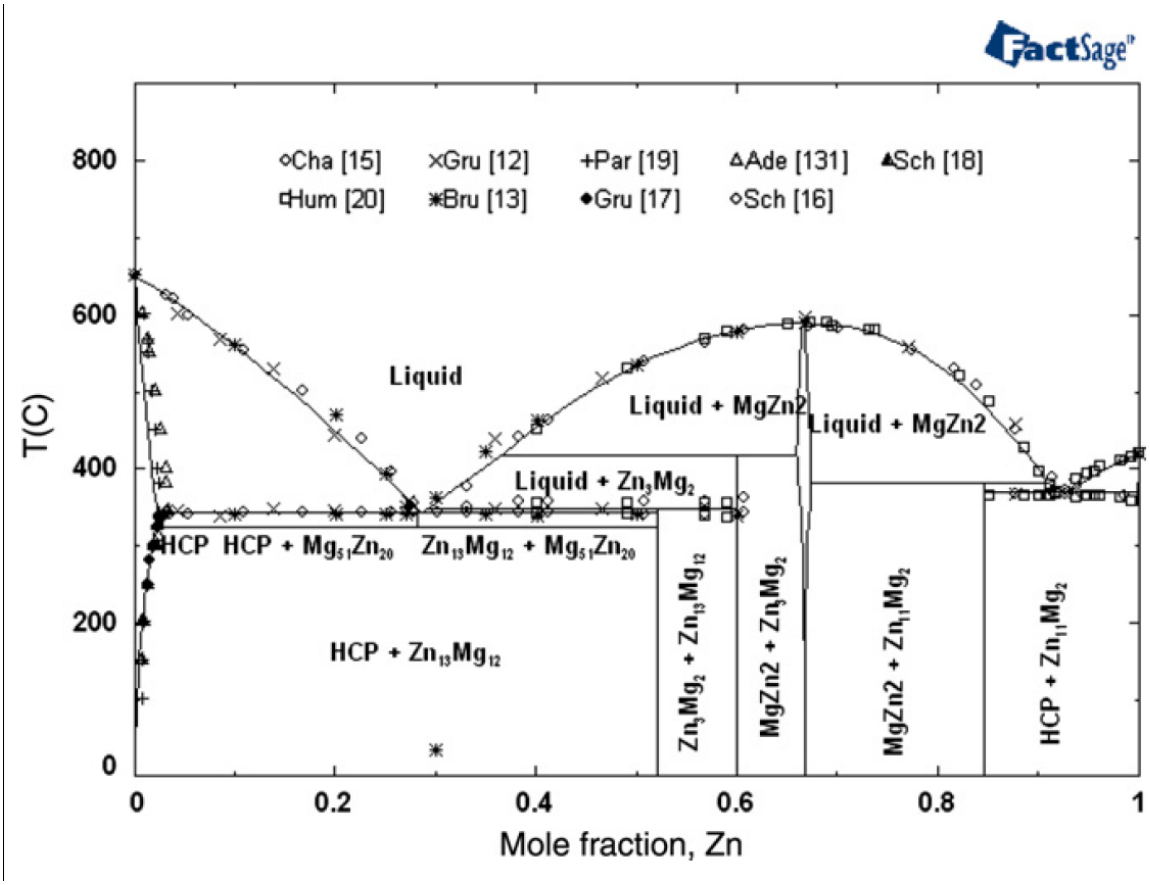

Figure 2.1 Mg-Zn Phase diagram [40].

2.2 Mg-Zr system

To date, only partial experimental data in the Mg-rich part of the Mg-Zr phase diagram is available [41, 42, 43, 44, 45]. Two earlier works [41, 42] tried to determine the liquidus of the Mg-Zr system. Their results, however, are inaccurate due to the lack of protective atmosphere and severe oxidation [43]. Later, the liquidus results obtained by Vesey and Bray [44] are considered to be more reliable since they used high purity starting materials and protective atmosphere to avoid contamination. In terms of solidus, Emley et al. [45] used solid diffusion technologies to determine the maximum solid solubility (1.042 at.%) of Zr in Mg. The maximum solid solubility of Mg in Zr is negligible [45]. Based on previous works, Schaum [42] studied the Mg-rich side with the limited composition range from 0 to 2 wt% Zr and constructed the partial Mg-Zr phase diagram which is shown in Figure 2.2. He determined the liquidus and solidus in the Mg-rich corner. In addition, a peritectic reaction ($L1+\alpha Zr \rightarrow \alpha Mg$) at $654^{o}C$ was reported in the Mg-rich part [42].

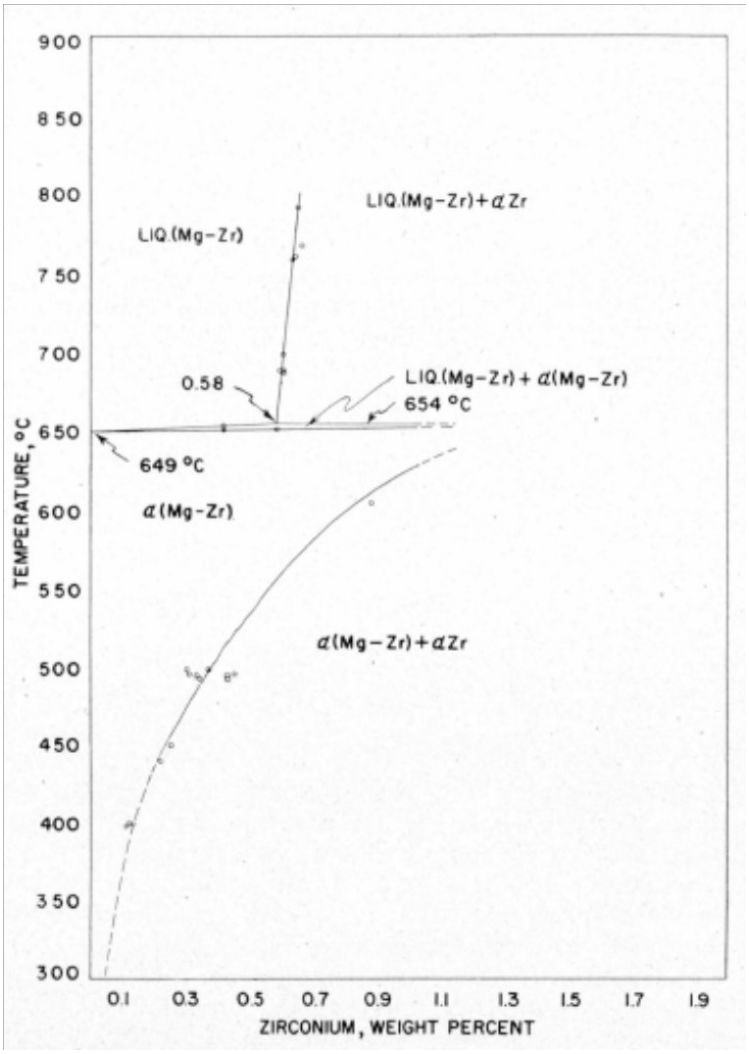

Figure 2.2 Partial Mg-Zr phase diagram at the Mg-rich corner [42].

Hämäläinen and Zeng [46] reported the full range of composition of the Mg-Zr phase diagram by thermodynamic calculation. However, the calculated results of Mg solidus are not completely in accord with the experimental data of Schaum [42]. Later, Arroyave et al. [47] improved the thermodynamic calculation of the Mg-Zr phase diagram using first-principles calculation method in combination with existing experimental data. The phase diagram of Mg-Zr system is shown in Figure 2.3. The maximum solubility of Zr in Mg is 0.766 at.%, and the solid solubility of Mg in Zr is negligible. The peritectic reaction (L1+hcp(Zr)→hcp(Mg)) happened at 654.6^{o}C. The

modeling results in the Mg-rich side show good agreement with the experimental results of Schaum [42]. Zr undergoes an allotropic phase transformation at 864°C from bcc(Zr) to hcp(Zr). The phase transformation reaction in the Zr rich side is: L ↔ L1 + bcc(Zr) (1848°C) and L1+bcc(Zr) ↔ hcp(Zr) (864°C) [47].

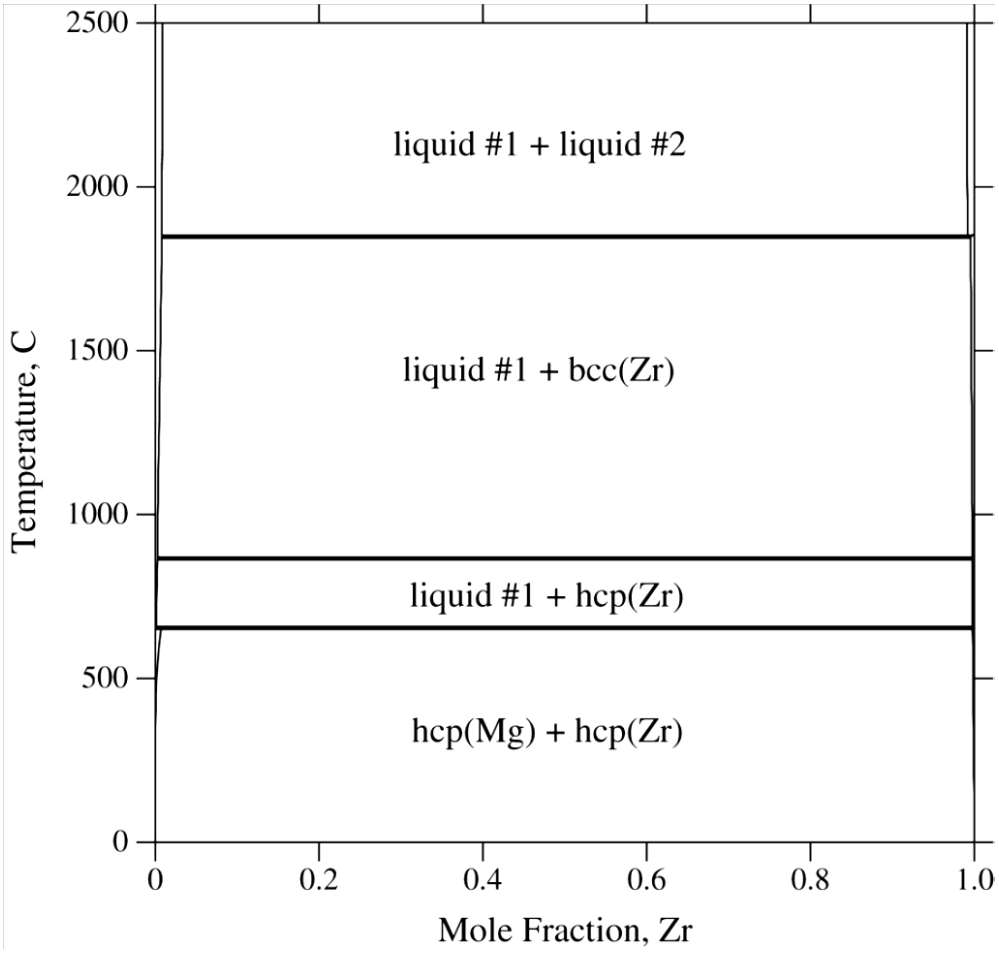

Figure 2.3 Calculated phase diagram of the Mg-Zr system [47].

2.3 Zn-Zr system

The Zn-Zr phase diagram is not well constructed because of the limited experimental data in the Zr-rich part. Gebbhardt [48] studied the liquidus in the Zn-rich part below 700^{o}C and reported

the Zn_6Zr phase. Chiotti and Kilp [49] measured the liquidus in the 800-950°C range and determined the $Zn_{14}Zr$, Zn_3Zr and ZnZr phases. Later, Chen and Jeitschko [50] replaced the $Zn_{14}Zr$ and Zn_6Zr by $Zn_{22}Zr$ and $Zn_{39}Zr_5$ respectively. The Zn_2Zr phase was reported by Pietrokowsky [51]. Figure 2.4 shows the Zn-Zr experimental phase diagram by Dutkiewicz [52] based on the previous findings [48, 49, 51]. Five intermetallic phases are shown in this phase diagram, and they are $Zn_{14}Zr$, Zn_6Zr, Zn_3Zr, Zn_2Zr and ZnZr. Zr undergoes an allotropic phase transformation at 863°C from βZr to αZr. There are two eutectic reactions, and the formula are: L ↔ Zr + ZnZr (1015°C); L ↔ Zn + $Zn_{14}Zr$ (419°C). One eutectoid reaction is βZr ↔ αZr + ZnZr (750°C). There are four peritectic reactions: L + Zn_6Zr ↔ $Zn_{14}Zr$ (545°C), L + Zn_3Zr ↔ Zn_6Zr (750°C), L + Zn_2Zr ↔ Zn_3Zr (910°C) and L + Zn_2Zr ↔ ZnZr (1110°C).

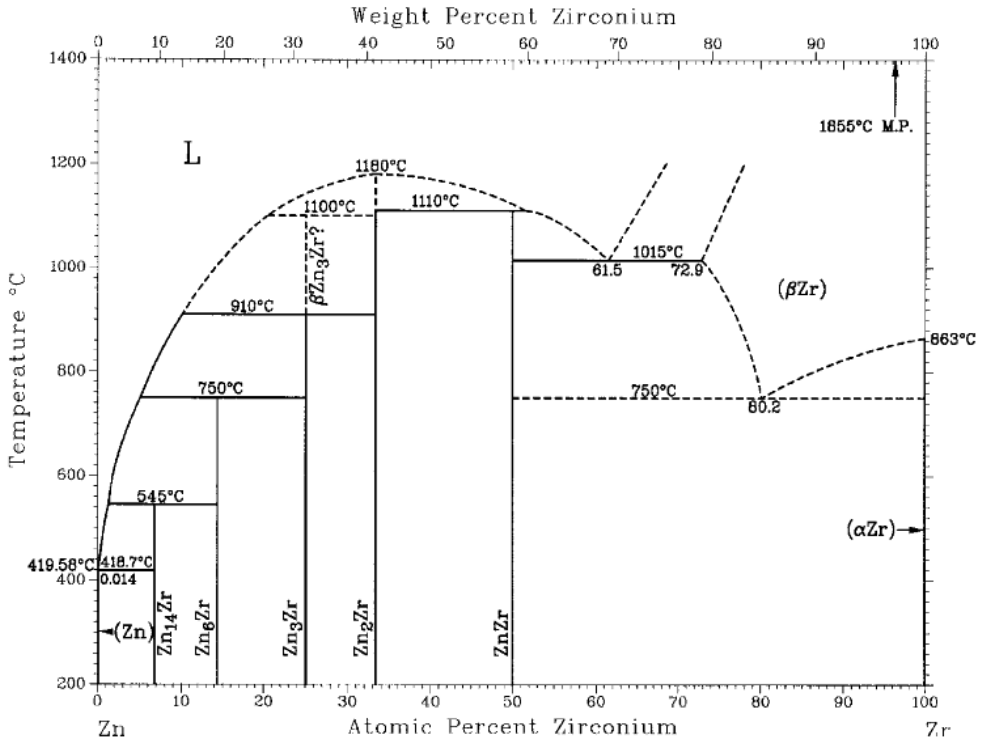

Figure 2.4 Experimental phase diagram of the Zn-Zr system [52].

Other researchers [53, 54, 55] studied the Zr-rich part of the Zn-Zr binary system and observed

the Zn_2Zr_3 and $ZnZr_2$ intermetallic phases. Williams et al. [56] experimentally studied the Zr-rich part of the Zn-Zr system and found that $ZnZr_2$ and Zn_2Zr_3 phases are metastable at room temperature. The stability range of $ZnZr_2$ is between 712°C and 775°C. The Zn_2Zn_3 phase was found to be not stable below 800°C. Williams et al.[56] also founded that the eutectic temperature in the Zr-rich part was 718 °C instead of 750°C.

Arroyave et al. [57] thermodynamically modeled the full range of composition of the Zn-Zr system combining the previous experimental results. The calculated phase diagram by Arroyave et al. [57] is shown in Figure 2.5. In another paper [58], Arroyave et al. indicated that Zn_2Zr_3 and $ZnZr_2$ are stable at 1000 ± 50°C and 750 ± 50°C, respectively. However, they also indicated that the stability range of Zn_2Zr_3 is not accurate due to the scarcity of experimental data.

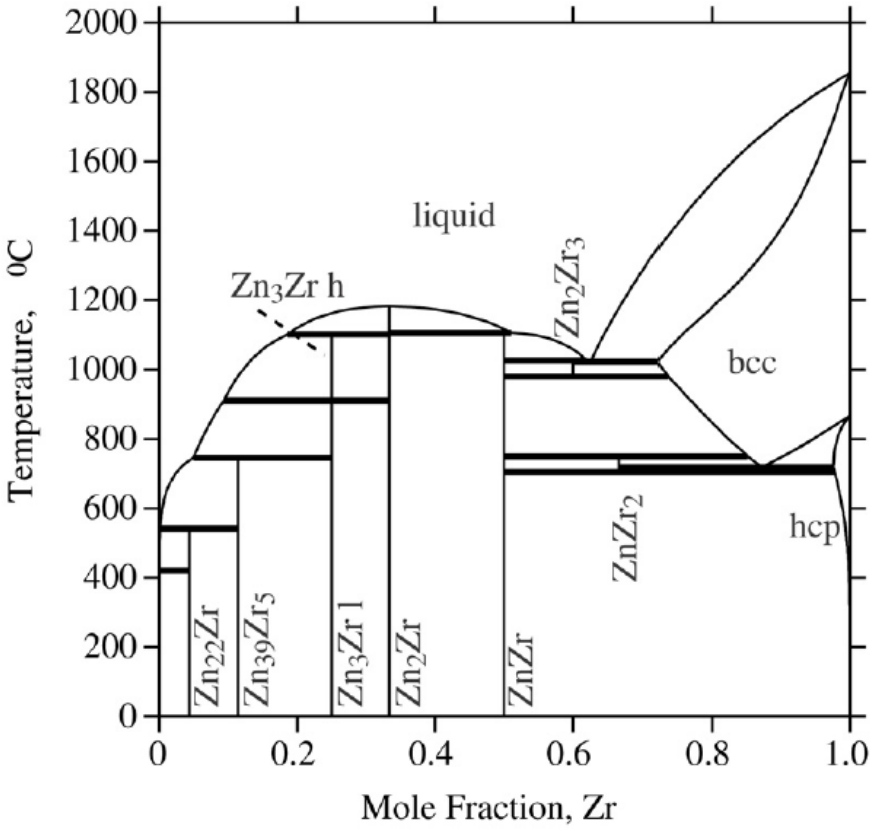

Figure 2.5 Thermodynamic modeling of the Zn-Zr system by Arroyave et al. [57].

Figure 2.6 represents a comparison between the experimental phase diagram [57] and the calculated phase diagram [52] of the Zn-Zr system. The black lines represent the calculated phase diagram by Arroyave et al. [57] while the red lines represent the experimental phase diagram by Dutkiewicz [52]. Comparing the two data sets, the intermetallic compounds in the calculated phase diagram, especially for $Zn_{22}Zr$, $Zn_{39}Zr_5$, Zn_2Zr_3, and $ZnZr_2$, could be represented more confidently since Arroyave et al. used the experimental results available in the literature [53, 54, 55, 56]. Furthermore, the liquidus phase can be considered acceptable in the range of 11 to 100 at.% Zr.

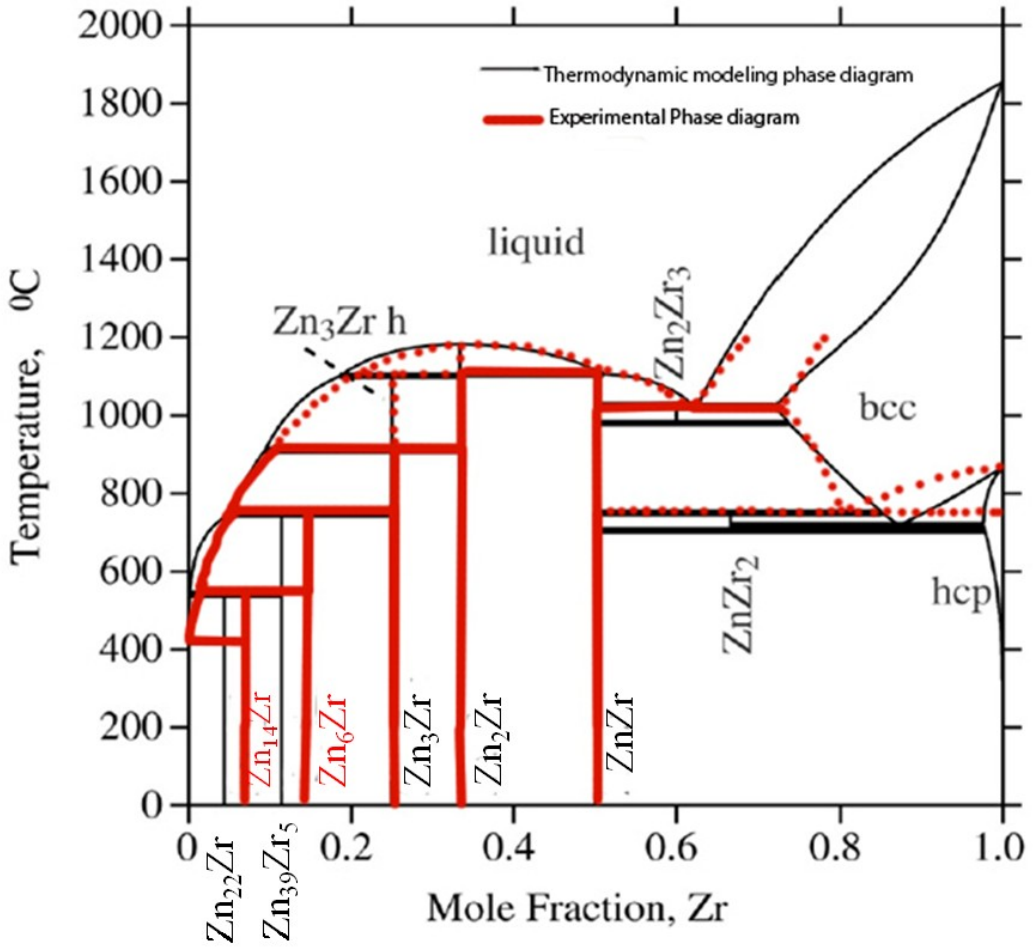

Figure 2.6 Comparison of the experimental [52] and thermodynamic modeling [57] phase diagram of the Zn-Zr system.

2.4 Mg-Zn-Zr system

To date, the Mg-Zn-Zr ternary system is not well studied. Lashkoi [59] identified the (Zn, $Mg)_2Zr$ and $Zn_2(Mg, Zr)$ phases in cast alloys. Babkin[60] studied the solubility of Zr in Mg, and he found that Zn did not affect Zr solubility in liquid Mg. Afterward, Lohberg et al. [61] determined the liquidus in Mg-rich part of the Mg-Zn-Zr system as shown in Figure 2.7.

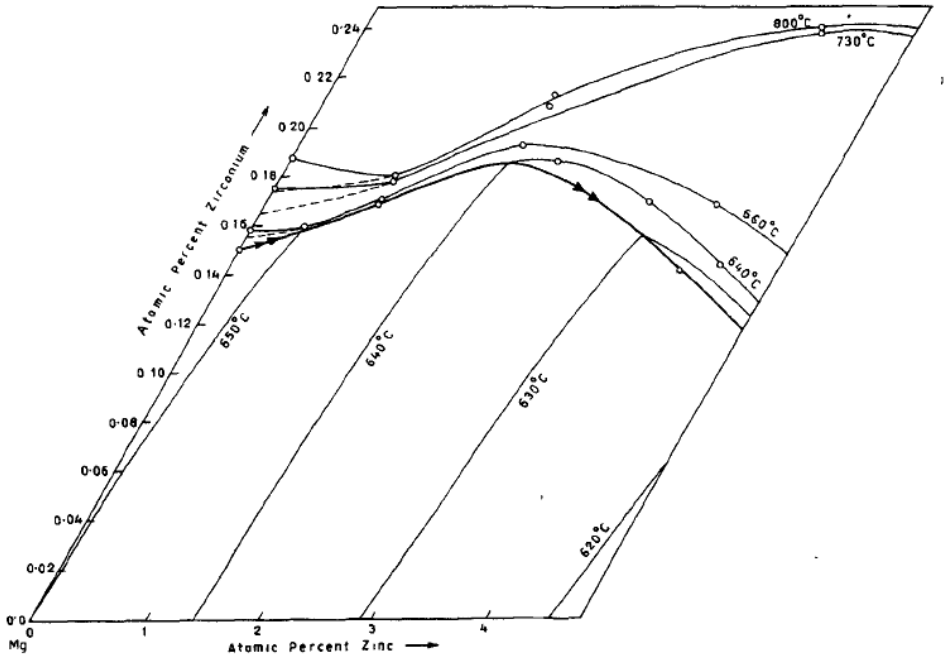

Figure 2.7 Partial liquidus projection for the Mg-Zn-Zr system [61].

The latest experimental isothermal section of the Mg-Zn-Zr ternary system was carried out by Ren et al. [62]. The phase diagram is shown in Figure 2.8. Nine key alloys in the Mg-rich part were prepared to obtain the isothermal section at 345°C. Six three-phase triangulations of Zr + Zn_2Zr_3 + Mg, Mg + ZnZr + Zn_2Zr_3, L + $(Mg,Zn)_2Zr$ + Mg, L + MgZn + $(Mg, Zn)_2Zr$ and MgZn + Mg_2Zn_3 + $(Mg, Zr)Zn_2$ were found. $(Mg, Zn)_2Zr$ is a substitutional solid solution where Mg replaces around 3 at.% of Zn in Zn_2Zr. The $(Mg, Zr)Zn_2$ is a substitutional solid solution of $MgZn_2$, in which around 15 at.% of Mg is replaced by Zr. However, the Zn-rich corner was not

well studied because all the key samples were in the Mg-rich region. Even in the Mg-rich corner, no alloys were prepared in the L + MgZn + $(Mg, Zn)_2Zr$ and MgZn + Mg_2Zn_3 + $(Mg, Zr)Zn_2$ region. Therefore, more work is still needed for this system.

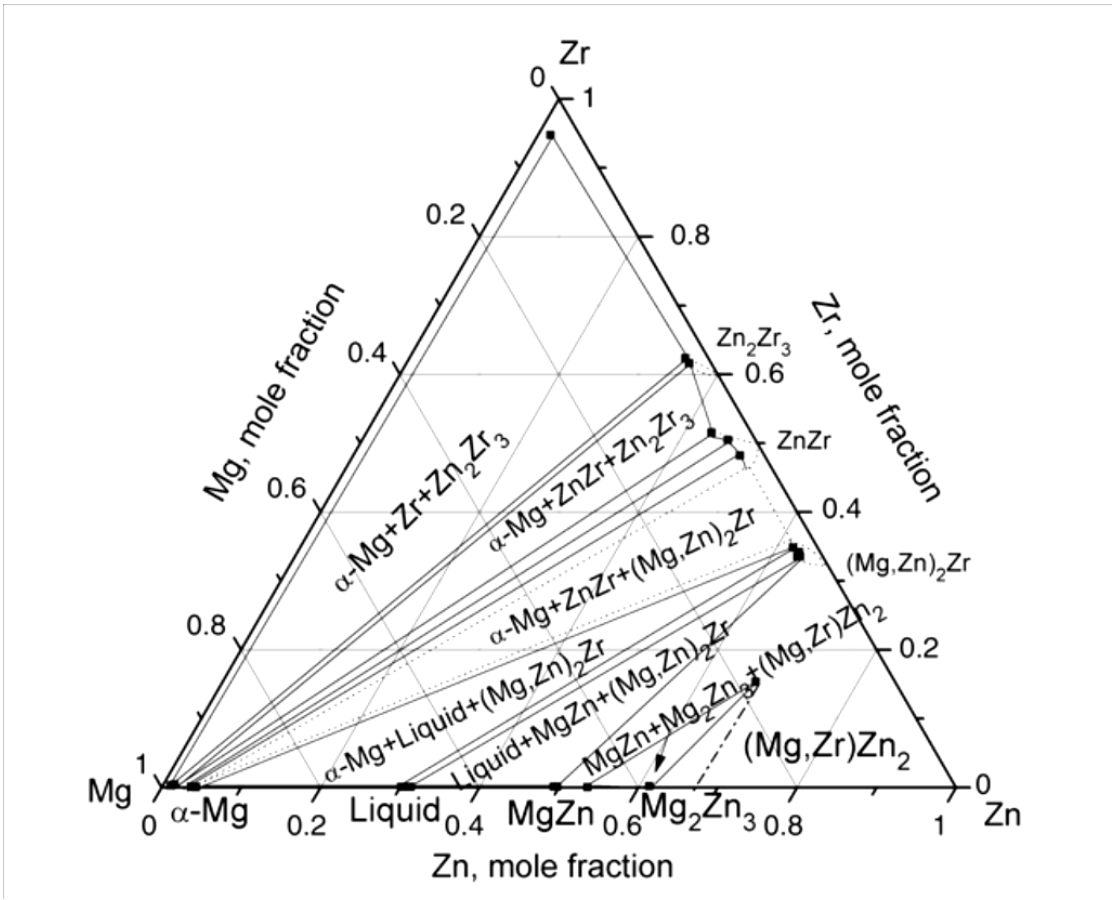

Figure 2.8 Isothermal section of the Mg-Zn-Zr ternary system at 345°C [62].

Chapter 3

Experimental Procedure

Figure 3.1 represents the preliminary phase diagram of the Mg-Zn-Zr ternary system at 450°C based on the available information in the literature. Several question marks are placed on the phase diagram. Firstly, at 450°C, the composition range of the liquid phase extending in the ternary phase diagram needs to be identified. Secondly, the phase relations in the Zn-rich part need to be constructed. Thirdly, the stability of Zn_2Zr_3 needs to be confirmed because contradiction regarding this compound could be found in the literature [57, 62]. Finally, the stability of $(Mg,Zr)Zn_2$ and $(Mg,Zn)_2Zr$ needs to be confirmed.

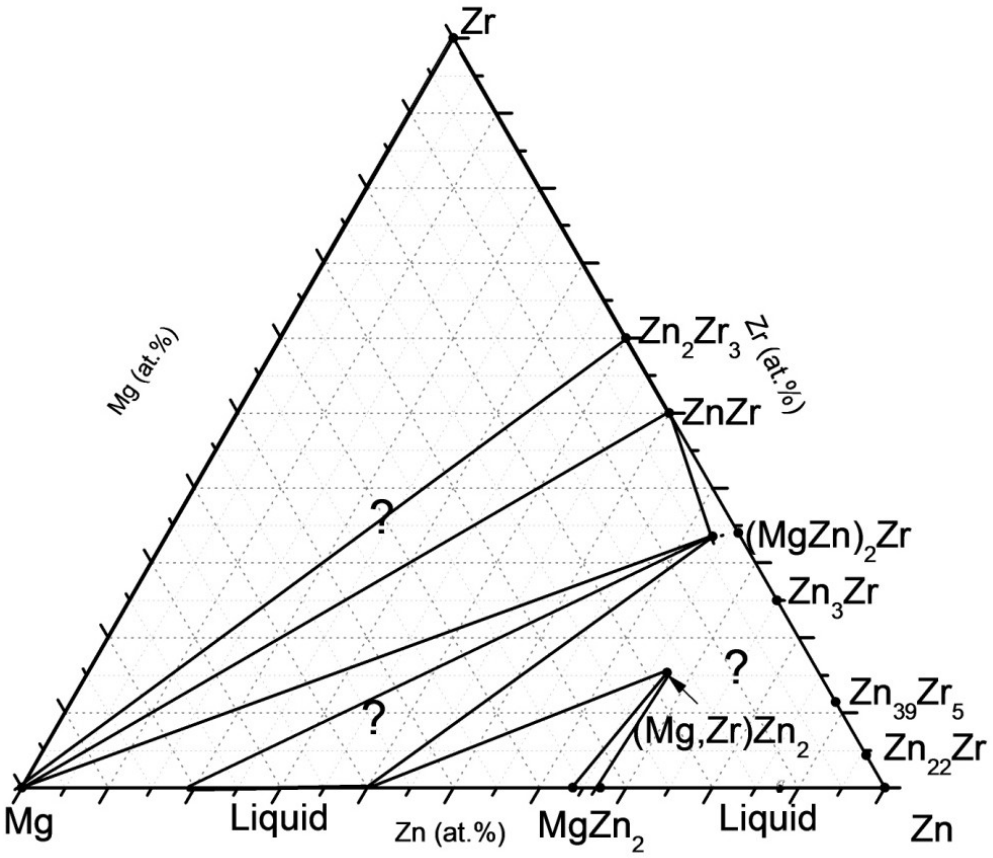

Figure 3.1 A preliminary phase diagram of the Mg-Zn-Zr ternary system at 450°C.

3.1 Annealing temperature and time

In this research, 450^{o}C was chosen as the annealing temperature, because our preliminary experiments at 335^{o}C and 400^{o}C showed that no diffusion layers formed in the diffusion couples. In addition, some key alloys did not equilibrate even after six weeks annealing at 335^{o}C and 400 ^{o}C. 450^{o}C was high enough to form diffusion layers and reach equilibrium of the key alloys. Liquid phase exists in this system over a wide range of compositions because the melting temperatures of $Mg_{51}Zn_{20}$, $Mg_{12}Zn_{13}$, Mg_2Zn_3, Mg_2Zn_{11} and Zn are lower than 450^{o}C. The presence of liquid increases the difficulty of studying the phase equilibria in this system.

Diffusion couple technique is a time dependent process. The annealing time should be sufficient for diffusion. However, if the annealing time is too long, the activation energy of the species forming intermetallic compounds might vary. Thus, missing phases can take place, or some phases are too thin to be detected, due to the initiation and growth kinetics of phases being different. The annealing time for diffusion couples was chosen as 7 days, based on the preliminary experimental results obtained during annealing at different time intervals. For key alloys, the annealing time should be relatively long to achieve equilibrium. The annealing time for key alloys was chosen as 28 days (4 weeks). However, the annealing time for specific compositions may vary.

In order to establish a systematic experimental investigation of the Mg-Zn-Zr ternary system, 6 diffusion couples and 16 key alloys were prepared using high purity Mg (99.8%), Zn (99.9%) ingots and Zr slugs (99.95%) supplied by Alfa Aesar (USA) and Mg-33 wt% Zr master alloy from Richest Group Company (China).

3.2 Key alloys

While preparing the alloys in this ternary system, it was difficult to prepare homogeneous samples, because of the significant differences in melting temperatures of the three elements. The

melting temperature of Zr (1852^{o}C) is higher than the boiling points of Mg (1107^{o}C) and Zn (907^{o}C). It will result in a very intensive evaporation of Mg and Zn during melting, which will lead to a problem of composition shifting and getting inhomogeneous samples. Therefore, an improved experimental procedure was designed to prepare homogeneous key alloys.

In order to prepare homogeneous samples, Zn-Zr master alloys were prepared using an arc melting furnace and water-cooled Cu crucible using a non-consumable tungsten electrode. Before melting, Zr slugs were cut to around 1 mm thick and were pressed to increase the contact area with the Zn ingot. Then the assembly as shown in Figure 3.2 was melted in the arc melting furnace. After melting, the master alloys were cut into small pieces that were then remelted 3-4 times to make sure all the Zr reacted with Zn. Before every melting process, around 0.50 g of Zinc was added to compensate for the evaporation of Zn during melting.

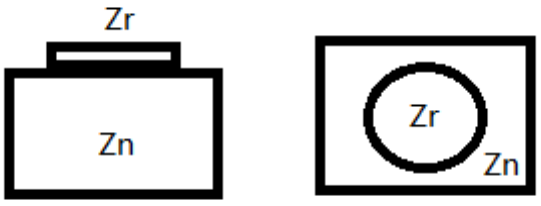

Figure 3.2 Schematic diagram of preparing Zn-Zr master alloy.

In the process of melting, the actual composition of the master alloy was not easily controlled. From the experimental experience, the maximum content of Zr in the Zn-Zr master alloy can be around 20 wt.%. The master alloys were located in the Zn_3Zr and $Zn_{39}Zr_5$ two-phase region. Afterwards, ternary alloys were prepared in an induction furnace by adding different amounts of Mg and Zn to the Zn-Zr master alloy. Figure 3.3 represents the area of the ternary phase diagram in which key alloys can be prepared using this method.

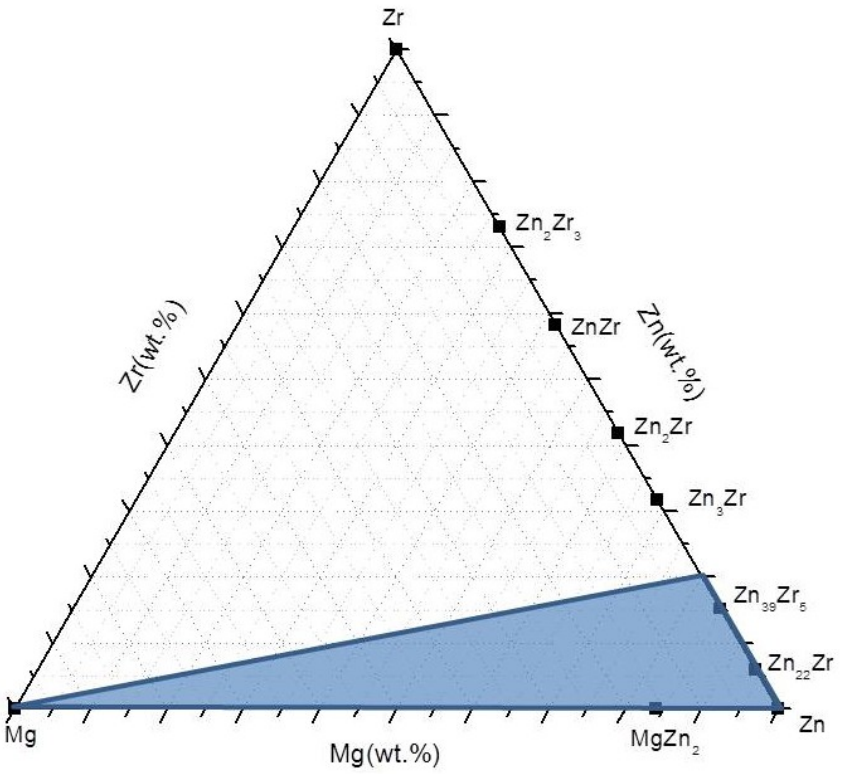

Figure 3.3 The key alloy region which can be investigated with the Zn-Zr master alloys.

As shown in Figure 3.3, the key alloys can be prepared in a limited area and key alloys in the Mg-rich could not be prepared this way. To solve this problem, the Mg-33 wt% Zr master alloy was used to prepare samples in the Mg-rich part. Unlike the Zn-Zr master alloy, the Mg-Zr master alloys were bought from Richest Group Company (China). Figure 3.4 shows the backscattered Scanning Electron Microscope (SEM) image of the Mg-Zr master alloy. White Zr particles are located in the gray Mg matrix randomly.

To prepare ternary alloys, the Mg-Zr alloy and Zn were melted in an induction furnace. The highest temperature of the induction melting furnace in our lab is lower than the melting temperature of Zr. However, Zr can be dissolved in the liquid Mg and Zn if the induction melting time is relatively long. Similarly, Figure 3.5 shows the region of key alloys prepared using the Mg-Zr master alloy.

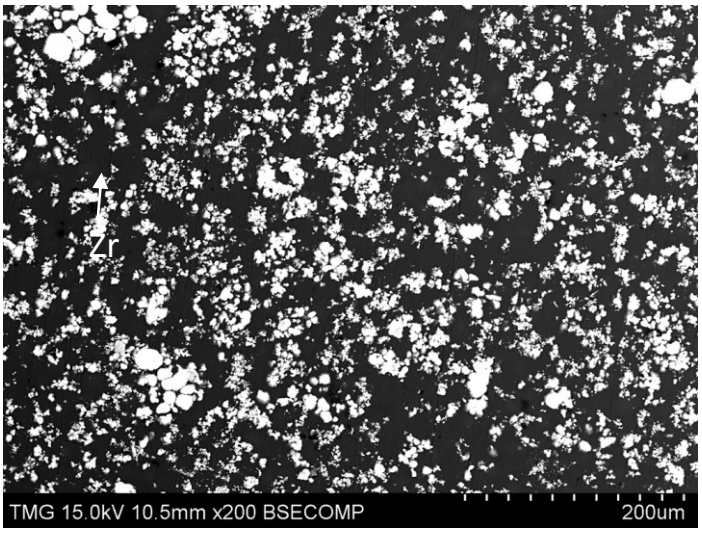

Figure 3.4 SEM micrograph of the Mg-Zr master alloy.

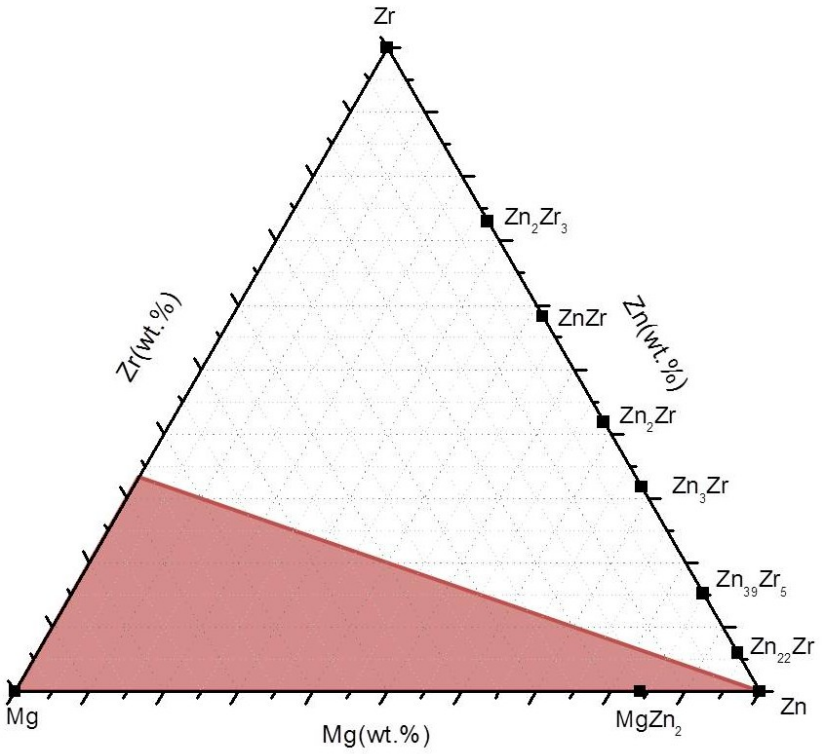

Figure 3.5 The key alloy region which can be prepared using the Mg-Zr master alloys.

Theoretically, more area of the phase diagram can be covered if mixing the Zn-Zr and Mg-Zr

master alloys. The composition of the alloy, however, cannot be easily controlled because of the significant evaporation of both Zn and Mg elements in the master alloys. Therefore, the method of preparing key alloys using both master alloys was abandoned. In this case, more diffusion couples were designed and prepared to cover more area of the phase diagram.

Ternary key alloys were cut into two pieces. One piece was used for the ICP test and SEM study as an as-cast sample. The other piece was wrapped in tantalum foil, sealed in argon-purged quartz tube and annealed in the box furnace at 450^{o}C for a predefined period. After annealing, the quartz tube was quenched in water and the samples were mounted in epoxy. Then it was ground up to 1200 grit SiC grinding papers and then polished by 1μm colloidal silica polishing suspensions (OP-S suspension). During grinding and polishing, ethanol was used as a lubricant. Afterward, the polished samples were examined by SEM coupled with EDS. Then, the key alloys were analysed using X-ray Powder Diffraction (XRD).

3.3 Diffusion couples

The diffusion couple technique is an advanced tool that is often used to study the formation of phases in binary, ternary and multicomponent systems [63, 64]. First of all, compared with the key alloy study, diffusion couples can determine several ternary or binary phase equilibria in one sample. For this reason, diffusion couples can significantly decrease the required numbers of key alloys. However, the preparation of diffusion couples is more complex and difficult than key alloys. In addition, the possibility of obtaining a successful diffusion couple is much lower than that of key alloys. Also, some diffusion layers may form and grow faster than others since the initiation and growth kinetics of phases are different. Therefore, some layers may be too thick while some phases are too thin to be examined by SEM. To sum up, diffusion couples are useful to analyse phase equilibria. Diffusion couples need to be coupled with key samples to verify the phase relationships. In addition, diffusion couples having different compositions and covering different regions of the phase diagram should be prepared to compare and confirm the results.

To prepare diffusion couples, two end-members, which were prepared from pure metals or alloys, were ground up to 1200 grit SiC paper and were polished to 1 μm using colloidal silica polishing suspensions (OP-S suspension). Then the two end-members were clamped together using a clamping ring. The diffusion couples were wrapped in tantalum foil and were annealed at 450^{o}C for 7 days in a quartz tube filled with Ar. The annealing periods of some diffusion couples were adjusted to form thicker layers or to avoid intensive evaporation as can be seen in Table 3.1.

The following diffusion couples were prepared to map the phase diagram of the Mg-Zn-Zr ternary system at 450°C. The compositions of the end-members and the annealing conditions of the diffusion couples are summarized in Table 3.1. Figure 3.6 illustrates the diffusion couples in the Mg-Zn-Zr ternary system. Diffusion couples 1 and 2 allow us to determine the phase equilibria in the Mg-rich side as expected at 450°C. Diffusion couples 3, 4, 5, and 6 were prepared to determine the phase equilibria in the Zn-rich side, because of the existence of many intermetallic phases in the Zn-rich corner.

Table 3.1 List of the diffusion couples

Diffusion couple	End-member 1	End-member 2	Annealing condition
1	**Zr**	**45 Mg 55 Zn at.%**	**450^{o}C 3 days**
2	**Zr**	**45 Mg 55 Zn at.%**	**450^{o}C 7 days**
3	**Zr**	**43 Mg 57 Zn at.%**	**450^{o}C 7 days**
4	**Zr**	**36 Mg 64 Zn at.%**	**450^{o}C 7 days**
5	**Zr**	**30 Mg 70 Zn at.%**	**450^{o}C 10 days**
6	**Zr**	**20 Mg 80 Zn at.%**	**450^{o}C 2 days**

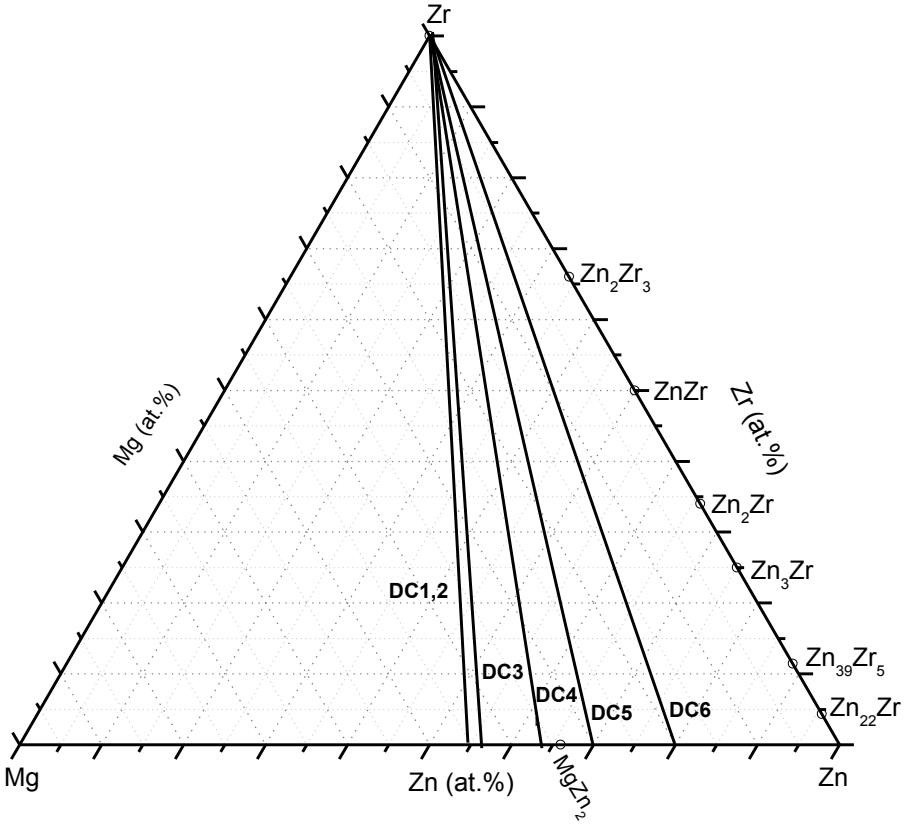

Figure 3.6 Terminal compositions of the diffusion couples in the Mg-Zn-Zr ternary system.

3.4 Characterization of samples

In this experimental investigation of the Mg-Zn-Zr ternary system, Inductively Coupled Plasma (ICP), Scanning Electron Microscopy (SEM) coupled with Energy-dispersive X-ray spectroscopy (EDS), X-ray Diffraction (XRD) were used to analyse the diffusion couples and key alloys.

3.4.1 Inductively Coupled Plasma Spectrometer

The actual compositions of the alloys vary significantly because of the intensive evaporation of Mg and Zn. Hence, it is extremely important to determine the global composition of the key samples and end-members of the diffusion couples. The actual compositions of the samples in this research were determined by Inductively Coupled Plasma (ICP). To prepare samples for ICP

test, 50 mg of the samples were cut from 3 different parts of the key samples, and they were put in a clean beaker. Concentrated nitric acid was slowly added in 0.5 ml installments in order to dissolve the sample completely. Once the sample was completely dissolved, more 1% diluted nitric acid was added in the beaker. Then the sample was transferred to a 50 ml clean and dry volumetric flask. Afterward, the sample was diluted to the concentrations of 5-15 ppm because it was found that the best calibration results were obtained in the interval 1 to 20 ppm. Before testing samples, element calibrations were required. Five calibration solutions with 5, 10. 15, 20 and 25 ppm concentrations of Mg, Zn and Zr elements were prepared. All the processes are done in the Fume-Hood using gloves and safety glasses. ICP is a precise technique to determined the global composition of the samples, the determination limit can be 0.2 ppm.

3.4.2 Scanning Electron Microscopy

Scanning Electron Microscopy (SEM) coupled with Energy-dispersive X-ray spectroscopy (EDS) was mainly used to analyse the diffusion couples and key alloys in terms of the constituent phases, compositions, and morphologies. Figure 3.7 represents a schematic of the SEM. The Backscattered Electrons (BSE) images are using high energy electrons reflected from the sample by elastic scattering. The Secondary Electrons (SE) images are using low-energy electrons ejected from the sample by inelastic scattering interaction. Both of the BSE and SE images provide the information about the phases. SE images are more powerful to observe the topography of samples' surface. BSE images are more useful to distinguish phases because BSE images have higher concentration contrast. In this research, BSE mode was mainly used to obtain pictures with good contrast. Hitachi S-3400N (SEM) coupled with Oxford Energy Dispersive Spectrometer (EDS) detector was used to analysis the diffusion couples and key alloys.

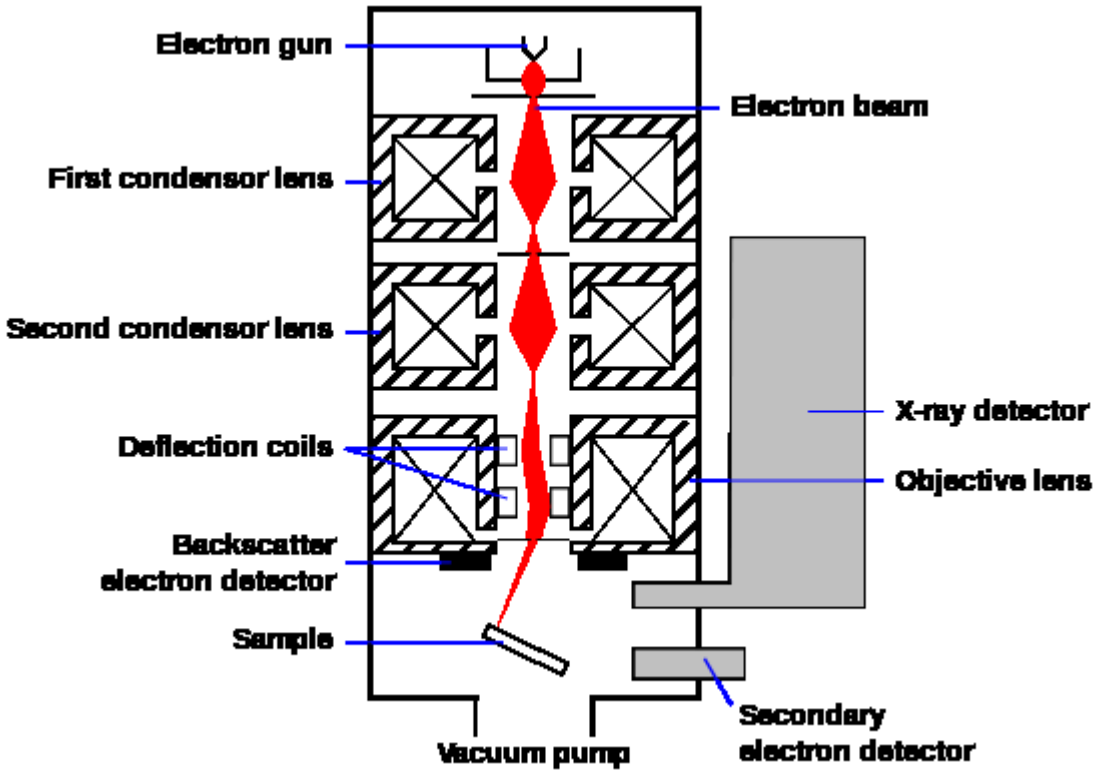

Figure 3.7 Schematic of the SEM [65].

EDS is a qualitative and quantitative X-ray micro analytical technique that can detect the chemical compositions of the phases. Because of the overlapping of peaks, there is an estimated 2-3 at.% error of EDS results. Therefore, for the chemical composition identification, 3-5 measurements were carried out on different locations for each phase and the average composition was taken as the actual composition. The determination limit of the EDS technique is around 1 at.%. The area EDS was also used to identify the composition of the key alloys. Both ICP and EDS results showed good agreement.

3.4.3 X-ray Diffraction

X-ray Diffraction is used to study the phases present in the key alloys and to determine the solubility limits of the phases. For some phases that have similar chemical composition, XRD is also used to distinguish the phases based on different crystal structure.

The crystal structure information of the pure elements and binary phases in this system were taken from the Pearson's Crystal Database [66] as CIF files. The Crystallographic information of the phases from the Pearson's Crystal Database is summarized in Table 3.3. The majority of the peaks of the pure elements and binary compounds are located in the range from 20^o to 90^o. Hence, the spectrum was acquired from 20 to 90º 2θ with a 0.02º step size. Silicon powder was added to the samples for calibrating the zero shift as well as specimen displacement. X-ray scans from a PANalytical X-ray Diffraction with a CuKα radiation at 45kV and 40mA were performed on key alloys. X'Pert HighScore Plus Rietveld analysis software was used for XRD patterns analysis. The determination limit of the XRD is around 3 volume percentage in a two phase mixture.

Table 3.3 The crystallographic information of the pure elements and binary compounds of the Mg-Zn-Zr ternary system.

Phase	Phase Prototype	Space Group	Lattice Parameter/nm		
			a	b	c
Mg	Mg, hP2	$P6_3/mmc$ (194)	0.3223	0.3223	0.5219
Zn	Mg, hP2	$P6_3/mmc$ (194)	0.2652	0.2652	0.5025
Zr	Mg, hP2	$P6_3/mmc$ (194)	0.3229	0.3229	0.5164
$MgZn_2$	$MgZn_2$, hP2	$P6_3/mmc$ (194)	0.5220	0.5220	0.5220
$Zn_{22}Zr$	$Zn_{22}Zr$, hP12	Fd-3m O2 (227)	1.4103	1.4103	1.4103
$Zn_{39}Zr_5$	$Zn_{39}Zr_5$, mS88	C12/m1 (12)	1.7855	0.8596	1.2546
Zn_3Zr	Cu_3Au, cP4	Pm-3m (221)	0.4074	0.4074	0.4074
Zn_2Zr	$MgCu_2$, cF24	Fd-3m O2 (227)	0.7400	0.7400	0.7400
ZnZr	CsCl, cP2	Pm-3m (221)	0.3336	0.3336	0.3336
Zn_2Zr_3			0.7633	0.7633	0.6965

Chapter 4

Results and discussion

4. 1 Experimental investigation through diffusion couples

4. 1. 1 Diffusion couple #1: Zr - Mg45Zn55 at.% (annealed at 450^{o}C for 3 days)

Backscattered electron (BSE) images of diffusion couple #1; Zr-Mg45Zn55 at.% are presented in Figure 4.1 (a). One end-member was made from Zr, and the other was made from the $Mg_{12}Zn_{13}$ + Mg_2Zn_3 two-phase alloy, as shown in Figure 4.1 (b). Diffusion couple #1 was annealed for three days at 450^{o}C. EDS spot analysis was carried out to measure the compositions of phases, and the results are summarized in Table 4.1. After analysis, eight layers were observed. The phases in Figure 4.1 (a) were colored for clearer presentation. Three ternary compounds, labeled as IM1, IM2 and IM3, were detected. In addition, a very thin layer was observed between Zone 6 (Zn_2Zr) and Zone 8 (Zr). The composition of this layer could not be determined by EDS because this layer was too thin. The layer was determined as ZnZr phase based on the Zn-Zr binary system phase diagram [57].

According to the binary phase diagram of the Mg-Zn system [40], the peritectic reactions: $Mg_{12}Zn_{13} \leftrightarrow L + Mg_2Zn_3$, $Mg_2Zn_3 \leftrightarrow L + (MgZn_2)$, occur at 347^{o}C and 410^{o}C respectively. Therefore, the Mg45Zn55 at.% alloy transforms to liquid and $MgZn_2$ while annealing at 450^{o}C. The composition of the liquid could be obtained from the binary phase diagram [40], which was around Mg60Zn40 at.%. Interdiffusion happened between Zr and the semi-solid end-member that contained liquid and $MgZn_2$. ZnZr, Zn_2Zr, IM3, IM2 and IM1 phases formed during diffusion. While quenching, the liquid solidified and formed Mg_2Zn_3 and $Mg_{12}Zn_{13}$ phases. However, Mg_2Zn_3 and $Mg_{12}Zn_{13}$ phases were not considered to be equilibrium phases as they are not stable at 450^{o}C.

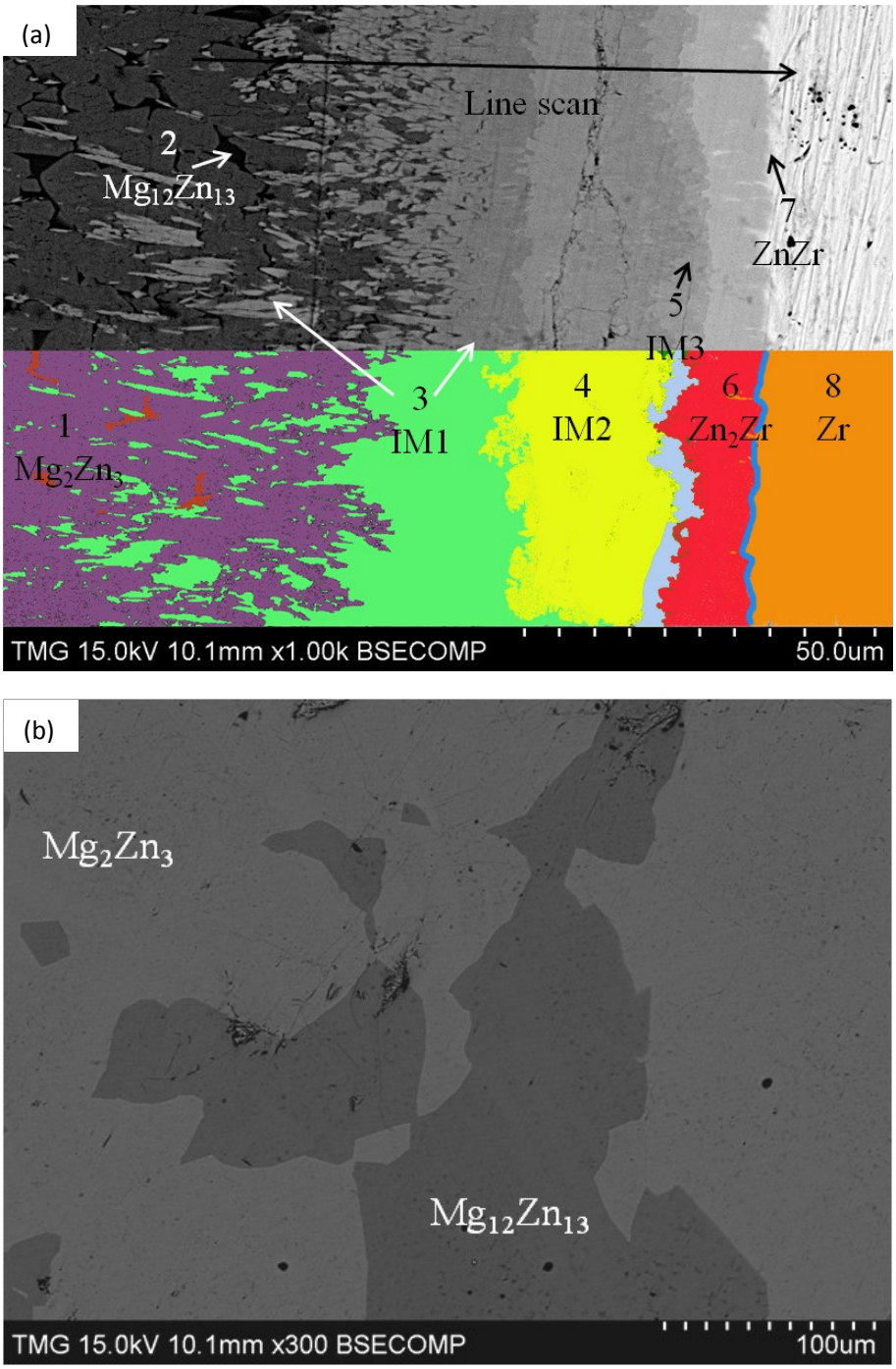

Figure 4.1 (a) SEM micrograph of diffusion couple #1; (b) SEM micrograph of the Mg45Zn55 (at.%) end-member before annealing.

Table 4.1 EDS spot analysis of diffusion couple #1.

Phases	Composition (at.%)			Corresponding phase
	Mg	Zn	Zr	
1	39	61	0	Mg_2Zn_3
2	47	53	0	$Mg_{12}Zn_{13}$
3	22-26	66	8-12	IM1
4	16	66	18	IM2
5	10	66	24	IM3
6	0	64	36	Zn_2Zr
7	0	50	50	ZnZr
8	0	0	100	Zr

EDS line scan was carried out across the diffusion couple to determine the homogeneity ranges of the ternary and binary phases. The results, shown in Figure 4.2, indicate that the IM1 ternary compound is a substitutional solid solution, where Mg is substituted by Zr at constant Zn concentration of 66 at.%. The homogeneity range of IM1 is estimated as $Mg_{(22-26)}Zn_{66}Zr_{(8-12)}$. No solid solution for IM2 phase was detected by EDS line scan, and its average composition was determined as $Mg_{16}Zn_{66}Zr_{18}$. The homogeneity range of IM3 phase could not be determined from this diffusion couple because the layer of IM3 was too thin to perform several EDS points across the layer. The average composition of some points of IM3 along the layer is $Mg_{10}Zn_{66}Zr_{24}$. ZnZr phase was not detected in the EDS line scan, because the layer of this phase is too thin. When performing EDS line scan, some points were taken at the interface of two layers. These points were abandoned when determining the homogeneity ranges of the detected phases. No solid solutions were observed for the binary compounds.

The $(Mg,Zr)Zn_2$, which was reported in the literatures as $Mg_{17.54}Zn_{67.11}Zr_{15.35}$ [62], has similar composition to the IM2 ($Mg_{16}Zn_{66}Zr_{18}$). In the literature, $(Mg,Zr)Zn_2$ was considered as a solid

solution of $MgZn_2$, because it has similar XRD pattern to that of $MgZn_2$ phase. This is doubted because two compounds can have the same prototype and similar XRD patterns. Further studies in terms of the crystal structure and composition of the ternary compounds are required and will be carried out in this work.

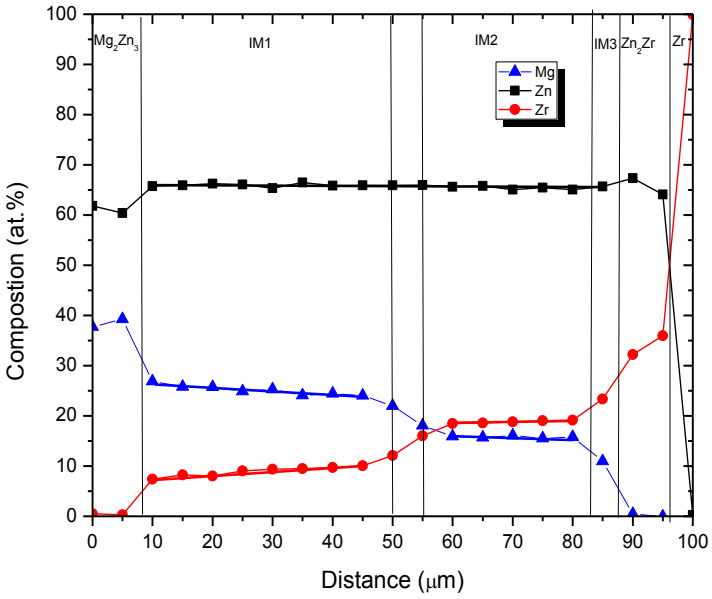

Figure 4.2 EDS line scan across diffusion couple #1.

4.1.2 Diffusion couple #2: Zr - Mg45Zn55 at.% (annealed at 450°C for 7 days)

Diffusion couple #2, which had the same end-members to diffusion couple #1, was prepared to study the stability of the existing phases with longer annealing time. Diffusion couple #2 was annealed at 450°C for 7 days. The SEM micrographs including a magnified microstructure of the area of interest are demonstrated in Figure 4.3. As shown in Figure 4.3 (a) to (c), six diffusion zones were identified by EDS spot analysis. The compositions and corresponding phases are summarized in Table 4.2. The phases in Figure 4.3 (b) are colored to improve clarity.

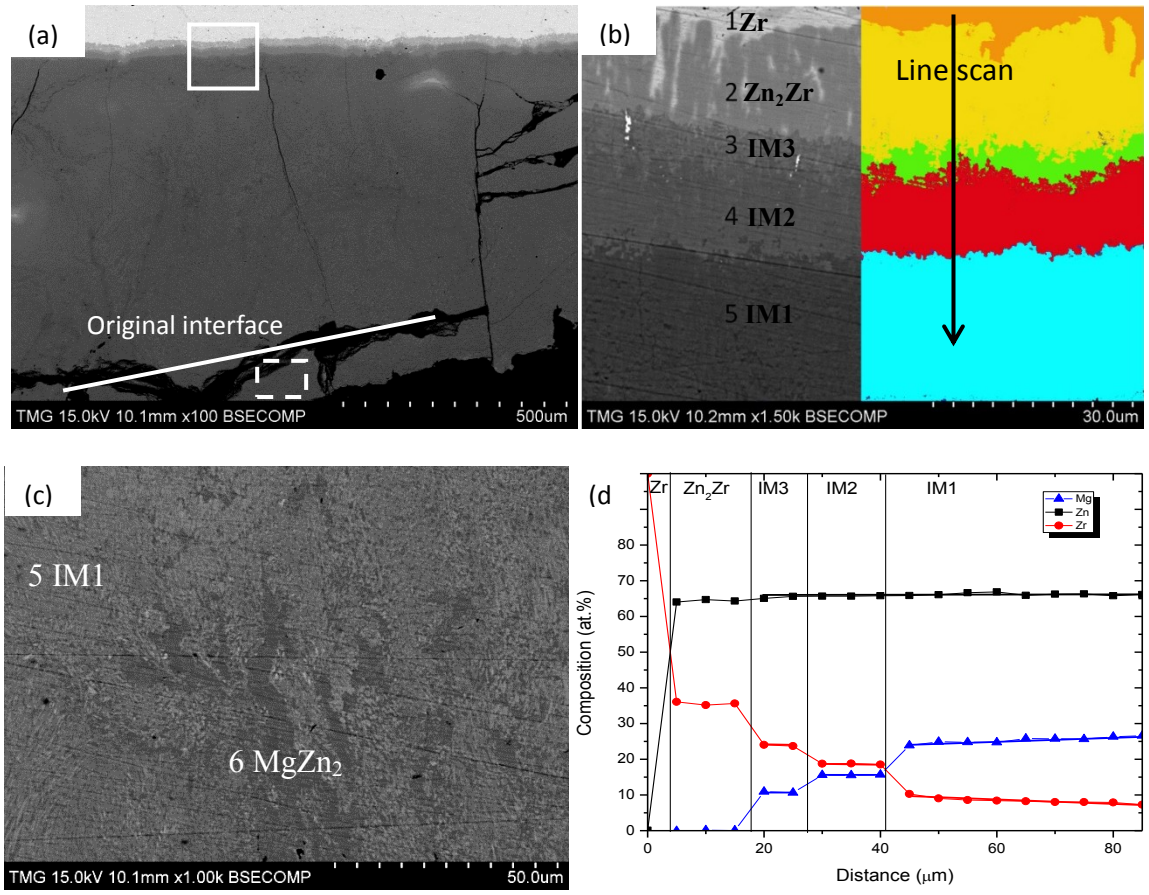

Figure 4.3 (a) SEM micrograph of diffusion couple #2; (b) Magnified micrograph of the white square area shown in (a); (c) Magnified micrograph of the dashed white square area shown in (a); (d) EDS line scan across the diffusion zones in (b).

The sequence of diffusion from zone 1 to zone 6 can be written as: Zr → Zn_2Zr → IM3 → IM2 → IM1 → $MgZn_2$. Except for ZnZr, which could be missing because it is too thin, the other phases show good consistency with diffusion couple #1. Zone 6 ($MgZn_2$), as shown in Figure 4.2 (c), is in equilibrium with zone 5 (IM1), that is different from diffusion couple #1. The morphology in Figure 4.3 (c) indicates the liquid forms. During annealing, Mg_2Zn_3 and $Mg_{12}Zn_{13}$ phases transformed to $MgZn_2$ phase and liquid (Mg60Zn40 at.%) through two peritectic reactions: $Mg_{12}Zn_{13} \leftrightarrow L + Mg_2Zn_3$ (347°C), $Mg_2Zn_3 \leftrightarrow L + (MgZn_2)$ (410°C). Subsequently, interdiffusion happened between Zr and the semi-solid end-member that contained liquid and $MgZn_2$ phase.

The crack in Figure 4.3 (a) is where the original interface of diffusion was. It was clear that major diffusion happened at the Zr end-member side, because Mg and Zn were more active than Zr at 450°C. A small quantity of Zr diffused to the Mg45Zn55 at.% alloy end-member side and formed IM1 phase. The liquid evaporated completely due to the long annealing time, $MgZn_2$ phase remained in the end-member after annealing for 7 days. Diffusion couple #2 confirmed that Mg_2Zn_3 and $Mg_{12}Zn_{13}$ phases are not stable at 450°C.

Table 4.2 Results of EDS spot analysis across diffusion couple #2.

Zone	Composition (at.%)			Corresponding phase
	Mg	Zn	Zr	
1	0	0	100	Zr
2	0	64	36	Zn_2Zr
3	10	66	24	IM3
4	15 - 7	66	17-19	IM2
5	24 -27	66	7-10	IM1
6	34	66	0	$MgZn_2$

EDS line scan was used to determine the homogeneity ranges of the phases and the results are shown in Figure 4.3 (d). The homogeneity range of IM1 in diffusion couple 2 was detected as $Mg_{(24\text{-}27)}Zn_{66}Zr_{(7\text{-}10)}$. The compositions of the IM2 and IM3 were $Mg_{16}Zn_{66}Zr_{18}$ and $Mg_{10}Zn_{66}Zr_{24}$, respectively. The determined compositions and the thicknesses of the ternary and binary compounds in diffusion couples #1 and #2 are summarized in Table 4.3. In terms of composition, all phases in diffusion couple #1 showed good consistency with diffusion couple #2. The slight difference in the composition of IM1 was within the error range of the EDS measurements. After 7 days annealing, the thickness of IM1 layer increased significantly, which means that the kinetic of formation of this phase is high compared to other phases. The layer thickness of IM2 phase decreased. The probable cause of it is the higher diffusivity of Mg and Zn in IM2 compared to

other phases. The other cause of the thickness reduction of IM2 layer could be due to more negative energy of formation and the high growth rate of IM1 layer. The layer thickness of IM3 and Zn_2Zr increased slightly with longer diffusion time. ZnZr phase was not observed in diffusion couple #2 and the thickness of ZnZr layer in diffusion couple #1 was very thin, that indicates the kinetic of formation and diffusion of the ZnZr phase is too slow.

Table 4.3 Compositions and layers thicknesses of the diffusion couple #1 and #2

Phase	Composition (at.%)		Layer thickness (μm)	
	DC1	DC2	DC1	DC2
IM1	$Mg_{(22-26)}Zn_{66}Zr_{(8-12)}$	$Mg_{(24-27)}Zn_{66}Zr_{(7-10)}$	45.9	300
IM2	$Mg_{16}Zn_{66}Zr_{18}$	$Mg_{16}Zn_{66}Zr_{18}$	24.2	12.7
IM3	$Mg_{10}Zn_{66}Zr_{24}$	$Mg_{10}Zn_{66}Zr_{24}$	3.5	5.9
Zn_2Zr	$Zn_{64}Zr_{36}$	$Zn_{64}Zr_{36}$	10.9	16.2
ZnZr			0.5	0

Based on the compositions of the diffusion zones and the EDS line scans, the sequence of the phases along the diffusion path can be depicted from diffusion couples #1 and #2 as follows: Liquid (Mg60Zn40 at.%) + $MgZn_2$ → IM1 → IM2 → IM3 → Zn_2Zr → ZnZr → Zr. The arrows indicate the phase boundary lines. The phase equilibria obtained from diffusion couples #1 and #2 are represented in Figure 4.4. The two end-members of diffusion couple #1 and #2 are connected by a dashed line in Figure 4.4. The ZnZr was not observed in diffusion couple #2, which could be due to this layer being too thin to be detected by SEM. The composition of the liquid was obtained from the Mg-Zn binary phase diagram [40]. Diffusion couple #1 and #2 obey the mass balance principle because the diffusion path crossed the dashed line at least once.

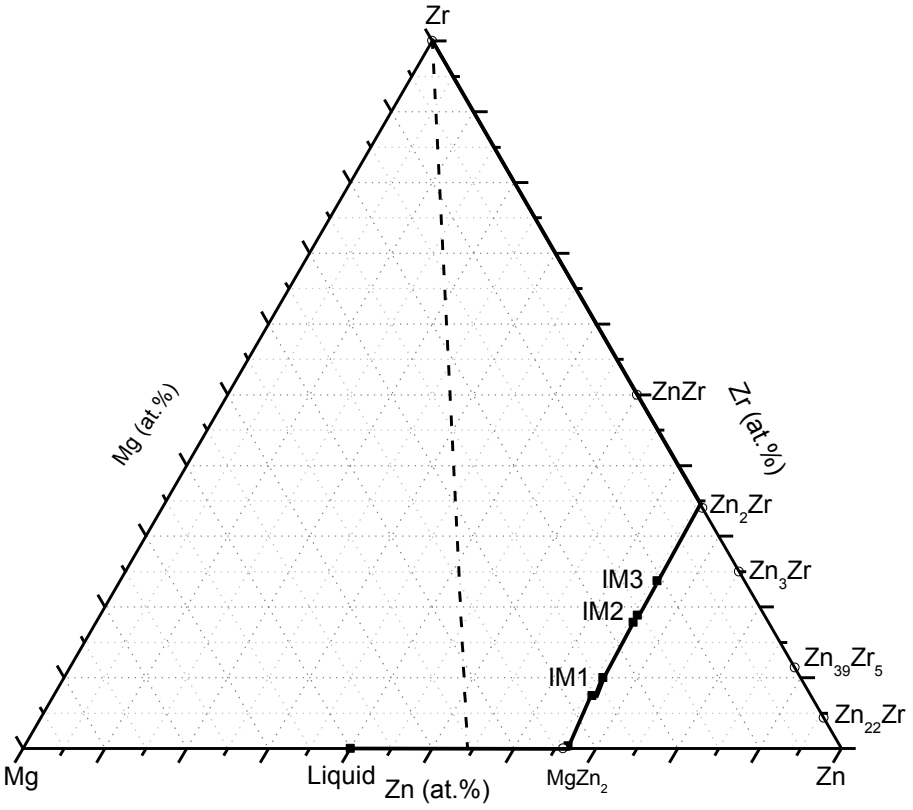

Figure 4.4 Diffusion path depicted from diffusion couple #1 and #2.

4. 1. 3 Diffusion couple #3: Zr - Mg43Zn57 at.% (annealed at 450^{o}C for 7 days)

Backscattered electron images of diffusion couple #3 are illustrated in Figure 4.5. The first end-member was made from Zr and the second end-member was made from Mg43Zn57 at.% alloy that is composed of $Mg_{12}Zn_{13}$ + Mg_2Zn_3. After annealing at 450^{o}C for 7 days, four layers were observed, and they were colored in Figure 4.5 (a) for better observation. The phases were analysed by EDS spot analysis, and the results are listed in Table 4.4. Zone 1, 2, 3 and 4 were identified to be Zr, Zn_2Zr, Zn_3Zr and IM1, respectively. Figure 4.5 (b) represents the magnified SEM image near the Zr end-member. Zone 1 was detected as Zr and zone 2 was detected as Zn_2Zr. The ZnZr phase was not observed in this image, which might be because the layer was too thin to be detected. As shown in Figure 4.5 (c), a thick layer of Zn_3Zr was formed during

annealing. Similar to the previous two diffusion couples, Mg_2Zn_3 and $Mg_{12}Zn_{13}$ were melted and transformed into liquid and $MgZn_2$ during annealing. Zn diffused faster than Mg in the Zr end-member, hence the sequence of Zn-Zr binary compounds were formed (zone 1 to zone 3). The forming of a thick Zn_3Zr layer consumed large amounts of Zn from the semi-solid end-member. The diffused Zn atoms were from the liquid and $MgZn_2$. Meanwhile, the liquid composition shifted towards the Mg-rich side. The composition of the liquid has the tendency to be constant at Mg60Zn40 at.% at 450^{o}C. Other Zn sources could be from the decomposition of $MgZn_2$ phase. Zr diffused to the Mg43Zn57 at.% alloy side and started forming IM1. The IM1 phase with porosity was observed in Figure 4.5 (d). The forming of porosity was due to liquid evaporation during annealing.

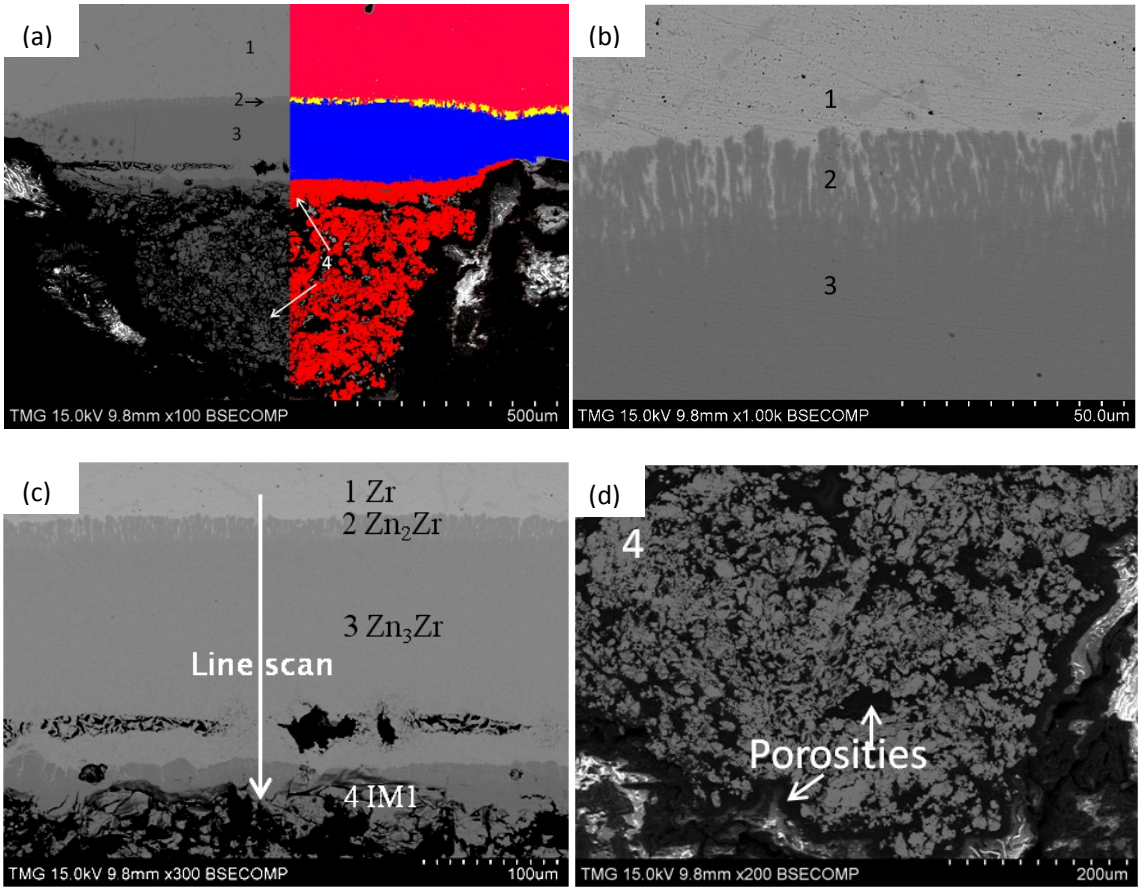

Figure 4.5 (a), (b), (c), (d) SEM micrographs of diffusion couple #3.

The EDS line scan, shown in Figure 4.6, was performed on the diffusion zones to measure the homogeneity ranges of the existing phases. The homogeneity range of IM1 was estimated as $Mg_{(23-25)}Zn_{67}Zr_{(7-10)}$ which showed a good consistency with the findings obtained from the previous two diffusion couples. No solid solubility of the third element was detected for Zn_2Zr and Zn_3Zr.

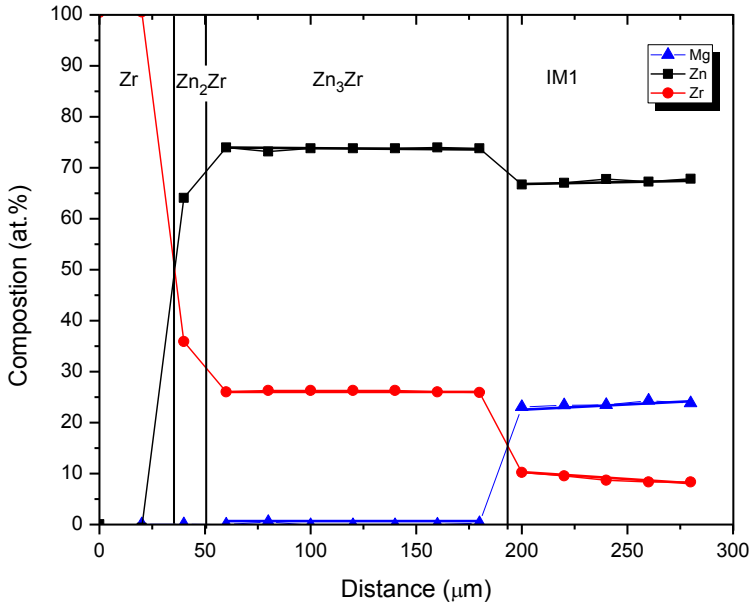

Figure 4.6 EDS line scan results across diffusion couple #3.

Table 4.4 EDS spot analysis of diffusion couple #3.

Zone	Composition (at.%)			Corresponding phase
	Mg	Zn	Zr	
1	0	0	100	Zr
2	0	64	36	Zn_2Zr
3	0	74	26	Zn_3Zr
4	23-25	67	8-10	IM1

The phase equilibria obtained from diffusion couple #3 are represented in Figure 4.7. The dashed line represents the location of the end-members. The sequence of phases along the diffusion path in diffusion couple #3 can be depicted as follows: Zr → Zn_2Zr → Zn_3Zr → IM1 → Liquid (Mg60Zn40 at.%) + $MgZn_2$.

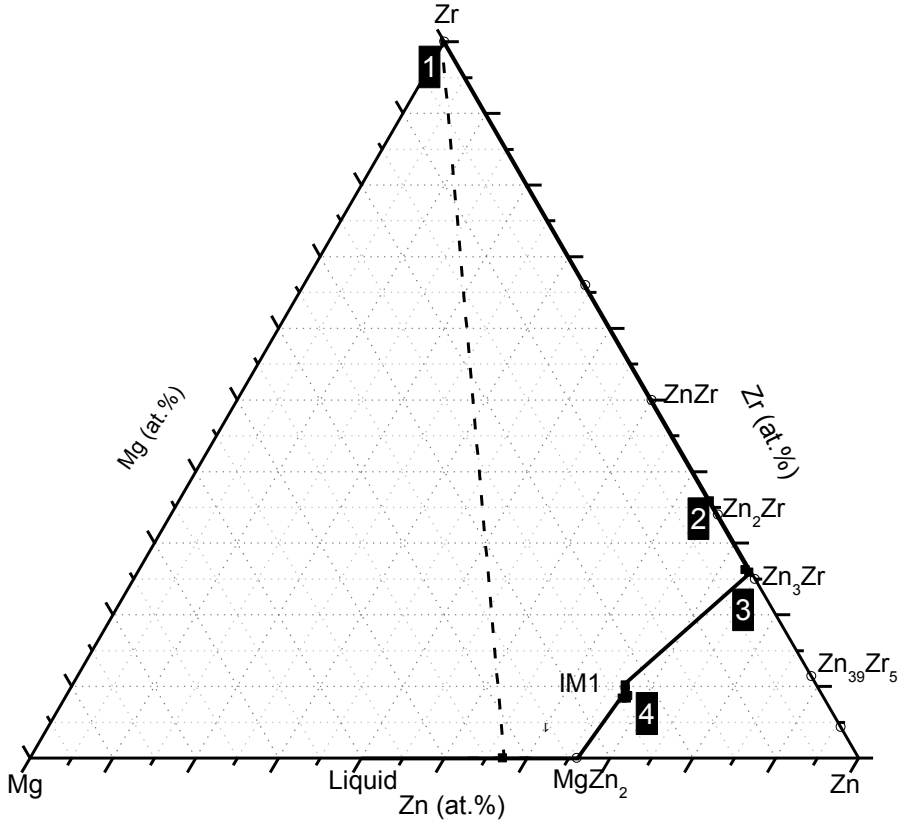

Figure 4.7 Diffusion path depicted from diffusion couple #3. Numbers in the black boxes represent the diffusion layers in Figure 4.5.

4. 1. 4 Diffusion couple #4: Zr-Mg36Zn64 at.% (annealed at 450°C for 7 days)

The SEM micrograph of diffusion couple #4 is presented in Figure 4.8. The first end-member was made from Zr, and the second end-member was made from the two-phase alloy that contained $MgZn_2$ and Mg_2Zn_3 phases as shown in Figure 4.8 (c). After 7 days annealing at 450°C, seven diffusion zones were observed in Figure 4.8 (a) and (b). The diffusion zones were colored

for clearer observation. EDS spot analysis was performed to identify each phase. The EDS results are summarized in Table 4.5. Figure 4.8 (b) represents the magnified image of this diffusion couple near the Zr end-member side. A very thin layer was observed between Zone 1 (Zr) and Zone 2 (Zn_2Zr), which was recognized as ZnZr based on the Zn-Zr binary system phase diagram [57]. However, the actual composition of this layer was not determined by EDS because this layer was too thin to be detected. EDS line scan was carried out across this diffusion couple, and the composition profile is shown in Figure 4.9. Accordingly, IM3 compound was recognized as $Mg_{11}Zn_{65}Zr_{24}$. The homogeneity range of IM2 compound was determined as $Mg_{(14-16)}Zn_{66}Zr_{(18-20).}$ The homogeneity range of IM1 compound was $Mg_{(22-26)}Zn_{66}Zr_{(8-12),}$ which agrees well with the results obtained from previous diffusion couples. As mentioned before, Ren et al. [62] reported that (Mg,Zr)Zn_2 ($Mg_{17.54}Zn_{67.11}Zr_{15.35}$) is an extended solid solubility of Zr in $MgZn_2$. In the current work, IM3, IM2 and IM1 phases are considered as ternary compounds based on the clear boundaries of the IM3, IM2, IM1 and $MgZn_2$ phases in the SEM images. IM1 (zone 6) is formed near to $MgZn_2$ (zone 7) in this diffusion couple. Therefore, the phase equilibria between IM1 and $MgZn_2$ phases can be established. The homogeneity range of $MgZn_2$ was estimated as $Mg_{(32-34)}Zn_{(66-68)}$.

Figure 4.8 (c) represents the second end-member of diffusion couple #4 before annealing. $MgZn_2$ is located in the matrix of Mg_2Zn_3. During annealing, the second end-member decomposed into liquid and $MgZn_2$ through the peritectic reaction: L + ($MgZn_2$) ↔ Mg_2Zn_3 (410^oC). The composition of the liquid is Mg60Zn40 at.%. The interdiffusion started between Zr and the semi-solid end-member that contained liquid and $MgZn_2$. ZnZr, Zn_2Zr, IM3, IM2, and IM1 formed during diffusion. Residual liquid evaporated from the Mg-Zn end-member, because the annealing time was relatively long.

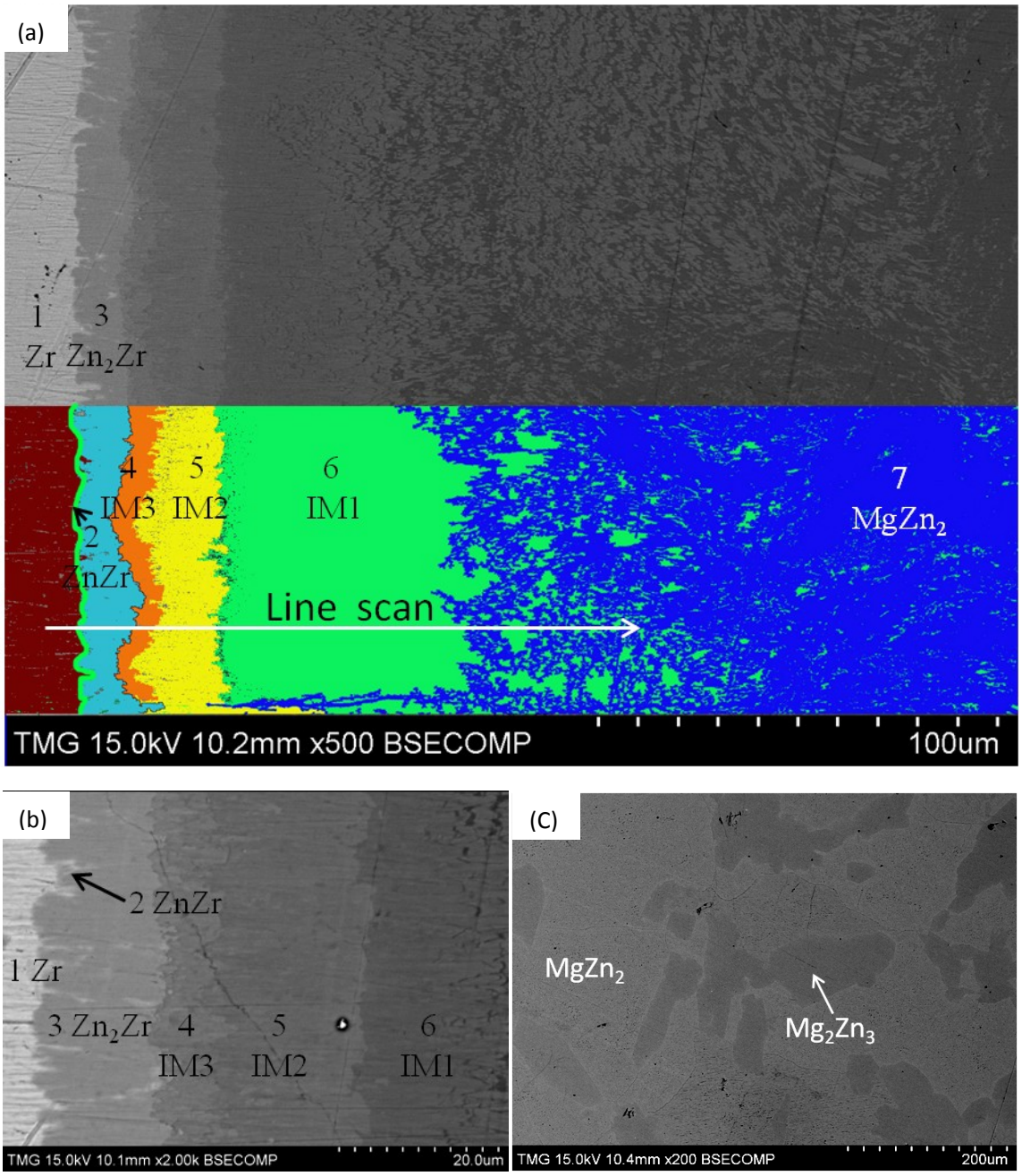

Figure 4.8 (a), (b) SEM micrograph of diffusion couple #4; (c) SEM micrograph of the Mg36Zn64 (at.%) end-member before annealing.

Table 4.5 EDS spot analysis of diffusion couple #4.

Zone	Composition (at.%)			Corresponding phase
	Mg	Zn	Zr	
1	0	0	100	Zr
2	0	50	50	ZnZr
3	0	67	33	Zn_2Zr
4	11	65	24	IM3
5	14-16	66	18-20	IM2
6	22-26	66	8 -12	IM1
7	32-34	66-68	0	$MgZn_2$

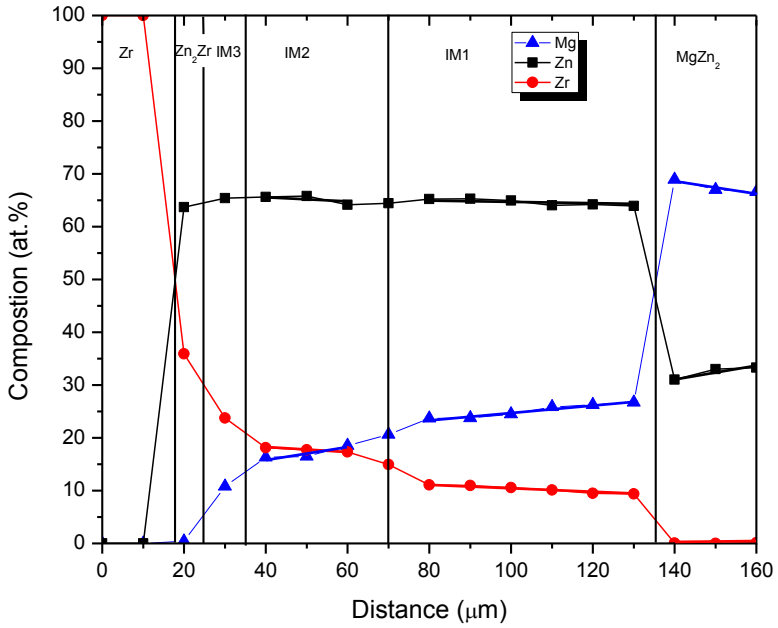

Figure 4.9 EDS line scan across diffusion couple #4.

The diffusion path of this diffusion couple can be depicted as follows: Zr → ZnZr → Zn_2Zr → IM3 → IM2 → IM1 → $MgZn_2$ + Liquid (Mg60Zn40 at.%). The phase equilibria obtained from diffusion couple #4 are represented in Figure 4.10. The two end-members of diffusion couple #4 are connected by a dashed line. Numbers in the black boxes represent the diffusion layers in Figure 4.10.

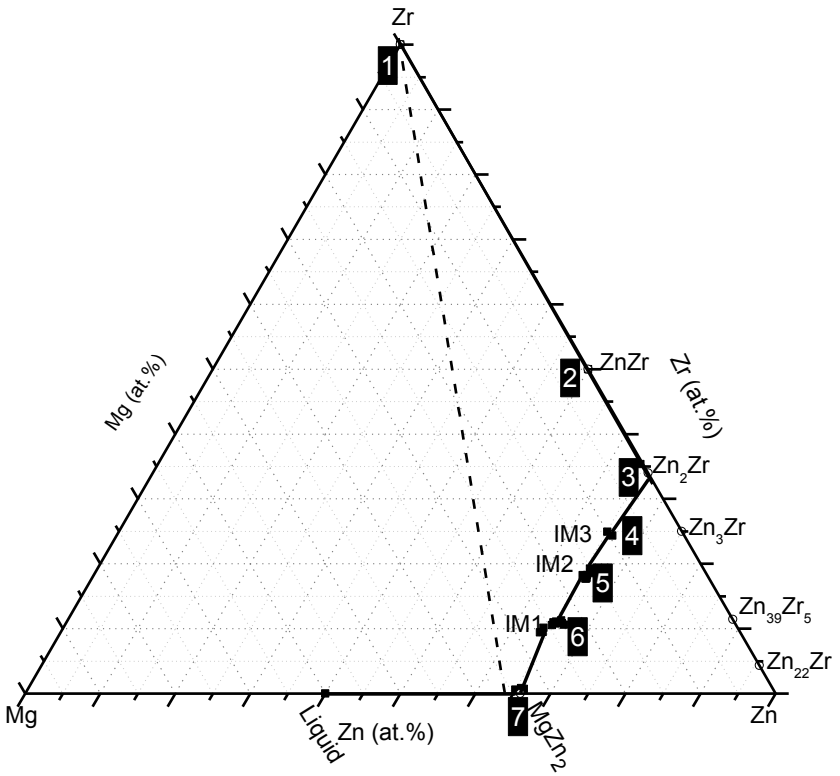

Figure 4.10 Diffusion path depicted from diffusion couple #4. Numbers in the black boxes represent the diffusion layers in Figure 4.8.

4. 1. 5 Diffusion couple #5: Zr-Mg30Zn70 at.% (annealed at 450^{o}C for 10 days)

The first end-member of diffusion couple #5 was made from Zr, and the second end-member was made from Mg30Zn70 at.% binary alloy that contained $MgZn_2$ and Mg_2Zn_{11} phases. Two diffusion couples with the same end-members were annealed for 7 days and the other for 10 days. However, diffusion layers were observed only in the diffusion couple annealed for 10 days, because the diffusion rate in this diffusion couple was slow. After annealing at 450^{o}C for 10 days, six diffusion zones were identified by EDS spot analysis, as shown in Figure 4.11 (a) and (b). The EDS spot analysis was performed to each phase, and the results are summarized in Table 4.6. Zone 1, 2, 3 and 4 were identified as Zr, Zn_2Zr, Zn_3Zr and IM2, respectively. The equilibrium between Zn_3Zr and IM2 was observed in this diffusion couple.

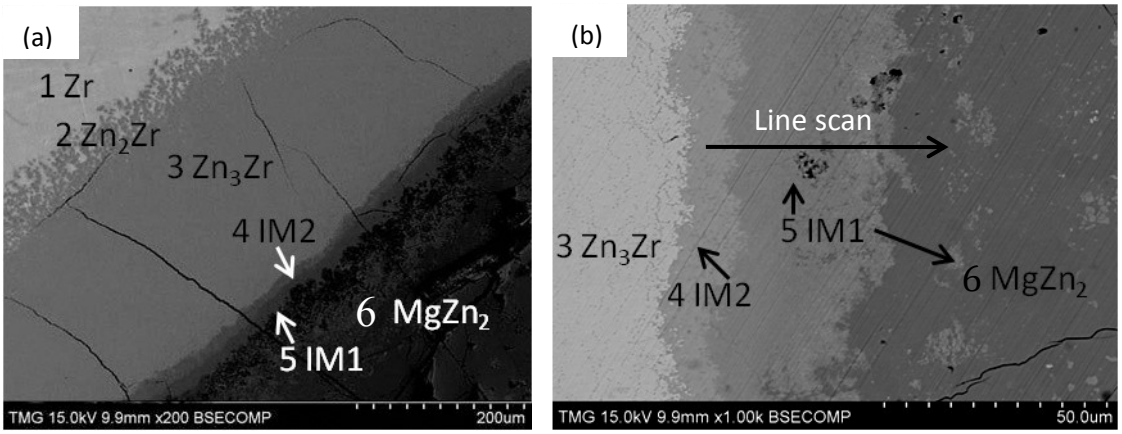

Figure 4.11 (a), (b) SEM micrographs of diffusion couple #5.

Before annealing, the second end-member contained $MgZn_2$ and Mg_2Zn_{11}. During annealing, Mg_2Zn_{11} transforms into liquid and $MgZn_2$ according to the peritectic reaction: L + ($MgZn_2$) ↔ Mg_2Zn_{11} (380^oC). The composition of the liquid is about Mg12.5Zn87.5 at.%, which was obtained from the binary phase diagram [40]. Afterward, interdiffusion took place between the solid Zr and the semi-solid end-member to form six diffusion layers. As shown in Figure 4.11 (b), IM1 phase was not only formed in zone 5 but also located within $MgZn_2$ layer. This is because Mg and Zn atoms diffused to the Zr end-member side and formed the IM1 layer (zone 5), and Zr atoms diffused into the semi-solid end-member and formed the IM1 phase in zone 6. Therefore, the layer structure of IM1 was observed in zone 5 and island structure of IM1 was observed in zone 6. Residual liquid evaporated since the annealing time was relatively long. The ZnZr was not observed in this diffusion couple, which could be because the layer was too thin to be detected by SEM. The possible reason is the kinetic of formation and diffusion of the ZnZr phase is too slow.

EDS line scan was carried out across zone 4 to zone 6 and the results are shown in Figure 4.12. For IM1 compound, Mg was replaced by Zr while Zn concentration was kept constant. The homogeneity range of IM1 was estimated to be $Mg_{(23-25)}Zn_{66}Zr_{(9-11)}$. For IM2, the homogeneity

range was estimated to be $Mg_{(15-16)}Zn_{66}Zr_{(18-19)}$.

Table 4.6 EDS spot analysis of diffusion couple #5.

Zone	Composition (at.%)			Corresponding phase
	Mg	Zn	Zr	
1	0	0	100	Zr
2	0	65	35	Zn_2Zr
3	0	73	28	Zn_3Zr
4	15-16	66	18-19	IM2
5	23-25	66	9-11	IM1
6	32	67	1	$MgZn_2$

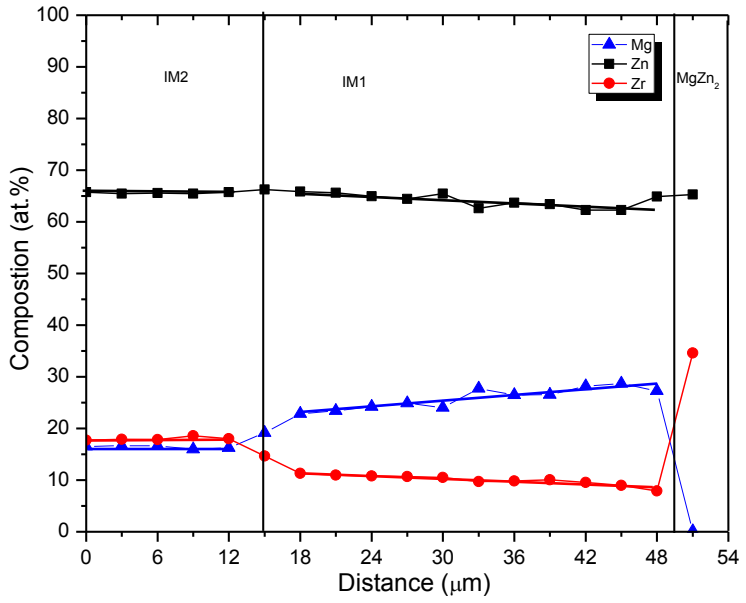

Figure 4.12 EDS line scan across diffusion zones 4, 5 and 6.

The sequence of the diffusion zones of this diffusion couple can be depicted as follows: Zr → Zn_2Zr → Zn_3Zr → IM2 → IM1 → $MgZn_2$ + Liquid (Mg12.5Zn87.5 at.%). The phase equilibria obtained from diffusion couple #5 are presented in Figure 4.13. The two end-members of

diffusion couple #5 are connected by a dashed line. Numbers in the black boxes correspond to diffusion layers in Figure 4.11.

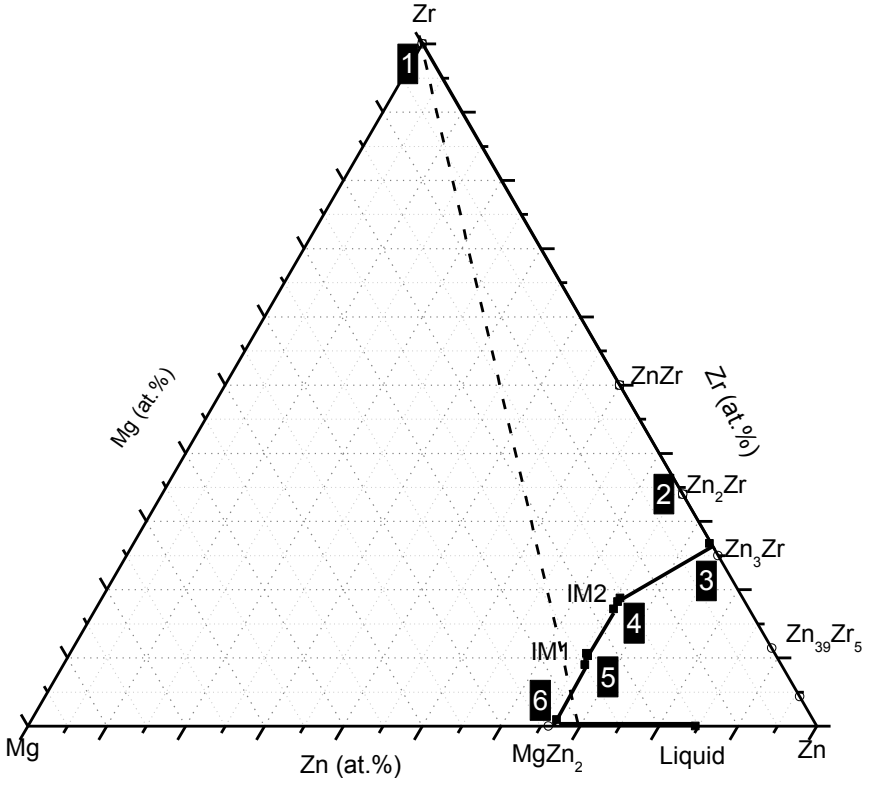

Figure 4.13 Diffusion path depicted from diffusion couple #5. Numbers in the black boxes correspond to the diffusion layers in Figure 4.11.

4. 1. 6 Diffusion couple #6: Zr-Mg20Zn80 at.% (annealed at 450^{o}C for 2 days)

The BSE images of diffusion couple #6 are presented in Figure 4.14 (a-b). The first end-member was made from Zr, and the second end-member was made from Mg20Zn80 at.% binary alloy containing $MgZn_2$ and Mg_2Zn_{11} phases. This diffusion couple was annealed at 450^{o}C for 2 days. After annealing, EDS spot analysis was used to identify the seven diffusion zones in Figure 4.14 (a). Chemical compositions and the corresponding phases are summarized in Table 4.7. A new ternary compound (IM4) was observed in zone 6. Besides, the equilibrium between IM4 (zone 6) and $Zn_{39}Zr_5$ (zone 5) could be established in this diffusion couple. Figure 4.14 (b) is a magnified

part of this diffusion couple. Zr, Zn_2Zr and Zn_3Zr were detected by EDS spot analysis. Besides, there is another phase between Zr and Zn_2Zr. It should be the ZnZr phase. However, this layer was too thin to be detected. In Figure 4.14 (c), a porous morphology was observed. As explained in diffusion couple #5, initially, Mg_2Zn_{11} transformed to liquid (Mg12.5Zn87.5 at.%) and solid $MgZn_2$ phase. Mg and Zn atoms from the liquid and $MgZn_2$ diffused to Zr, and Zr atoms from the Zr end-member diffused to the semi-solid end-member side. The diffusion rate was fast because of a large amount of liquid. Therefore, the annealing period of this diffusion couple was short. ZnZr, Zn_2Zr, Zn_3Zr, $Zn_{39}Zr_5$ and IM4 layers formed during annealing. After annealing, the end-member created a porous structure because of the liquid evaporation.

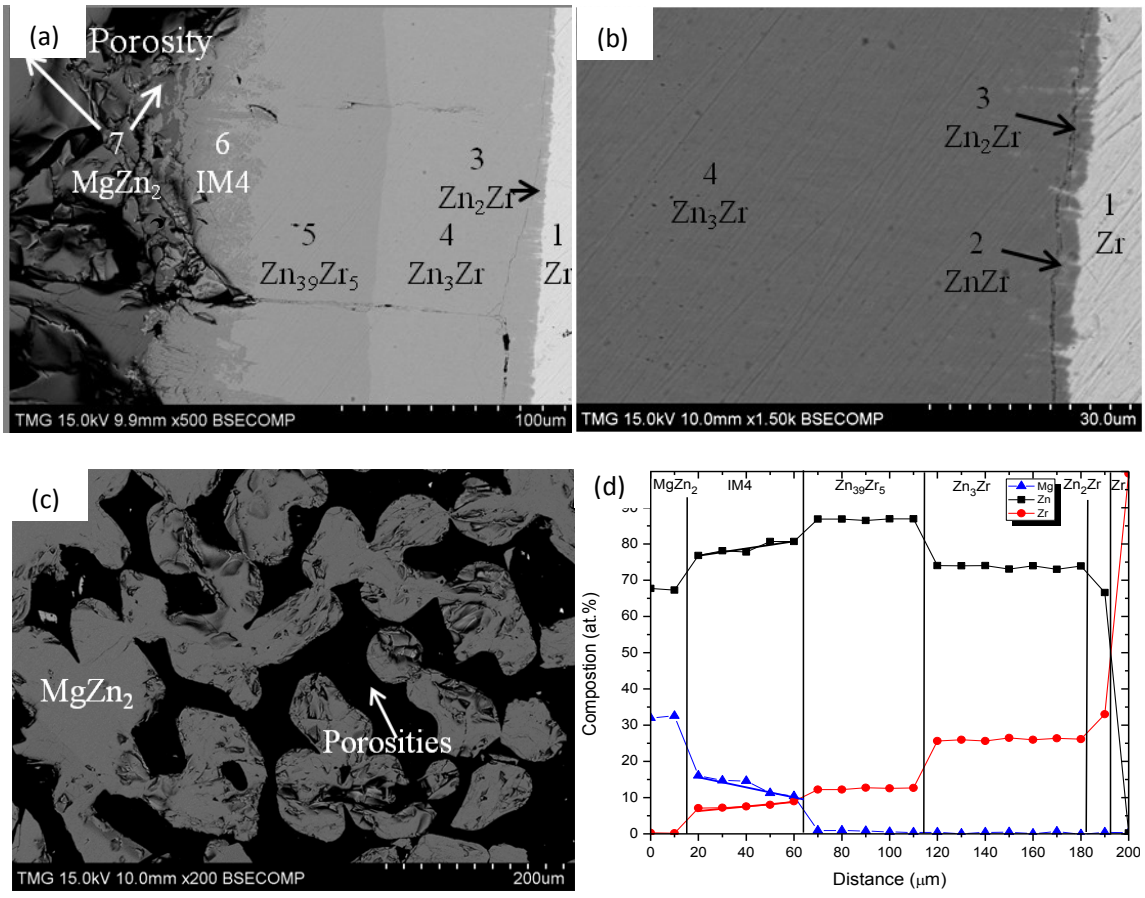

Fig 4.14 (a), (b), (c) SEM micrographs of diffusion couple #6; (d) EDS line scan across diffusion layers.

EDS line scan was carried out through this diffusion couple to determine the homogeneity ranges of the ternary and binary phases and the results were presented in Figure 4.14 (d). EDS line scan was used to study the homogeneity range of the IM4, and the results showed Mg was substituted by both Zr and Zn. The homogeneity range of IM4 was estimated as $Mg_{(7-9)}Zn_{(77-81)}Zr_{(10-15)}$.

The sequence of diffusion in this diffusion couple can be depicted as follows: Zr → ZnZr → Zn_2Zr → Zn_3Zr → $Zn_{39}Zr_5$ → IM4 → $MgZn_2$ + Liquid (Mg12.5Zn87.5 at.%). The phase equilibria obtained from diffusion couple #6 are presented in Figure 4.15. The two end-members of diffusion couple #6 are connected by a dashed line. Numbers in the black boxes represent the diffusion layers in the Figure 4.15. Compared to diffusion couple #5, diffusion couple #6 followed a different diffusion path, which is due to the different composition of the second end-member. The composition of the second end-member of diffusion couple #6 was close to $Mg_2Zn_{11,}$ which means more liquid at 450°C (20 at.% liquid in Mg30Zn70 at.% and 75 at.% liquid in Mg20Zn80 at.%) [40].

Table 4.7 EDS spot analysis results of diffusion couple #6.

Zone	Composition (at.%)			Corresponding phase
	Mg	Zn	Zr	
1	0	0	100	Zr
2	0	50	50	ZnZr
3	0	64	36	Zn_2Zr
4	0	74	26	Zn_3Zr
5	0	87	13	$Zn_{39}Zr_5$
6	7-9	77-81	10-15	IM4
7	33	67	0	$MgZn_2$

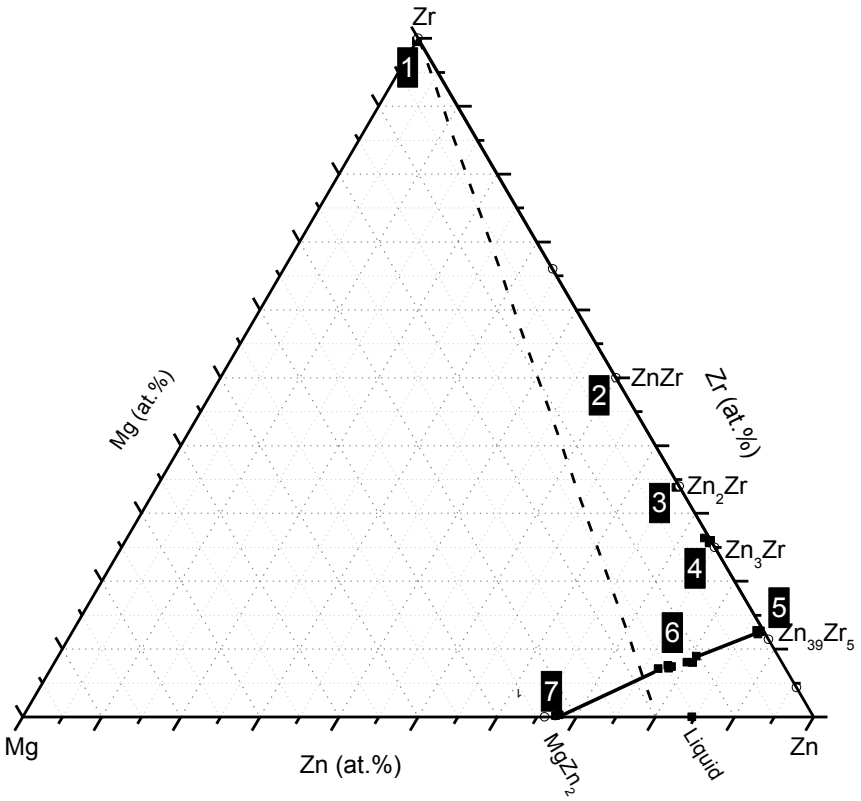

Fig 4.15 Diffusion path depicted from diffusion couple #6. Numbers in the black boxes represent the diffusion layers in Figure 4.14.

4. 1. 7 Summary of the diffusion couples results

In this work, 6 diffusion couples were prepared and annealed at 450^{o}C. A partial isothermal section of the Mg-Zn-Zr ternary system at 450^{o}C was constructed by combining the results of these six diffusion couples. The phase relations are demonstrated in Figure 4.16.

The diffusion path depicted from the diffusion couples are listed as follows:

Diffusion couple #1: Zr → ZnZr → Zn_2Zr → IM3 → IM2 → IM1;

Diffusion couple #2: Zr → Zn_2Zr → IM3 → IM2 → IM1 → $MgZn_2$ + Liquid (Mg60Zn40 at.%);

Diffusion couple #3: Zr → Zn_2Zr → Zn_3Zr → IM1 → $MgZn_2$ + Liquid (Mg60Zn40 at.%);

Diffusion couple #4: Zr → ZnZr → Zn_2Zr → IM3 → IM2 → IM1 → $MgZn_2$ + Liquid (Mg60Zn40 at.%);

Diffusion couple #5: Zr → Zn_2Zr → Zn_3Zr → IM2 → IM1 → $MgZn_2$ + Liquid (Mg12.5Zn87.5 at.%);

Diffusion couple #6: Zr → ZnZr → Zn_2Zr → Zn_3Zr → $Zn_{39}Zr_5$ → IM4 → $MgZn_2$ + Liquid (Mg12.5Zn87.5 at.%).

It is clear that diffusion couple #1, #2 and #4 followed the same diffusion path. Three ternary compounds were detected in these diffusion couples confirming the results of one another. Equilibria between Zn_2Zr and IM3, IM3 and IM2, IM2 and IM1, IM1 and $MgZn_2$ could be established through these experiments. Zn_3Zr layer was in equilibrium with IM1 in diffusion couple #1, and it was in equilibrium with IM2 in diffusion couple #5. Based on the phase diagram rules, phase equilibrium between Zn_3Zr and IM3 should be established. The Zn_2Zr + Zn_3Zr + IM3, IM3 + IM2 + Zn_3Zr, and IM2 + IM1 + Zn_3Zr three-phase equilibria were established through these diffusion couples. The compositions of the ternary phases detected by EDS in diffusion couple #1 - #6 are summarized in Table 4.8. The compositions of the ternary compounds are consistent among the different diffusion couples. The deviation of the composition was within the error range of the EDS measurements (3 at.%). IM1 and IM2 ternary compounds have substitutional solid solubilities that Mg is substituted by Zr at constant Zn concentration (66 at.%). The homogeneity range of IM1 and IM2 are $Mg_{(23\text{-}25)}Zn_{66}Zr_{(8\text{-}11)}$ and $Mg_{(15\text{-}16)}Zn_{66}Zr_{(18\text{-}19),}$ respectively. No solid solubility of IM3 was observed in the diffusion couples, and the composition of IM3 compound was determined as $Mg_{10}Zn_{66}Zr_{24.}$ IM4 was

detected by EDS measurements in diffusion couple #6. EDS line scan results showed that Mg atoms were substituted by both Zr and Zn atoms. The homogeneity range of IM4 was $Mg_{(7-9)}Zn_{(77-81)}Zr_{(10-15)}$. In addition, the phase equilibria between Zn_3Zr and $Zn_{39}Zr_5$, $Zn_{39}Zr_5$ and IM4, IM4 and $MgZn_2$ were established based on diffusion couple #6 results. The layer of ZnZr was observed only in diffusion couple #1, #4 and #6. The possible reason for that was this layer was too thin to be observed. The possible reason is the kinetic of formation and diffusion of the ZnZr phase is too slow.

Table 4.8 Compositions of the ternary compounds based on diffusion couples analysis.

Diffusion Couple	IM1			IM2			IM3			IM4		
	Composition (at.%)			Composition (at.%)			Composition (at.%)			Composition (at.%)		
	Mg	Zn	Zr	Mg	Zn	Zr	Mg	Zn	Zr	Mg	Zn	Zr
DC1	22- 26	66	8 - 12	16	66	18	10	66	24			
DC2	24- 27	66	7 - 10	15- 17	66	17- 19	10	66	24			
DC3	23- 25	67	8 - 10									
DC4	22- 26	66	8 - 12	14- 16	66	18- 20	11	65	24			
DC5	23- 25	66	9 -11	15- 16	66	18- 19						
DC6										7-9	77-81	10-15

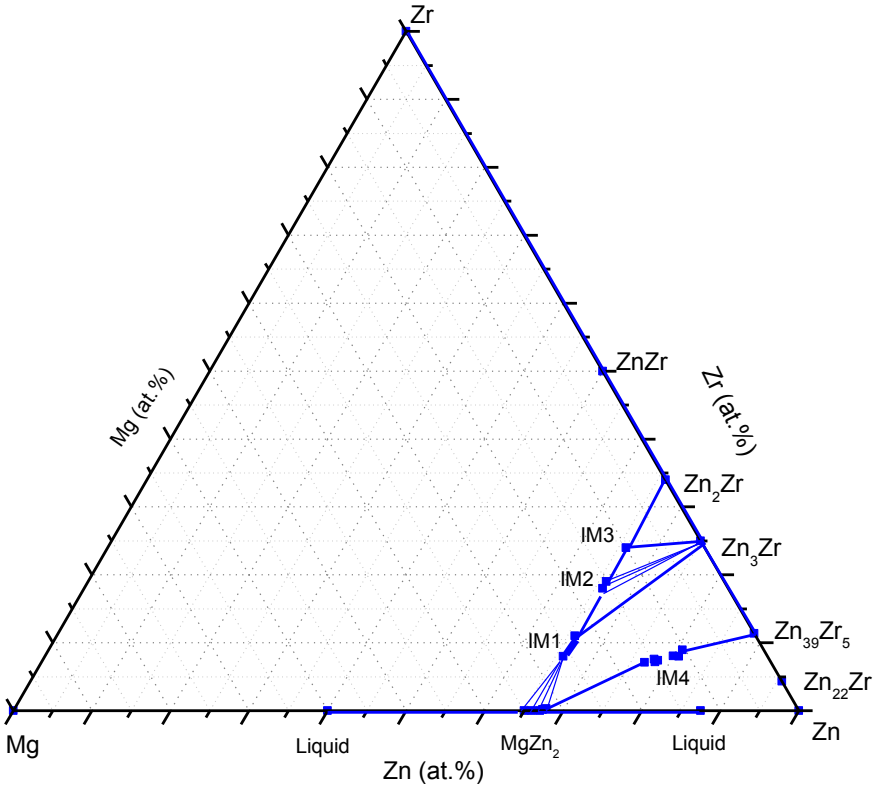

Figure 4.16 Partial phase diagram depicted from diffusion couples.

The compositions of the liquid were taken from the Mg-Zn binary phase diagram [40]. However, the liquid range will be extended to the ternary area, which needed to be verified by key alloys. The phase equilibria in the Mg-rich corner and Zn-rich corners were not clear. Key alloys were designed and prepared to confirm these findings of the diffusion couples and to identify other regions in this system.

4. 2 Experimental investigation through key alloys

4. 2. 1 IM1, IM2 and IM3 ternary compounds study

4. 2. 1. 1 IM1, IM2 and IM3 ternary compounds phase transformations study

Four ternary compounds, namely: IM1, IM2, IM3 and IM4 were determined by diffusion couples experiments. The key alloys No. 1-3 were prepared to verify the formation of the ternary compounds IM1, IM2 and IM3, and the phase equilibria in the Mg - $MgZn_2$ - Zn_2Zr as shown in Figure 4.17 (d). The key alloys were annealed at 450^{o}C for 4 weeks, and the backscattered electron images of these key alloys are presented in Figure 4.17 (a) - (c). SEM coupled with EDS was used to determine the observed phases. The actual chemical compositions of the key alloys were identified by ICP tests and confirmed by EDS area analysis. The actual chemical compositions and the corresponding phases of the key alloys are listed in Table 4.9. In these key alloys, $MgZn_2$ was found in equilibrium with IM1, IM2 and IM3. As shown in Figure 4.17 (d), this phase relation results in crossing tie lines. The possible reason for the crossing tie lines is that the key alloys could not reach equilibrium, because of the slow formation kinetics of IM1, IM2 and IM3. Another assumption is that IM1, IM2 and IM3 are only compositions of one extended solid solution between $MgZn_2$ and Zn_2Zr. However, this assumption cannot be adopted, because clear boundaries between IM1, IM2 and IM3 were observed in diffusion couples #1, #2 and #4, which indicated that they are three different ternary compounds. This point will be tackled further using key alloy No. 4. In addition, Mg_2Zn_3 was observed at the edge of the $MgZn_2$ grains. Liquid formed in these alloys at 450^{o}C, and the Mg_2Zn_3 formed because of the diffusion during liquid solidification. This point will be tackled further using key alloy No. 5.

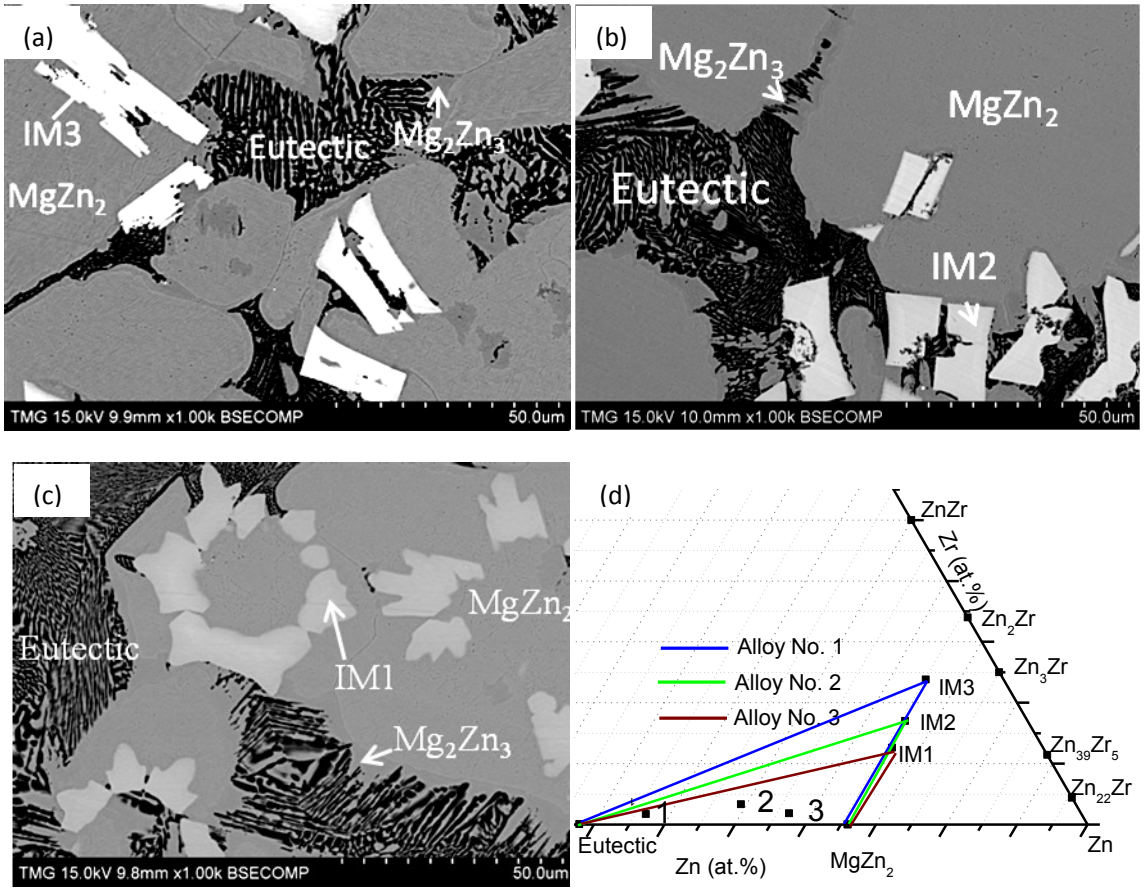

Figure 4.17 (a) SEM micrograph of key alloy No. 1; (b) SEM micrograph of key alloy No. 2; (c) SEM micrograph of key alloy No. 3; (d) Phase equilibria depicted from the key alloys.

Table 4.9 List of key alloys No. 1-3.

Sample Number	Actual composition (at.%)			EDS composition (at.%)			Corresponding Phases
	Mg	Zn	Zr	Mg	Zn	Zr	
1	61.74	36.54	1.72	11	65	24	IM3
				37	63	0	$MgZn_2$
				40	60	0	Mg_2Zn_3
				70	30	<1	Eutectic
2	47.46	49.25	3.29	18	65	17	IM2
				36	64	0	$MgZn_2$
				40	60	0	Mg_2Zn_3
				73	27	<1	Eutectic
3	41.37	56.77	1.86	22	66	12	IM1
				35	65	0	$MgZn_2$
				40	60	0	Mg_2Zn_3
				77	23	<1	Eutectic

From the phase analysis above, it can be seen that IM1, IM2 and IM3 have the same Zn concentration, which may suggest that these phases could be a ternary solid solution extending from $MgZn_2$. Key alloy No. 4 (Mg60.5Zn36.4Zr3.1 at.%) was prepared to provide a better understanding of the phase relationships with the target composition. Key alloy No. 4 was annealed at 450^{o}C for 1 week. The backscattered electron images of this key alloy are demonstrated in Figure 4.18. The as-cast sample, shown in the Figure 4.18 (a), contained IM3, Mg_2Zn_3 and Mg + Mg_2Zn_3 eutectic. Figure 4.18 (b) and (c) present the same key sample after 1 week of annealing at 450^{o}C. According to the Gibbs' phase rule ($F = C - P + 2$), maximum three phases can be detected in the equilibrium samples. Although the microstructure of this sample changed dramatically after annealing, it is still not in equilibrium. This could be attributed to the short annealing time, which was not sufficient for the phase transformation being observed in this sample. After 1 week annealing at 450^{o}C, IM3 phase is decomposing, and IM1 is forming

instead. Between IM3 and IM1, there is another layer which is recognized as IM2. Therefore, the clear grain boundaries between IM1, IM2 and IM3 compounds confirmed that three ternary compounds form between the Zn_2Zr and $MgZn_2$ binary phases. The results showed good consistency with the results obtained from diffusion couples. Since IM1, IM2 and IM3 are determined as three ternary compounds, some samples of the key alloys 1, 2, 3 were not in equilibrium after 4 weeks annealing. Therefore, the phase relations and triangulations will be different from what is presented in Figure 4.17 (d) as will be discussed below.

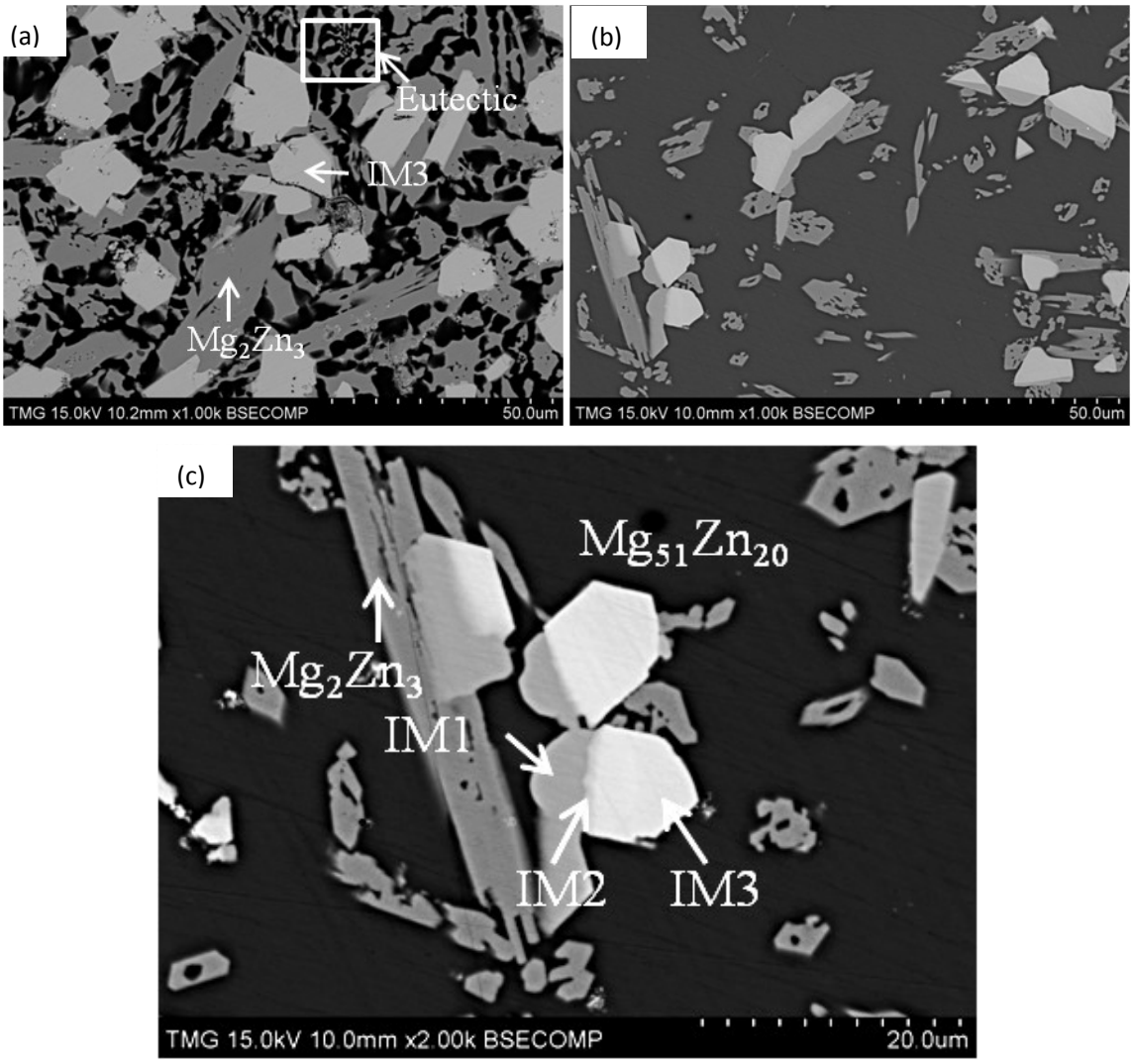

Figure 4.18 SEM micrographs of sample No. 4 (a) As-cast; (b), (c) annealed for 1 week at 450°C.

To study the phase transformations of the IM1, IM2 and IM3 ternary compounds and to solve the crossing tie lines problem, new key alloys (No. 5 and No. 6) were prepared and annealed in 2 steps instead of one. The first step involves heating the alloys up to 450^{o}C and holding them for 2 weeks. Then they were analysed using SEM and XRD. The second step involves annealing the same alloys for 2 more weeks at 450^{o}C, then analyzing them using SEM and XRD. The backscattered images of key alloy No. 5 (Mg42.16Zn53.52Zr4.32 at.%) are shown in Figure 4.19. Figure 4.19 (a) shows the SEM 4.19 (b) and (c) demonstrate the microstructures of the same sample (Mg42.16Zn53.52Zr4.32 at.%) after 2 weeks annealing at 450^{o}C. $MgZn_2$, IM2 phases and eutectic structure of Mg + $MgZn_2$ were detected by EDS spot analysis. During annealing, Mg_2Zn_3 phase decomposed according to the peritectic reaction: $Mg_2Zn_3 \leftrightarrow L + MgZn_2$ (410^{o}C) into $MgZn_2$ and liquid. IM3 phase transformed creating IM2 phase. If the cooling rate is slow, the liquid will form Mg_2Zn_3 and $Mg_{12}Zn_{13}$ through two peritectic reactions: L + ($MgZn_2$) $\leftrightarrow$ Mg_2Zn_3 (410^{o}C), L + $Mg_2Zn_3 \leftrightarrow Mg_{12}Zn_{13}$ (347^{o}C). However, the liquid formed the eutectic structure of Mg + $MgZn_2$, due to quenching. In addition, Mg_2Zn_3 was observed at the edge of the $MgZn_2$ grains. It formed by diffusion during liquid solidification. It was expected that a very thin layer of $Mg_{12}Zn_{13}$ also forms at the edge of Mg_2Zn_3. EDS area analysis on the eutectic structure and Mg_2Zn_3 phase were used to obtain the composition of liquid. The composition was estimated as Mg71Zn29 at.% and the amount of Zr was less than 1 at.%. After 4 weeks annealing at 450^{o}C, the key alloy (Mg28.51Zn66.99Zr4.5 at.%) achieved equilibrium containing $MgZn_2$ and IM1. Therefore, the IM2 was not a stable phase in this key alloy. The liquid, however, evaporated and left porosity as shown in Figure 4.19 (d). The composition of the key alloy No. 5 did not change after 2 weeks annealing, indicates that the liquid evaporation is not a fast process. Even after 4 weeks annealing, the composition of the sample shifted but it was still in the same triangulation, therefore, the three-phase equilibrium of $MgZn_2$ + IM1 + Liquid can be determined because only liquid evaporated during annealing. In addition, the three-phase equilibrium of $MgZn_2$ + IM1 + Liquid can be supported by key alloy No. 3 which is annealed at 450^{o}C for 4 weeks, because

alloy No. 3 and No. 5 are in the same triangluation. The composition of liquid can be obtained from key alloy No. 3. The composition was estimated as Mg70Zn30 at.% and the amount of Zr was less than 1 at.%. The phase relationships could be inferred from alloy No. 5 in different conditions, and they are shown in Figure 4.20. Three phases of Mg + IM3 + Mg_2Zn_3 were observed in the as-cast alloy. $MgZn_2$ + IM2 + Liquid were determined in the annealed alloy after 2 weeks annealing at 450°C. The three-phase equilibrium of $MgZn_2$ + IM1 + Liquid is determined in the sample annealed for 4 weeks.

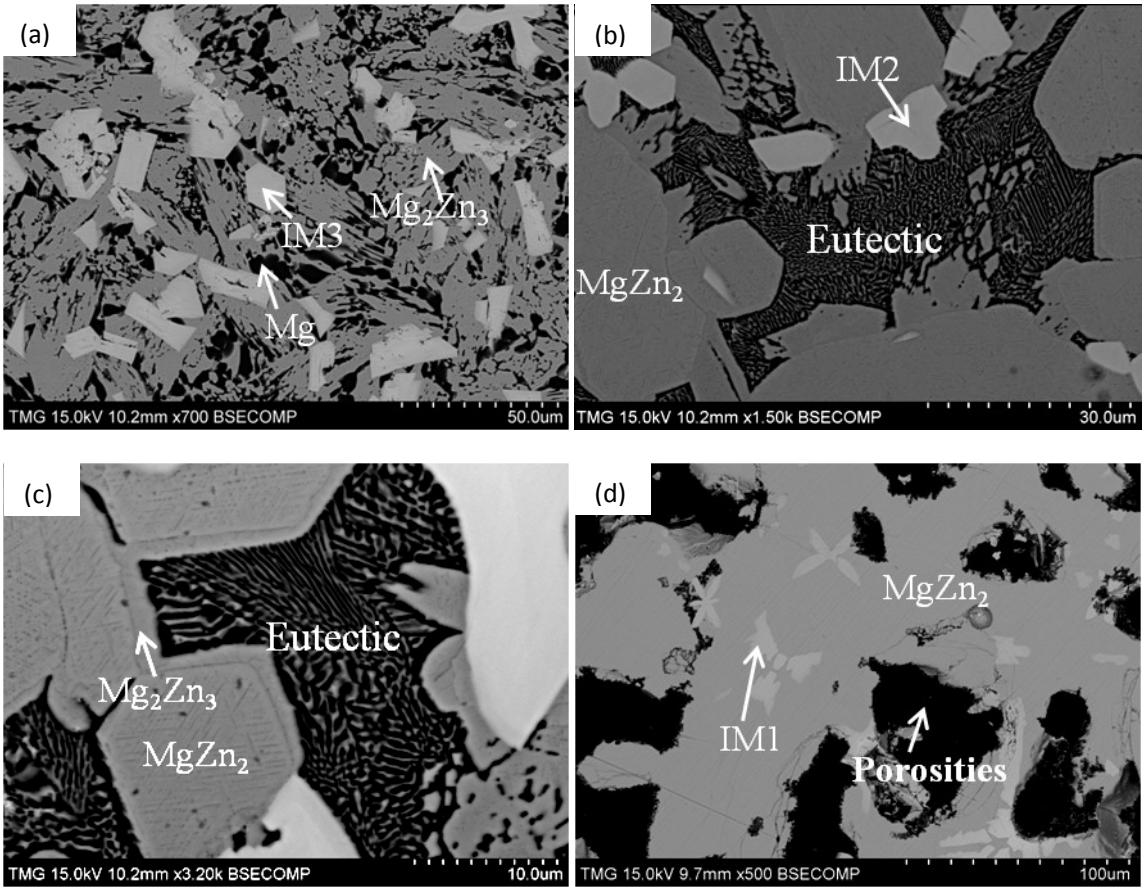

Figure 4.19 SEM micrographs of sample No. 5 (a) as-cast; (b), (c) annealed for 2 weeks at 450°C; (d) annealed for 4 weeks at 450°C.

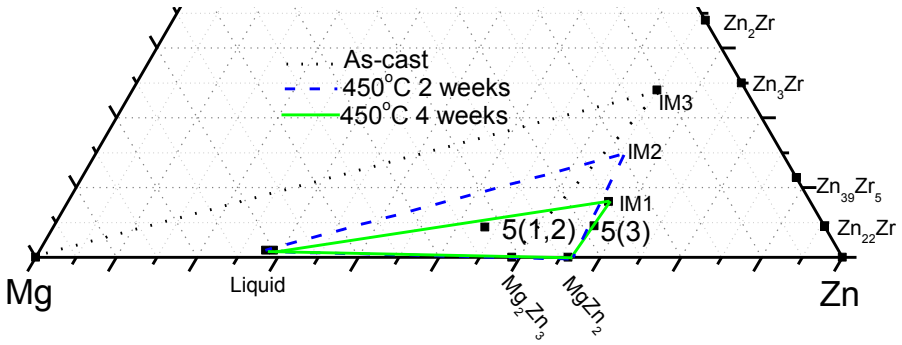

Figure 4.20 Phase relationships of key alloy No. 5 in as-cast, 2 weeks annealing and 4 weeks annealing conditions. The actual composition of the key alloy No. 5 in as-cast and 2 weeks annealing conditions is shown on the diagram and labeled as 5 (1, 2). The actual composition of the key alloy No. 5 at 4 weeks annealing condition is shown on the diagram and labeled as 5 (3).

The chemical compositions and the corresponding constituent phases of the key alloy No. 5 at each annealing stages are listed in Table 4.10. The composition of IM2 after 2 weeks annealing was $Mg_{20}Zn_{65}Zr_{15}$. This composition was reported in the literature [62] as $(Mg,Zr)Zn_2$ ($Mg_{17.54}Zn_{67.11}Zr_{15.35}$). It is highly probable that the key alloy in the literature was not equilibriated, because it was annealed only 15 days at 345°C, which proved to be insufficient in the current study. The current results confirm that key alloys No. 3 and No. 5 have reached equilibrium, whereas key alloys No. 1 and No. 2 did not. The three-phase equilibrium in key alloy No. 5 is $MgZn_2$+IM1+Liquid.

Table 4.10 Actual composition and corresponding phases of key alloy No. 5

Annealing condition	Actual composition (at.%)			EDS composition (at.%)			Corresponding Phases
	Mg	Zn	Zr	Mg	Zn	Zr	
As-cast	42.16	53.52	4.32	11	65	24	IM3
				40	60	0	Mg_2Zn_3
				100	0	0	Mg
450°C 2weeks	42.16	53.52	4.32	73	27	<1	Eutectic
				37	63	0	$MgZn_2$
				20	65	15	IM2
				41	59	0	Mg_2Zn_3
450°C 4weeks	28.51	66.99	4.50	25	67	8	IM1
				37	63	0	$MgZn_2$

Key alloy No. 6 (Mg75.52Zn22.59Zr1.89 at.%) was annealed at 450°C in two steps the same as key alloy No. 5. The backscattered images of this key alloy are shown in Figure 4.21. Figure 4.21 (a) represents the micrograph of the as-cast sample No. 6. Mg, Mg_2Zn_3, IM3, and Zn_2Zr phases were identified by EDS spot analysis. Around 3 at.% of Zr was substituted by Mg in the Zn_2(Zr, Mg) solid solution. A peritectic morphology containing Zn_2Zr as a primary phase and surrounded by the peritectic phase IM3 was observed. Zn_2Zr is decomposing to form IM3. However, the process was not completed during melting due to the short time. Meanwhile, Mg and Mg_2Zn_3 were observed in the as-cast alloy. Although Mg_2Zn_3 is not stable at 450°C, it forms in the as-cast conditions. Figure 4.21 (b) represents the sample after 2 weeks annealing at 450°C. Mg, IM2 and eutectic were observed. It was expected that the IM3 phase decomposed creating the IM2 compound, because IM2 is the only phase that contained Zr in Figure 4.21 (b). During the process of rapid quenching in water, partial liquid solidified to eutectic microstructure of Mg and $MgZn_2$. The BSE images of the same sample after 4 weeks annealing are shown in Figure

4.21 (c) and (d). IM1, Mg and eutectic were observed in the SEM images. For the Mg solid solution, it dissolves around 4 at.% Zn. With longer annealing, IM2 decomposed to form IM1. This key sample was finally brought to equilibrium after 4 weeks annealing, because the metastable phases were not observed and the Mg + IM1 + Liquid three-phase equilibrium has been reached. The composition of the eutectic area identified by EDS area mapping EDS was $Mg_{72}Zn_{28}$ at.%. The Zr amount in the eutectic composition was less than 1 at.%.

The actual chemical compositions and the corresponding constituent phases of the key alloys are listed in Table 4.11. The phase relationships could be inferred from alloy No. 6 in different conditions and they are shown in Figure 4.22. Four phases of Mg + IM3 + Zn_2Zr + Mg_2Zn_3 were observed in the as-cast alloy. Mg + IM2 + Liquid were determined in the annealed alloy after 2 weeks annealing at 450^{o}C. The three-phase equilibrium of Mg + IM1 + Liquid were determined in the 4 weeks annealing alloy.

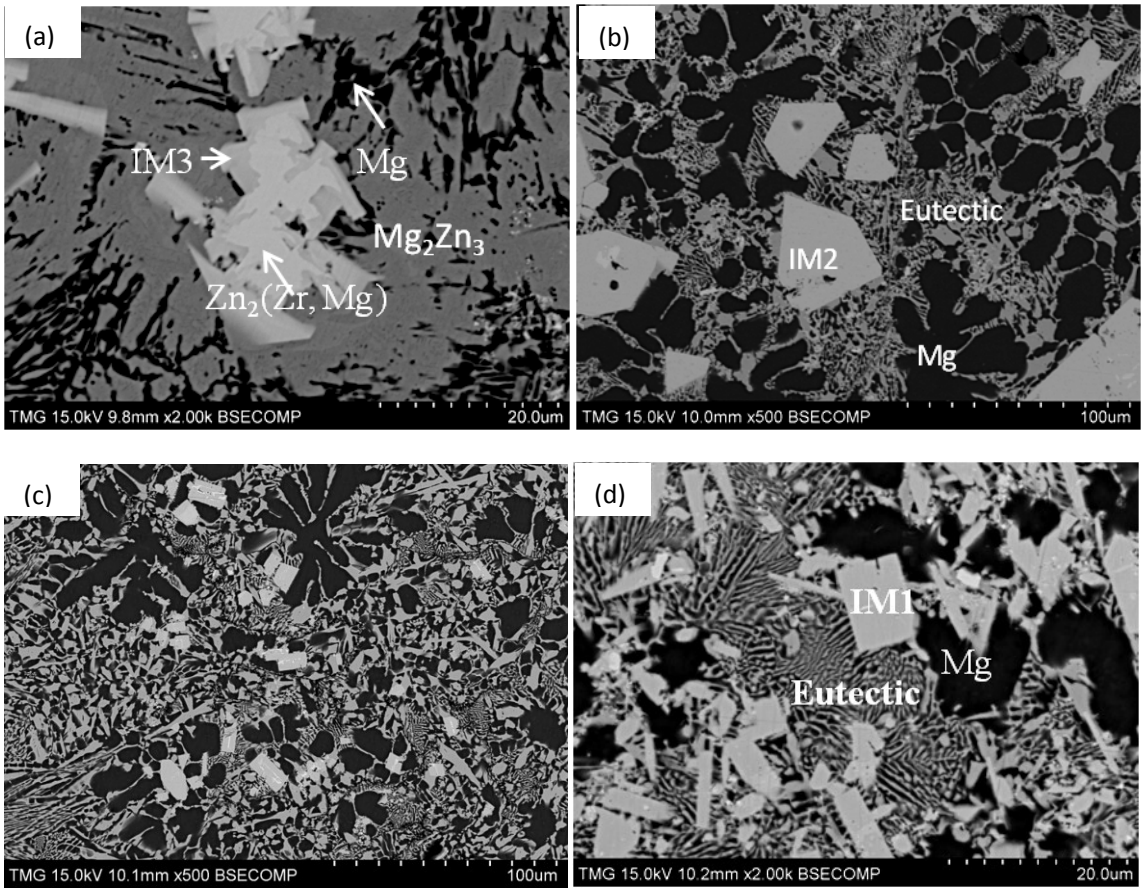

Figure 4.21 SEM micrographs of (a) as-cast sample No. 6; (b) after 2 week annealing at 450°C; (c), (d) after 4 weeks annealing at 450°C.

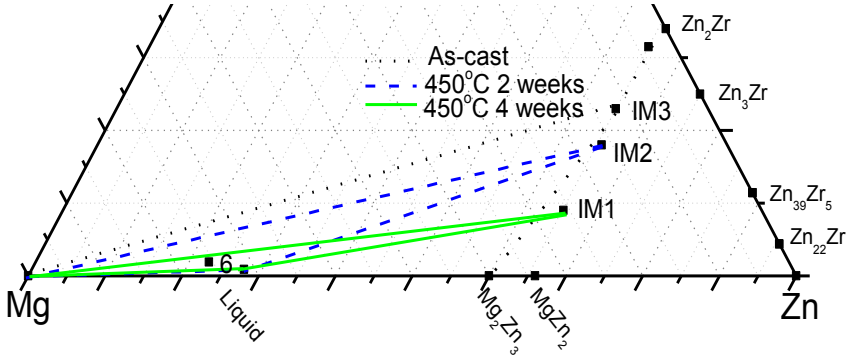

Figure 4.22 Phase relationships of key alloy No. 6 in as-cast, 2 weeks annealing and 4 weeks annealing conditions. The actual composition of the key alloy No.6 is shown on the diagram and labeled as 6.

Table 4.11 Actual composition and corresponding phases of key alloy No. 6

Sample Number	Actual composition (at.%)			EDS composition (at.%)			Corresponding Phases
	Mg	Zn	Zr	Mg	Zn	Zr	
As-cast	75.52	22.59	1.89	3	65	32	$Zn_2(Zr,Mg)$
				100	<1	<1	Mg
				40	60	0	Mg_2Zn_3
				11	65	24	IM3
450°C 2weeks	75.52	22.59	1.89	16	66	18	IM2
				96	4	0	(Mg)
				64	30	6	Eutectic
450°C 4weeks	75.52	22.59	1.89	26	65	9	IM1
				96	4	0	(Mg)
				72	28	<1	Eutectic

4. 2. 1. 2 IM1, IM2 and IM3 ternary compounds XRD study

IM1, IM2 and IM3 ternary compounds were detected in this system. The XRD data of these ternary compounds were not available in the literature. Alloys No.7-9 were prepared to obtain the crystallographic data of the ternary compounds. The actual compositions were obtained by ICP and the phases were confirmed by EDS and XRD as summarized in Table 4.12.

For crystal structure refinement study of a new compound, a single-phase sample is the best and first choice. However, it is difficult to prepare a single-phase samples for the ternary compounds in the Mg-Zn-Zr system, because of two reasons. Firstly, Mg and Zn evaporated during melting. Thus, the composition shifted from the nominal one. Secondly, as explained in the experimental procedure, it was difficult to prepare homogeneous key alloys with high Zr content. In the present work, a single phase sample of IM1 was successfully prepared after several attempts. The

SEM micrograph of the annealed sample No. 7 ($Mg_{27.25}Zn_{65.12}Zr_{7.63}$ at.%) is presented below in Figure 4.23. The single phase sample was studied by XRD using Rietveld analysis. The XRD pattern of IM1 is illustrated in Figure 4.24 (a). IM1 compound is determined to have the same prototype as $MgZn_2$ with the hexagonal structure and $P6_3/mmc$ space group.

Table 4.12 Actual compositions and corresponding phases of key alloys No. 7-9

Sample Number	Actual composition (at.%)			EDS composition (at.%)			Corresponding Phases	
	Mg	Zn	Zr	Mg	Zn	Zr	By EDS	By XRD
7	27.25	65.12	7.63	27	65	8	IM1	IM1
8	90.97	6.54	2.50	17 97	65 3	18 0	IM2 (Mg)	IM2 (Mg)
9	72.63	19.62	7.76	13 98	64 2	23 0	IM3 (Mg)	IM3 (Mg)

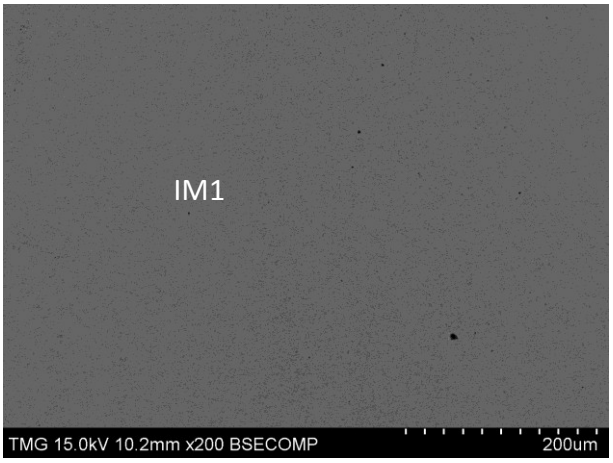

Figure 4.23 SEM micrograph of the key alloy No. 7.

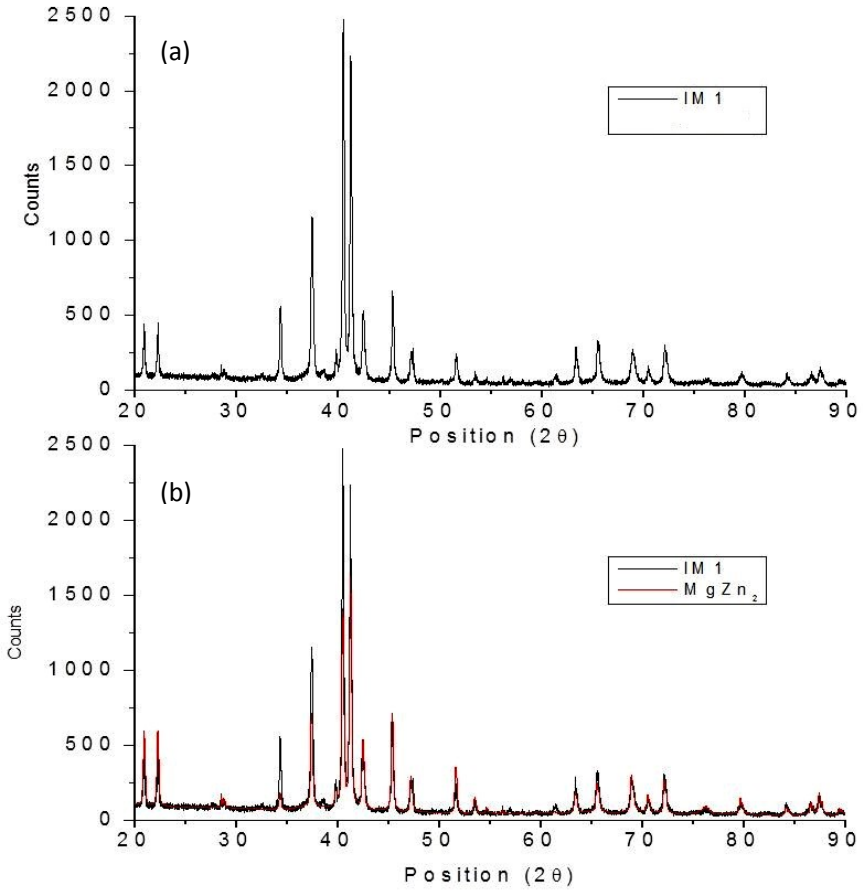

Figure 4.24 (a) XRD pattern of IM1; (b) XRD pattern of IM1 and modified $MgZn_2$ phase.

The XRD patterns of IM1 are very similar to the $MgZn_2$ XRD patterns. By replacing 30% of Mg by Zr, the modified $MgZn_2$ patterns, as shown in Figure 4.24 (b), are perfectly corresponding to IM1 patterns. This substitution did not shift the peaks because there is no large difference in the atomic size between Mg (r=0.16 nm) and Zr (r=0.159 nm) [67]. The calculated chemical composition of IM1 was $Mg_{24}Zn_{66}Zr_{10,}$ which was consistent with the EDS results obtained from the key alloys and diffusion couples.

Although the single-phase IM2 and IM3 alloys were not prepared successfully, two-phase samples No. 8 ($Mg_{90.97}Zn_{6.54}Zr_{2.50}$ at.%) and No. 9 ($Mg_{72.63}Zn_{19.62}Zr_{7.76}$ at.%) containing these

phases were successfully prepared. The micrographs of the equilibrated samples are presented below in Figure 4.25 (a) and (b). SEM coupled with EDS was used to determine the phases and their chemical compositions. Two-phase equilibria of Mg + IM2 and Mg + IM3 were illustrated from key alloys No. 8 and No. 9 respectively. EDS results show that 3 at.% and 2 at.% of Mg in the Mg solid solution was replaced by Zn in No. 8 and No. 9 respectively, which is consistent with the literature [40].

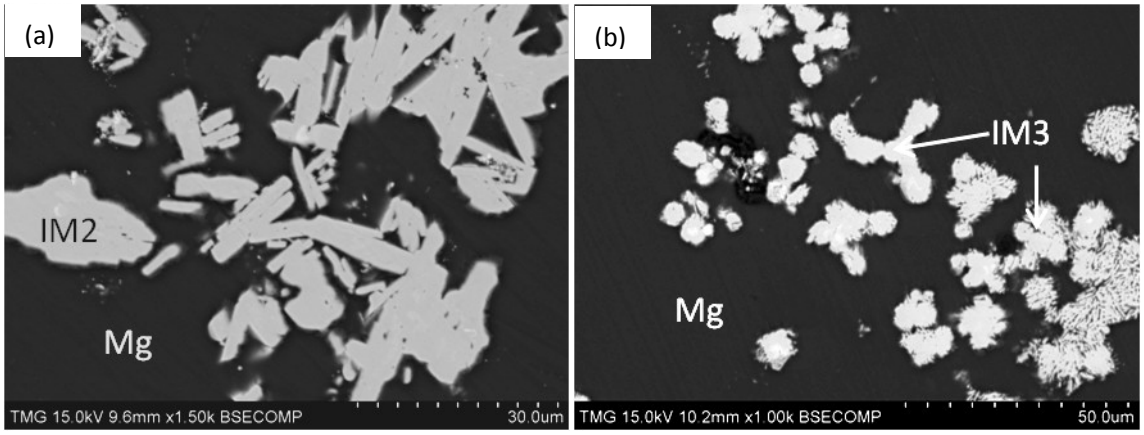

Figure 4.25 (a) SEM micrograph of sample No. 8 after 4 weeks annealing at 450^{o}C; (b) SEM micrograph of sample No. 9 after 4 weeks annealing at 450^{o}C.

The XRD patterns of these samples with identified phases are shown in Figures 4.26 (a) and 4.27 (a). As shown in Figure 4.26 (a), despite Mg and the internal calibration standard Si, it was obvious that another phase was in this sample. Because Mg and IM2 were identified in the EDS analysis, the unknown peaks were determined as IM2 phase. The XRD pattern of the IM2 was shown in Figure 4.26 (b). The crystal structure and prototype of the IM2 have not been determined yet. Studies regarding the crystal structure of the IM2 are still needed in the future work.

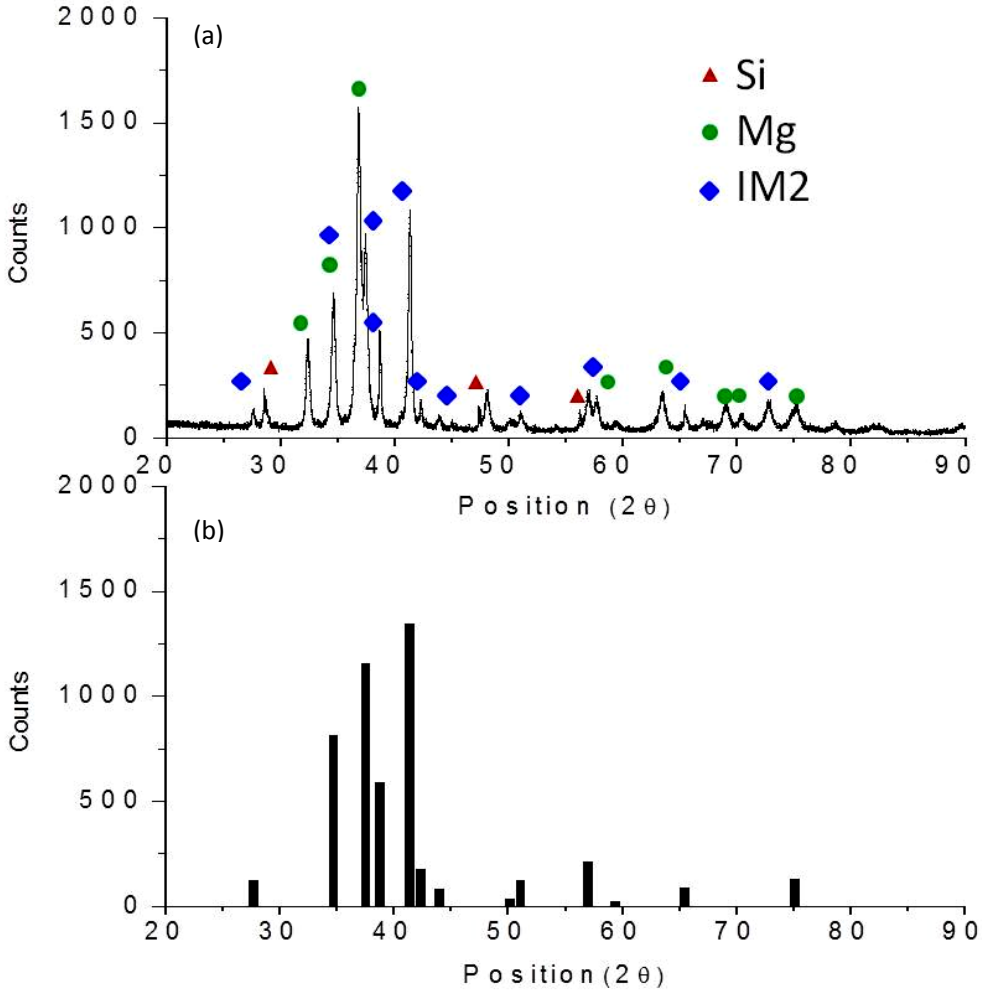

Figure 4.26 (a) XRD pattern of sample No. 8; (b) XRD pattern of IM2.

The XRD pattern of sample No. 9 is presented in Figure 4.27 (a). The peaks of IM3 were identified positively using the same method as sample No. 8. The XRD pattern of IM3 was shown in Figure 4.27 (b). The crystal structure and prototype of the IM3 have not been determined yet. Studies regarding the crystal structure of the IM3 are still needed in the future work.

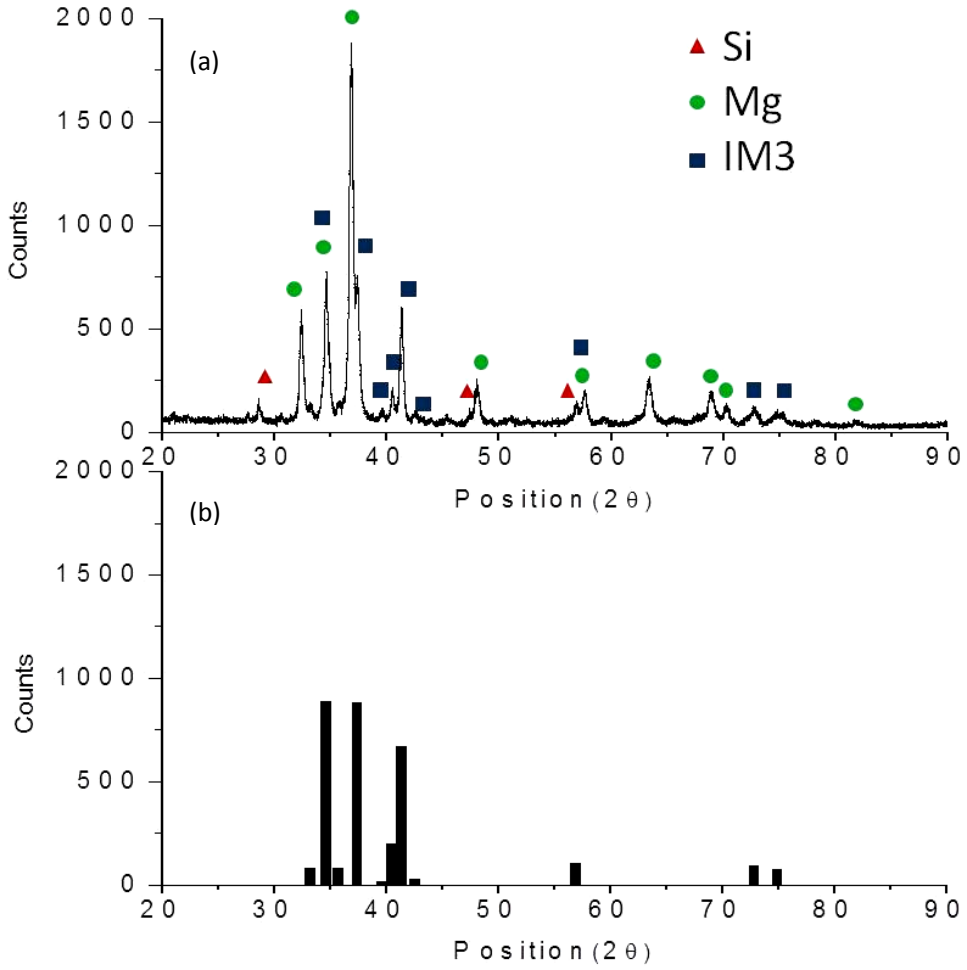

Figure 4.27 (a) XRD pattern of sample No. 9; (b) XRD pattern of IM3.

The crystal structure and prototype of IM1 are determined in this work. The XRD peaks of IM2 and IM3 can be obtained from key alloy No. 8 and No. 9, respectively, although the crystal structure and prototype of the IM2 and IM3 have not been determined, the peaks can be used to analyse the samples in this system. Therefore, the XRD analyses of the key alloys containing IM1, IM2 and IM3 become feasible. Figure 4.28 represents the refined XRD pattern of key alloy No. 5 in two annealing conditions. As shown in 4.28 (a), IM2, $MgZn_2$, Mg_2Zn_3 and Mg were observed in the sample after 2 weeks annealing. Mg and $MgZn_2$ formed the eutectic structure. In the sample annealed for 4 weeks, IM1 and $MgZn_2$ were detected. These results are consistent with the EDS results as shown in Table 4.10.

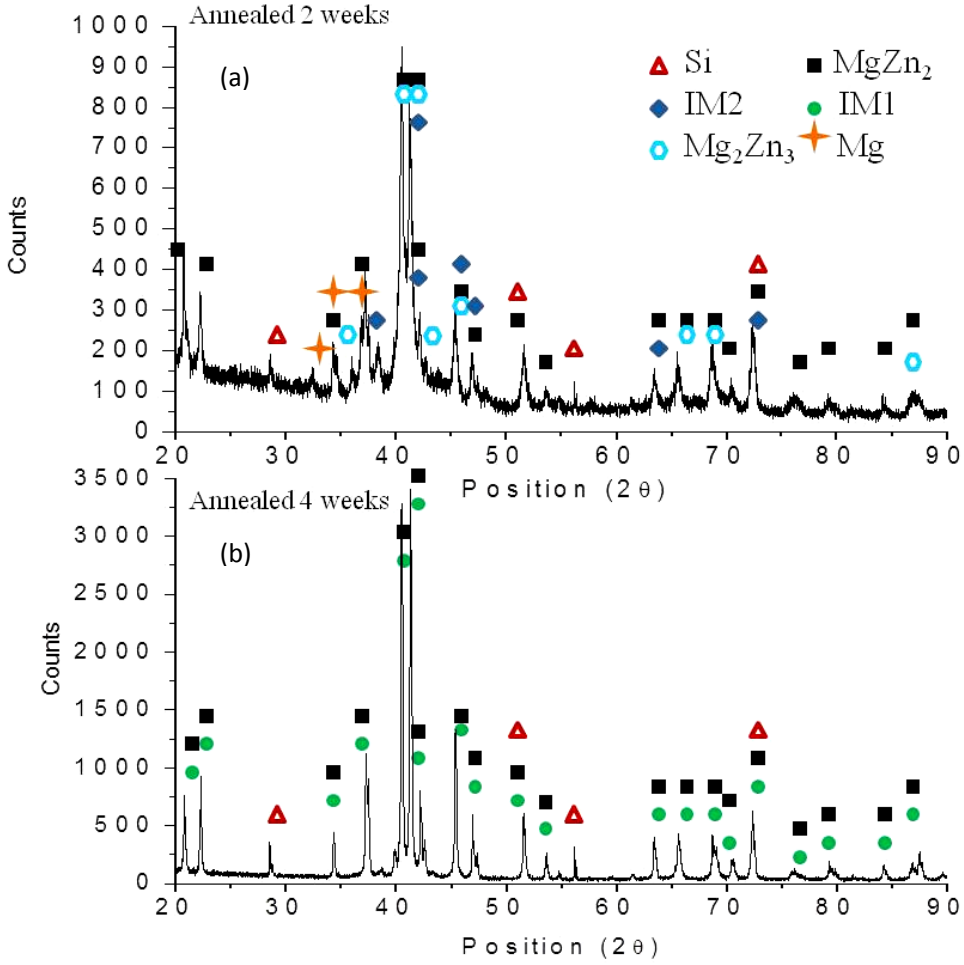

Figure 4.28 XRD results of key alloy No. 5 annealed at 450°C for (a) 2 week and (b) 4 weeks.

The XRD analysis of key alloy No. 6 is presented in Figure 4.29. Figure 4.29 (a) shows the XRD pattern of the sample after 2 weeks annealing. IM2, Mg and $MgZn_2$ were detected in the XRD analysis. As illustrated in Figure 4.29 (b), IM1, Mg and $MgZn_2$ were determined by XRD. Hence, the XRD results confirmed that the IM2 decomposed to IM1 when samples were subjected to long annealing. The existence of $MgZn_2$ indicated that the eutectic was composed of Mg and $MgZn_2$.

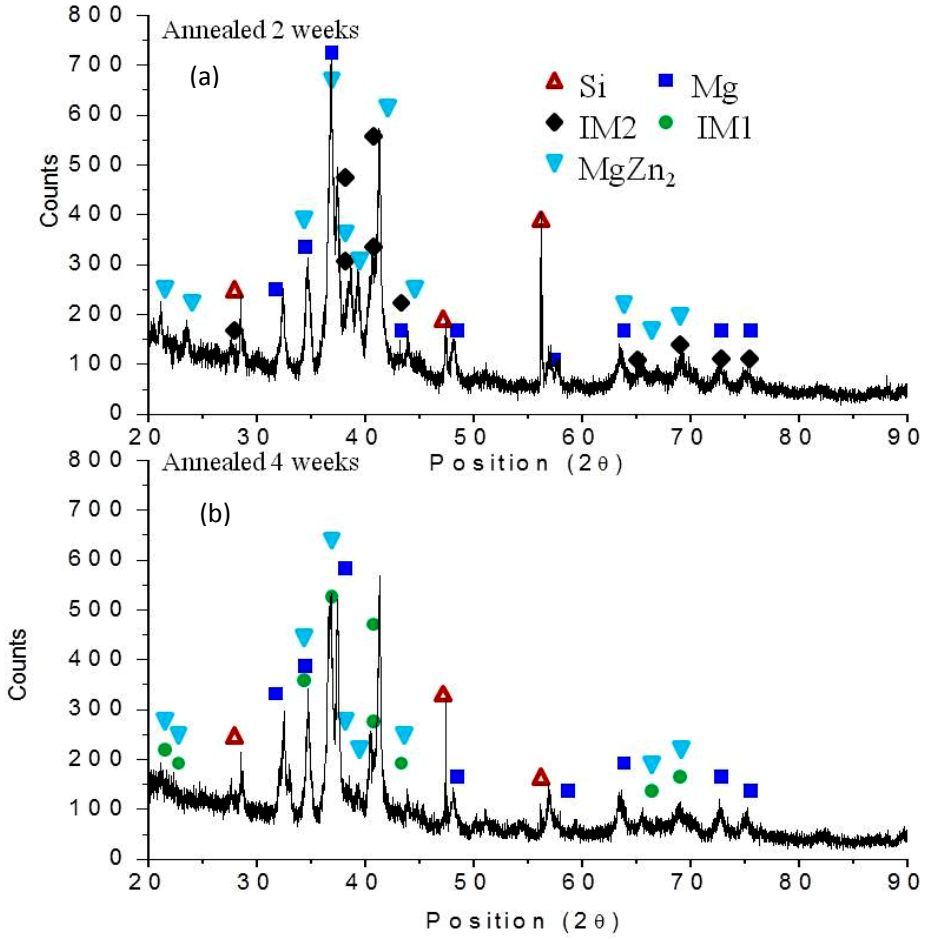

Figure 4.29 XRD results of key alloy No. 6 annealed at 450°C for (a) 2 weeks (b) 4 weeks

4. 2. 2 Other parts in the Mg corner

The SEM micrographs of the annealed key alloys No. 10 (Mg90.97Zn6.54Zr2.50 at.%) and No. 11 (Mg72.63Zn19.62Zr7.76 at.%) are shown in Figure 4.30 (a) and (c) respectively. As shown in Figure 4.30 (a), three-phase equilibrium of Mg + IM2 + IM1 was detected by EDS spot analysis. The solid solubility of Zn in Mg was around 3 at.%. The contrast of Figure 4.30 (a) was increased to distinguish IM1 from IM2. In addition, IM2 was colored in Figure 4.30 (b) for better observation. Another three-phase equilibrium of Mg + ZnZr + Zr, was observed in sample No. 11 as shown in Figure 4.30 (c). The white phase with a square shape is ZnZr, and the white phase

with the irregular shape is Zr. XRD was performed on these two samples, and the XRD patterns of these two samples are shown in Figure 4.31. The XRD results are consistent with the EDS results. The peaks of IM1 and IM2 phases were taken from key alloys No. 7 and No. 8, respectively. The actual compositions of these key alloys obtained by ICP and the experimental results are summarized in Table 4.13.

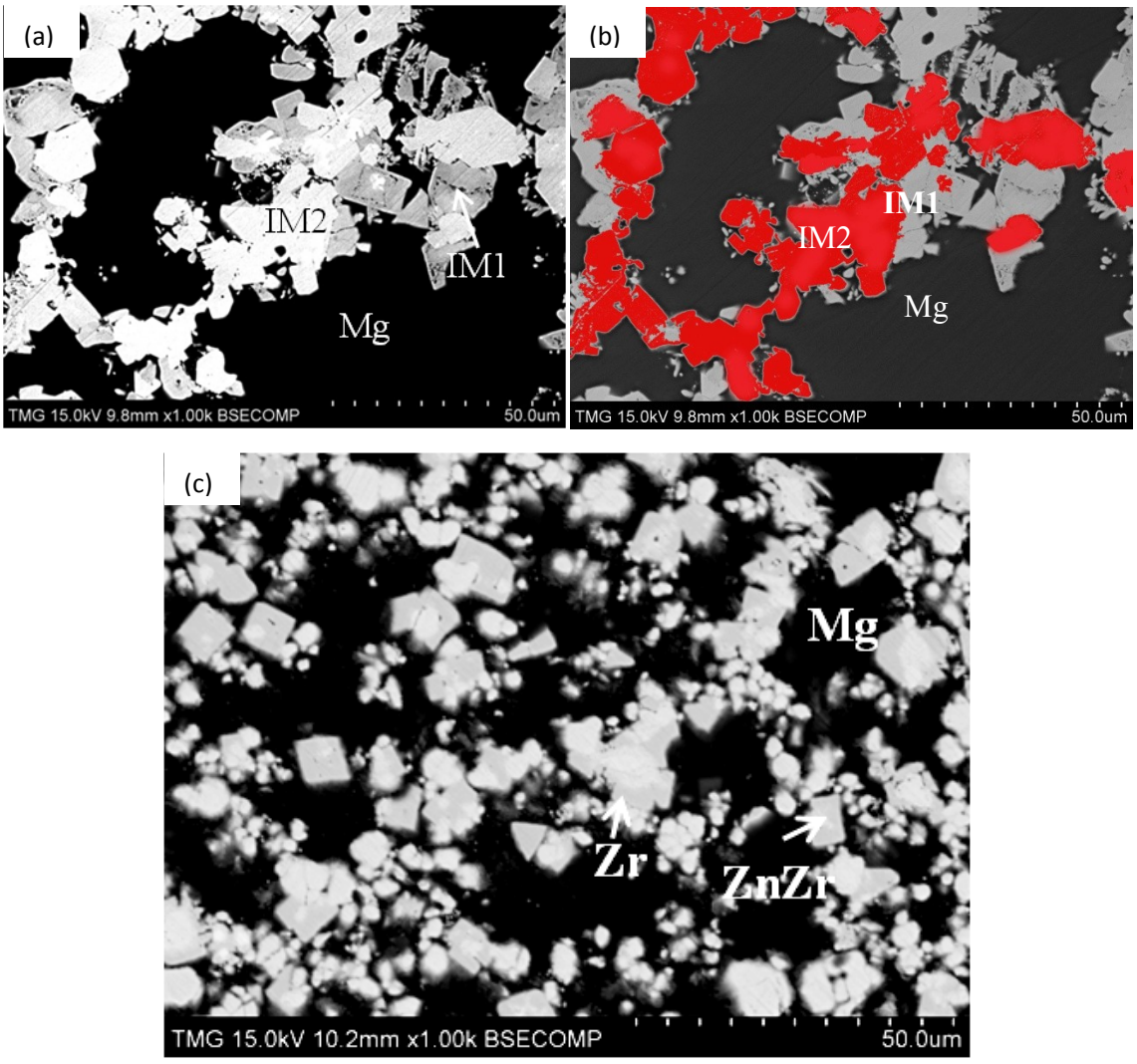

Figure 4.30 (a), (b) SEM micrographs of alloy No. 10 annealed at 450°C for 4 weeks; (c) SEM micrographs of alloy No. 11 annealed at 450°C for 4 weeks.

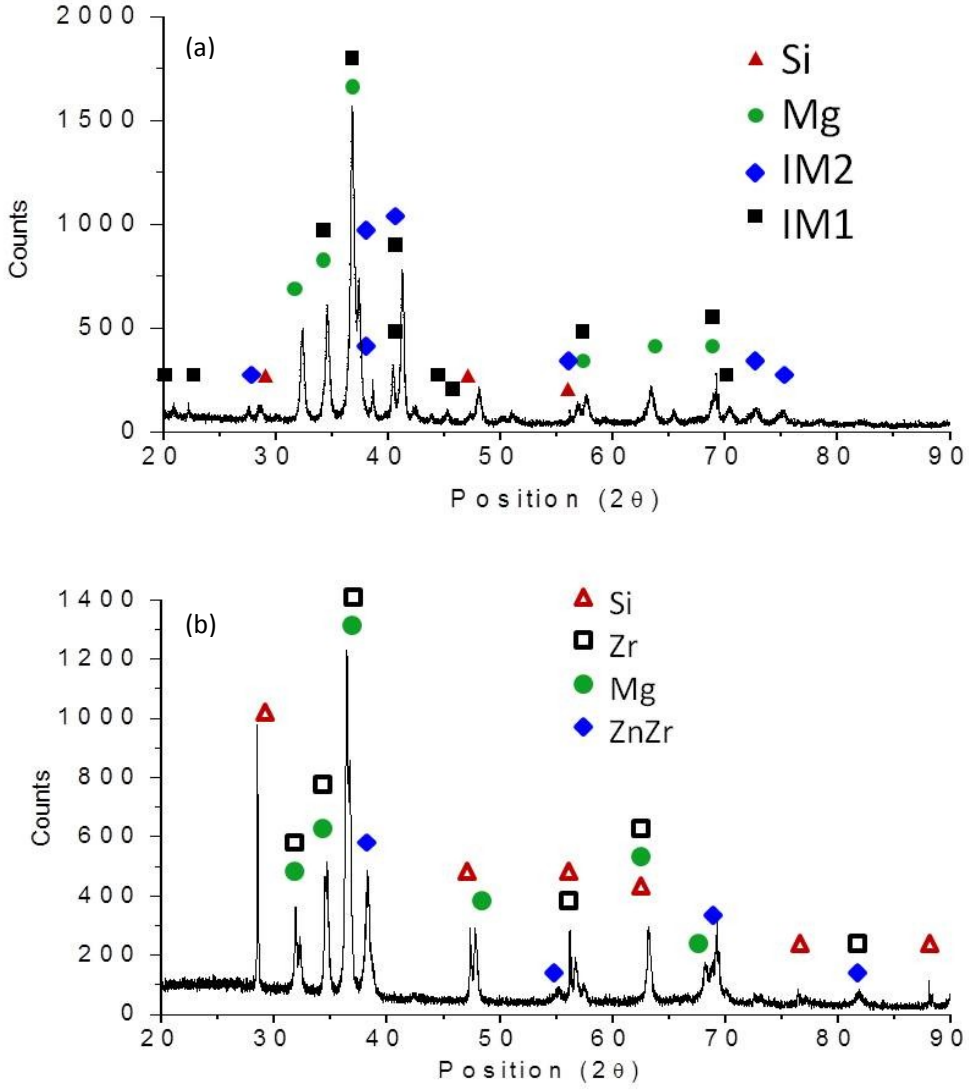

Figure 4.31 (a) XRD pattern of the alloy No. 10, (b) XRD pattern of the alloy No. 11.

Table 4.13 Actual composition and corresponding phases of key alloys No. 10 and No. 11.

Sample Number	Actual composition (at.%)			EDS composition (at.%)			Corresponding Phases	
	Mg	Zn	Zr	Mg	Zn	Zr	By EDS	By XRD
10	90.97	6.54	2.50	16	65	18	IM2	IM2
				24	65	11	IM1	IM1
				97	3	0	(Mg)	(Mg)
11	72.63	19.62	7.76	0	49	51	ZnZr	ZnZr
				0	0	100	Zr	Zr
				98	2	0	(Mg)	(Mg)

A partial isothermal section of the Mg-Zn-Zr system at 450^{o}C is illustrated in Figure 4.32. Key alloys could not be prepared successfully in the Mg + ZnZr + Zn_2Zr and Mg + Zn_2Zr + IM3 regions because the key alloys shifted to another area. In addition, as explained in the experimental procedure chapter, it was difficult to prepare the samples with high Zr concentration. However, the proposed tie line relationships were drawn by the dotted lines based on the phase diagram construction rules. In the Mg-rich part, Mg + Zr + ZnZr, ZnZr + Zn_2Zr + Mg, Zn_2Zr + IM3 + Mg, IM3 + IM2 + Mg, IM2 + IM1 + Mg, IM1 + Mg + Liquid, and Liquid + $MgZn_2$ + IM1 three-phase equilibria are confirmed by the current key alloys results. The liquid was ranging between Mg80Zn20 at.% and Mg60Zn40 at.%, and extended up to around 1 at.% Zr. The homogeneity ranges of IM1, IM2 and IM3 were estimated as $Mg_{(23-26)}Zn_{66}Zr_{(8-11)}$, $Mg_{(15-16)}Zn_{66}Zr_{(18-19)}$ and $Mg_{(10-11)}Zn_{66}Zr_{(23-24)}$, respectively.

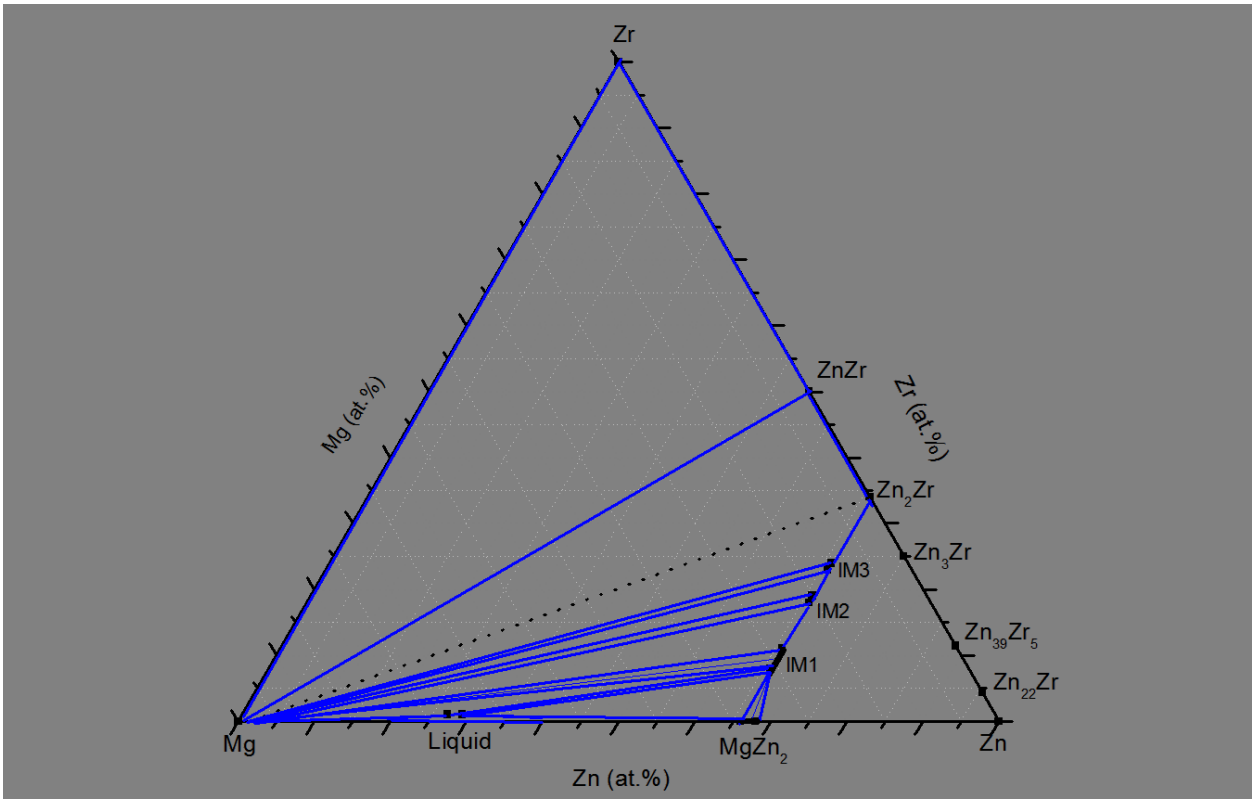

Figure 4.32 A partial phase diagram of the Mg-Zn-Zr system at 450°C.

4.2.3 Key alloys in the Zn-rich part

Three-phase equilibria of Zn_2Zr + Zn_3Zr + IM3, Zn_3Zr + IM3 + IM2 and Zn_3Zr + IM2 + IM1 were determined from the diffusion couples results. In addition, the ternary compound of IM4 was detected in diffusion couple #6 in the Zn rich area. Key alloys No. 12 - No. 16 were prepared to verify the results of diffusion couples including the presence of IM4 and to identify the other part in the Zn-rich part.

4.2.3.1 IM4 ternary compound XRD study

Since no XRD data was available in the literature, a single phase sample No. 12 ($Mg_{8.6}Zn_{84}Zr_{7.4}$ at.%), which only contains IM4 was prepared. The XRD pattern of IM4 was obtained in Figure

4.33. The crystal structure and prototype of the IM4 have not been determined yet. Studies regarding the crystal structure of the IM4 are still needed in the future work.

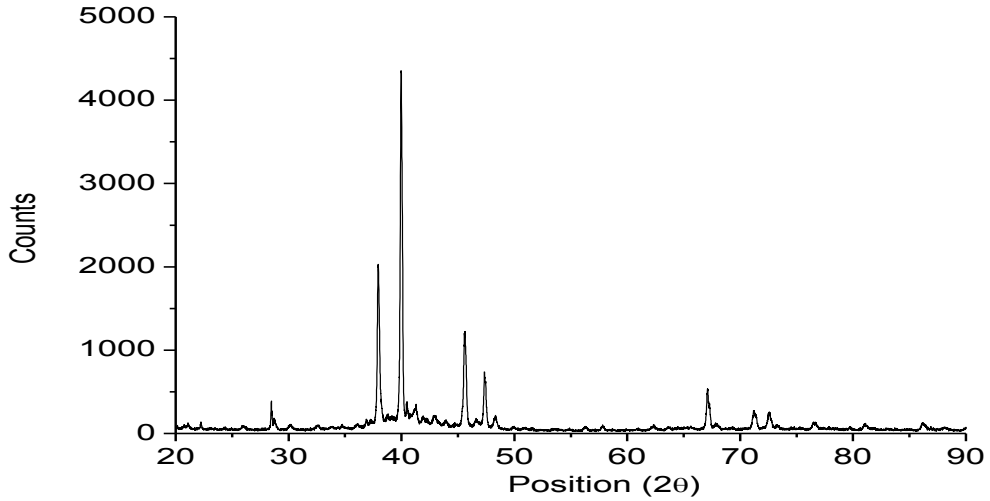

Figure 4.33 XRD pattern of IM4 obtained from key alloy No. 12 (annealed at 450°C for 4 weeks).

4. 2. 3. 2 Zn-rich area

The composition of IM4 in alloy No. 12 is $Mg_{8.6}Zn_{84}Zr_{7.4}$ at.%. IM4 was found to have solid solubility in the diffusion couples #6. Four key alloys were selected to study the phase relations in the Zn-rich area and the solid solubility range of IM4. The actual compositions of the key alloys obtained by ICP and the phases confirmed by EDS and XRD are summarized in Table 4.14. The micrograph images of the equilibrated alloys were presented in Figure 4.34.

The as-cast sample No. 13 (Mg17.38Zn80.12Zr2.50 at.%) along with the equilibrated sample after 2 days annealing at 450°C are demonstrated in Figure 4.34 (a) and (b). $Zn_{39}Zr_5$, IM4, $MgZn_2$ and eutectic of $MgZn_2$ and Zn were observed in the as-cast sample as shown in Figure 4.34 (a). After 2 days annealing at 450°C, IM4, $MgZn_2$ and the $MgZn_2$ + Zn eutectic were detected by EDS spot analysis in Figure 4.34 (b). The annealing time was 2 days to avoid liquid

evaporation. The binary $Zn_{39}Zn_5$ phase was observed in the as-cast sample, and it was not observed in the sample after 2 weeks annealing at 450°C. The $Zn_{39}Zr_5$ phase is a metastable phase for this key alloy having $MgZn_2$ + IM4 + liquid three-phase equilibria. $Zn_{39}Zr_5$ was formed at around 750°C during melting and it did not decompose because the melting time in the arc melting furnace was short. After annealing, the $Zn_{39}Zn_5$ phase transforms to IM4. $MgZn_2$ was a stable phase in the key alloy. Zn melted to liquid and formed eutectic structure with $MgZn_2$ upon quenching. The composition of IM4 was identified as $Mg_{11}Zn_{84}Zr_{5,}$ and the liquid composition was determined as $Mg_{13}Zn_{87}$ by EDS area analysis. The Zr amount in the eutectic composition was less than 1 at.%. The three-phase equilibrium of $MgZn_2$ + IM4 + liquid was determined.

Figure 4.34 (c) shows the two-phase equilibrium of $MgZn_2$ and IM4 in key alloy No. 14 (Mg20.18Zn75.15Zr4.67 at.%). The composition of the IM4 was determined as $Mg_{11}Zn_{82}Zr_7$. The black spots were porosities, which were caused by liquid evaporation.

Figure 4.34 (d) represents the three-phase key alloy No. 15 (Mg22.64Zn71.09Zr6.27 at.%) after 4 weeks annealing at 450°C. IM4, IM1 and $MgZn_2$ phases were observed in the micrograph. The composition of IM4 was determined as $Mg_{13}Zn_{79}Zr_8$. The composition of IM1 was detected as $Mg_{23}Zn_{67}Zr_{10}$. The three-phase equilibrium of $MgZn_2$ + IM4 + IM1 was determined.

After 4 weeks annealing, sample No. 16 (Mg4.45Zn88.30Zr7.25 at.%) was brought to equilibrium. As shown in Figure 4.34 (e), $Zn_{39}Zr_5$, $Zn_{22}Zr$ and IM4 demonstrated three-phase equilibrium. The composition of IM4 was detected as $Mg_9Zn_{85}Zr_6$.

Based on these four key alloys, the phase relationships in the Zn-rich part are presented in Figure 4.31(f). The homogeneity range of the ternary compound IM4 was obtained from the EDS results of key alloys No. 13-16 and diffusion couples #6. IM4 has a homogeneity range of 9 - 13 at.% Mg, 79 - 87 at.% Zn and 5 - 8 at.% Zr.

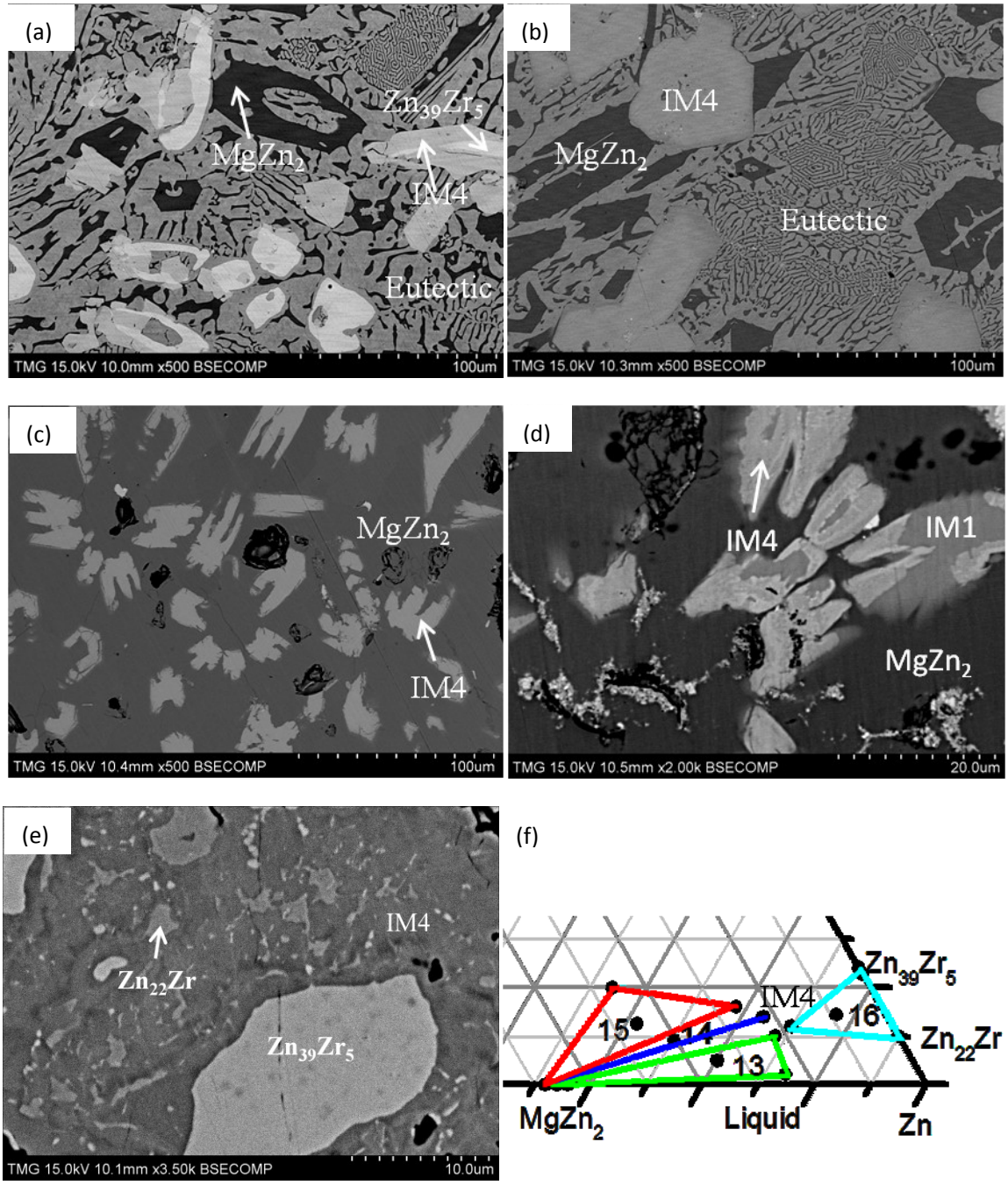

Figure 4.34 SEM micrographs of (a) as-cast sample No. 13; (b) sample No. 13 after 2 days annealing at 450°C; (c) sample No. 14 after 2 weeks annealing at 450°C; (d) sample No. 15 after 4 weeks annealing at 450°C;(e) sample No. 16 after 4 weeks annealing at 450°C; (f) partial phase diagram in the Zn-corner of the Mg-Zn-Zr system at 450°C.

Table 4.14 Actual composition and corresponding phases of key alloys No. 13-16

Sample Number	Actual composition (at.%)			EDS composition (at.%)			Corresponding Phases	
	Mg	Zn	Zr	Mg	Zn	Zr	By EDS	By XRD
13	17.38	80.12	2.50	11	84	5	IM4	IM4
				13	87	<1	Liquid	Liquid
				33	67	0	$MgZn_2$	$MgZn_2$
14	20.18	75.15	4.67	11	82	7	IM4	IM4
				33	67	0	$MgZn_2$	$MgZn_2$
15	22.64	71.09	6.27	23	67	10	IM1	IM1
				13	79	8	IM4	IM4
				32	68	0	$MgZn_2$	$MgZn_2$
16	4.45	88.30	7.25	0	88	12	$Zn_{39}Zr_5$	$Zn_{39}Zr_5$
				9	85	6	IM4	IM4
				0	95	5	$Zn_{22}Zr$	$Zn_{22}Zr$

The X-ray diffraction was performed on the key alloys in the Zn-rich part. The full pattern refinement along the identified phases in sample No. 14 and 15 are illustrated in Figures 4.35 and 4.36 respectively. The XRD results are consistent with the SEM results which are shown in Table 4.14. In key alloy No. 14, $MgZn_2$ and IM4 phases were detected in the XRD results. The peaks of IM4 in key alloy No. 14 matched well with the key alloy No. 12 which contained IM4 as a single phase. $MgZn_2$, IM1 and IM4 phases were detected in key alloy No. 15, which is consistent with the SEM results.

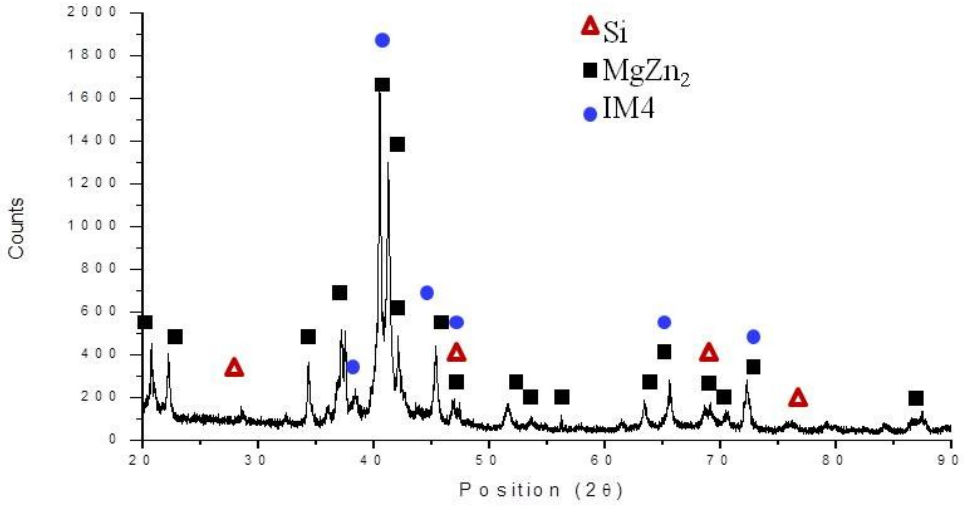

Figure 4.35 XRD results of sample No. 14 annealed at 450°C for 4 weeks.

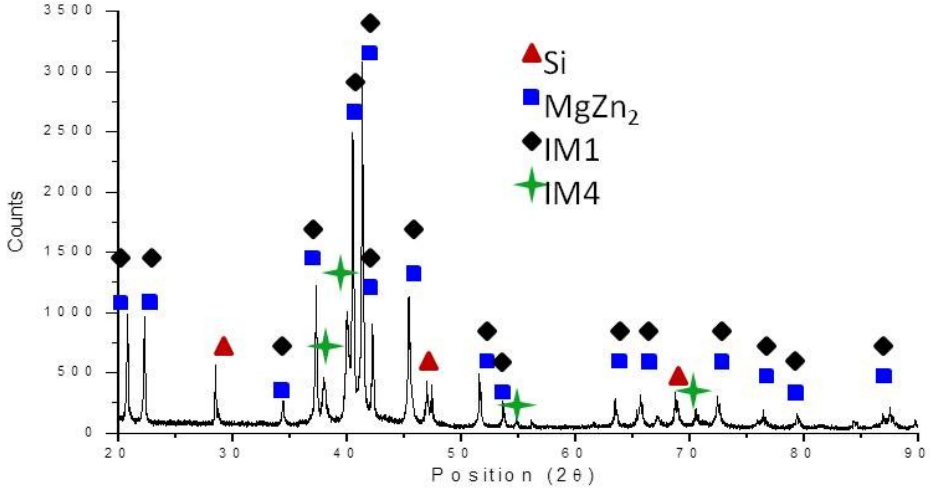

Figure 4.36 XRD results of sample No. 15 annealed at 450°C for 4 weeks.

4. 2. 4 Summary of the diffusion couples results and key alloys results

The isothermal section of the Mg-Zn-Zr ternary system at 450°C has been constructed via experimental data of diffusion couples and key alloys. The phase diagram is illustrated in Figure

4.37. No key alloys were prepared in the Zn_3Zr-IM1-IM4-$Zn_{39}Zr$ area because no key alloys can be prepared in this area using Zn-Zr and Mg-Zr master alloys. Therefore, the suggested tie lines were constructed by dotted line. Four ternary compounds were detected in the diffusion couples and key alloys. The homogeneity ranges of IM1, IM2, IM3 and IM4 were $Mg_{(23-26)}Zn_{66}Zr_{(8-11)}$, $Mg_{(15-16)}Zn_{66}Zr_{(18-19),}$ $Mg_{(10-11)}Zn_{66}Zr_{(23-24),}$ and $Mg_{(9-13)}Zn_{(79-87)}Zr_{(5-8)}$ respectively. Mg + Zr + ZnZr, ZnZr + Zn_2Zr + Mg, Zn_2Zr + IM3 + Mg, IM3 + IM2 + Mg, IM2 + IM1 + Mg, IM1 + Mg + Liquid, Liquid + $MgZn_2$ + IM1, Zn_2Zr + Zn_3Zr + IM3, Zn_3Zr + IM3 + IM2, Zn_3Zr + IM2 + IM1, $MgZn_2$ + IM4 + IM1, IM4 + $MgZn_2$ + Liquid, $Zn_{22}Zr$ + $Zn_{39}Zr_5$ + IM4, and IM4 + $Zn_{22}Zr$ + Liquid three-phase equilibria were constructed through diffusion couples and key alloys. As shown in Figure 4.38, although large regions of liquid exist in the Mg-Zn phase diagram at 450 ^oC, the single phase liquid region extended only around 1 at.% into the ternary phase diagram. Two and three-phase regions that contain liquid are up to around 10 at.% Zr. This is consistent with the Mg-Zr and Zn-Zr binary systems, which have steep liquidus lines in the Mg and Zn rich regions. No binary compounds were found to have extended solid solubility in the ternary system.

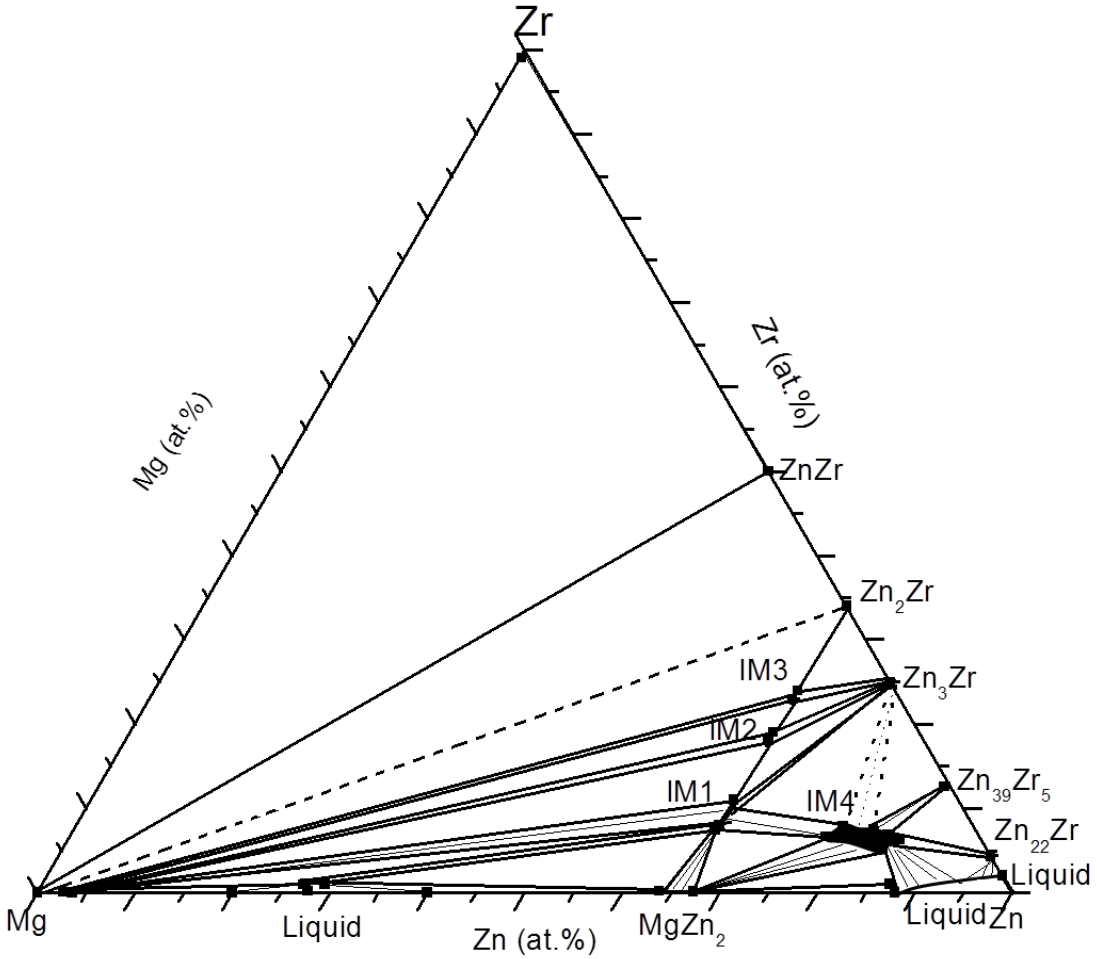

Figure 4.37 Partial isothermal section of the Mg-Zn-Zr system at 450°C.

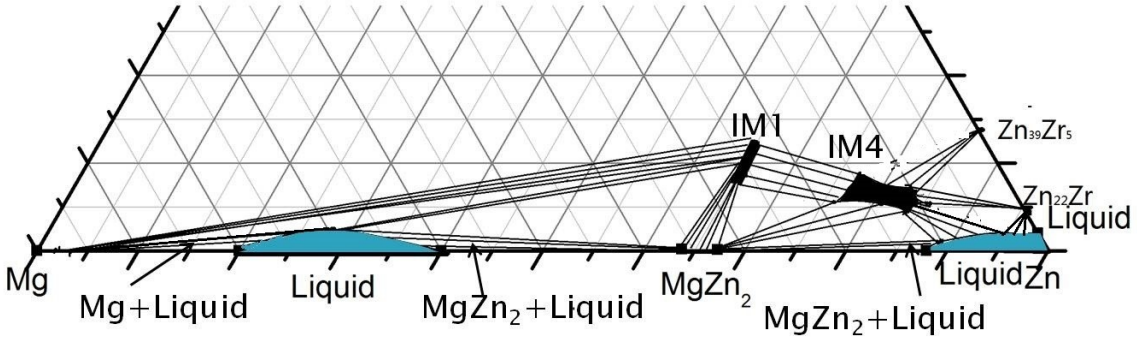

Figure 4.38 Liquid area of the Mg-Zn-Zr system at 450^{o}C.

Chapter 5

Concluding Remarks, Contributions, and Recommendations

5.1 Concluding Remarks

The isothermal section of Mg-Zn-Zr ternary system at 450^{o}C was experimentally constructed using six diffusion couples and 16 key alloys. SEM, EDS and XRD techniques are used to determine the phase relations, solubility limits and crystal structures information for binary and new founded ternary compounds. Four ternary compounds were observed. The composition, homogeneity ranges and the XRD patterns of these compounds were determined. The homogeneity ranges of IM1, IM2, IM3 and IM4 are $Mg_{(23\text{-}26)}Zn_{66}Zr_{(8\text{-}11)}$, $Mg_{(15\text{-}16)}Zn_{66}Zr_{(18\text{-}19),}$ $Mg_{(10\text{-}11)}Zn_{66}Zr_{(23\text{-}24),}$ and $Mg_{(9\text{-}13)}Zn_{(79\text{-}87)}Zr_{(5\text{-}8)}$ respectively. IM1 compound is determined to have the same prototype as $MgZn_2$ with the hexagonal structure and $P6_3/mmc$ space group. Although the crystal structures and prototypes of the IM2, IM3 and IM4 have not been determined, the XRD patterns of the ternary compounds can be used to analyse the key samples in this system. No binary compounds were found to have extended solid solubility in the ternary system. The liquid area in the Mg-Zn-Zr ternary system at 450^{o}C was verified by several key alloys. Although large regions of liquid exist in the Mg-Zn phase diagram at 450 ^{o}C, the single phase liquid region extended only around 1 at.% into the ternary phase diagram. Two and three-phase regions that contain liquid are up to around 10 at.% Zr. Current experimental results are compared with available literature data [62], and current study improves the accuracy of Mg-Zn-Zr ternary phase diagram.

5.2 Contributions

The Mg-Zn-Zr ternary system has been experimentally investigated combining the diffusion couple technique and selected equilibrated key alloys. The isothermal section of Mg-Zn-Zr at 450^{o}C has been constructed. In the present work, the following contributions have been achieved:

- Four ternary compounds of IM1, IM2, IM3 and IM4 were detected for the first time in the Mg-Zn-Zr system. The composition, homogeneity range and XRD patterns of the ternary compounds were confirmed by SEM, EDS and XRD techniques;

- The crystal structure of IM1 has been determined by the XRD analysis of a single phase key alloy;

- A combination of diffusion couples and key alloys is used to decrease the required experimental work;

- A two step annealing method was used to study the key alloys when the samples were difficult to eqilibrate.

5.3 Recommendations for the future work

- Future experimental work is needed to confirm the crystal structure of the IM2, IM3 and IM4 compounds;

- DSC study is suggested to determine the liquidus surface and the invariant reactions of the Mg-Zn-Zr system;

- Thermodynamic modeling of the Mg-Zn-Zr ternary system with full range of concentrations and temperatures is suggested;

- Development of the methodology for preparation of Zr rich alloys in this system is suggested.

References:

[1] B. L. Mordike, T. Ebert, Magnesium properties-applications-potential, Materials Science and Engineering A, Vol. 302, 2001, pp. 37-45.

[2] E. Aghion, B. Bronfin, Magnesium alloys development towards the 21st century, Materials Science Forum, Vol. 350-351, 2000, pp. 19-28.

[3] Y. N. Zhang, D. Kevorkov, F. Bridier, M. Medraj, Experimental investigation of the Ca-Mg-Zn system using diffusion couples and key alloys, Journal of Science and Technology of Advanced Materials, Vol. 12, No. 8, 2011, pp. 1-14.

[4] X. N. Gu, Y. F. Zheng, A review on magnesium alloys as biodegradable materials, Frontiers of Materials Science in China, Vol. 4, No. 2, 2010, pp. 111-115.

[5] Y. Xin, T. Hu, P. K. Chu, In vitro studies of biomedical magnesium alloys in a simulated physiological environment: a review, Acta Biomaterialia, Vol. 7, No. 2, 2011, pp. 1452-1459.

[6] K. U. Kainer, Magnesium-alloys and technology, Wiley-VCH Verlag GmbH & Co. KGaA, 2003, pp.16-25.

[7] F. W. Bach, M. Schaper, C. Jaschik, Influence of lithium on *hcp* magnesium alloys, Materials Science Forum,Vol. 419-422, No. 2, 2003, pp. 1037-1042.

[8] M. Avedesian, H. Baker, ASM specialty handbook-magnesium and magnesium alloys. ASM International, 1999.

[9] Z. H. Yu, H. G. Yan, J. H. Chen, Y. Z. Wu, Effect of Zn content on the microstructures and mechanical properties of laser beam-welded ZK series magnesium alloys. Journal of Materials Science, Vol. 45, 2010, pp. 3797-3803.

[10] Y. N. Zhang, D. Kevorkov, J. Li, E. Essadiqi, M. Medraj, Determination of the solubility range and crystal structure of the Mg-rich ternary compound in the Ca-Mg-Zn system, Intermetallics, Vol. 18, No. 12, 2010, pp. 2402-2411.

[11] Y. N. Zhang, X. D. Liu, Z. Altounian, M. Medraj, Coherent nano-scale ternary precipitates in crystallized Ca4Mg72Zn24 metallic glass, Scripta Materialia, Vol. 68, 2013, pp. 647-650.

[12] A. Becerra, M. Pekguleryuz, Effects of zinc, lithium, and indium on the grain size of magnesium, Journal of Materials Research, Vol. 24, No. 5, 2009, pp. 1722-1730.

[13] M. P. Staiger, A. M. Pietak, J. Huadmai, G. Dias, Magnesium and its alloys as orthopedic

biomaterials: a review, Biomaterials, Vol. 27, 2006, pp. 1728-1734.
[14] Z. Zhang, J. P. Li, J. X. Zhang, G. W. Lorimer, J. Robson, Review on research and development of magnesium alloys, Acta Metallurgica Sinica, Vol. 21, No. 5, 2008, pp. 313-328.
[15] M. Shahzad, L. Wagner, The role of Zr-rich cores in strength differential effect in an extruded Mg-Zn-Zr alloy, Journal of Alloys and Compounds, Vol. 486, 2009, pp. 103-108.
[16] E. F. Emely, Principles of magnesium technology, Pergamon, Oxford, 1966, pp. 127-130.
[17] Y. C. Lee, A. K. Dahle, D. H. St. John, The role of solute in grain refinement of magnesium, Metallurgical and Materials Transactions A, Vol. 31, 2000, pp. 2895-2906.
[18] J. Koike, T. Kobayashi, T. Mukai, H. Watanabe, M. Suzuki, K. Maruyama, K. Higashi, The activity of non-basal slip systems and dynamic recovery at room temperature in fine-grained AZ31b magnesium alloys, Acta Materialia, Vol. 51, No. 7, 2003, pp. 2055-2065.
[19] C. Y. Wang, X. J. Wang, H. Chang, K. Wu, M. Y. Zheng, Processing maps for hot working of ZK60 magnesium alloy, Materials Science and Engineering A, Vol. 464, 2007, pp. 52-58.
[20] X. N. Gu, N. Li, Y. F. Zheng, L. Q. Ruan, In vitro degradation performance and biological response of a Mg-Zn-Zr alloy, Materials Science and Engineering B, Vol. 176, No. 20, 2011, pp. 1778-1784.
[21] A. Hartwig, Role of magnesium in genomic stability, Mutation Research/ Fundamental and Molecular Mechanisms of Mutagenesis, Vol. 475, 2001, pp. 113-121.
[22] H. Tapiero, K. D. Tew, Trace elements in human physiology and pathology: Zinc and metallothioneins, Biomedicine & Pharmacotherapy, Vol. 57, 2003, pp. 399-411.
[23] M. Yamaguchi, Role of zinc in bone formation and bone resorption, The Journal of Trace Elements in Experimental Medicine, Vol. 11, 1998, pp. 119-135.
[24] L. Saldañ, A. Méndez-Vilas, L. Jiang, M. Multigner, J. L. González-Carrasco, M. T. Pérez-Prado, In vitro biocompatibility of an ultrafine grained zirconium, Biomaterials, Vol. 28, 2007, pp. 43-54.
[25] A. Bussiba, A. Ben Artzy, A. Shtechman, S. Ifergan, M. Kupiec, Grain refinement of AZ31 and ZK60 Mg alloys towards superplasticity studies, Materials Science and Engineering A, Vol. 302, 2001, pp. 56-62.
[26] I. J. Polmear, Overview Magnesium alloys and applications, Materials Science and Technology, Vol. 10, 1994, pp. 1-16.

[27] H. Watanabe, T. Mukai, M. Mabuchi, K. Higashi, High-strain-rate superplasticity at low temperature in a ZK61 magnesium alloy produced by powder metallurgy, Scripta Materialia, Vol. 41, 1999, pp. 209-213.

[28] R. Pinto, M. G. S. Ferreira, M. J. Carmezim, M. F. Montemor, The corrosion behaviour of rare-earth containing magnesium alloys in borate buffer solution, Electrochimica Acta, Vol. 56, 2011, pp. 1535-1545.

[29] L. Lin, Z. Liu, L. Chen, T. Liu, S. Wu, Microstructure evolution and low temperature superplasticity of ZK40 magnesium alloy subjected to ECAP, Metals and Materials International, Vol. 10, No. 6, 2004, pp. 501-506.

[30] O. Boudouard, Alloys of zinc and magnesium, Comptes Rendus Hebdomadaires des Seances de l'Academie des Sciences, Vol. 139, 1904, pp. 424-426.

[31] G. Grube, Alloys of magnesium with cadmium, zinc, bismuth and antimony, Zeitschrift fur Anorganische Chemie, Vol. 49, 1906, pp. 72-92.

[32] G. Bruni, C. Sandonnini, The ternary of magnesium, zinc and cadmium II, Zeitschrift fur Anorganische Chemie, Vol.78, 1913, pp. 273-297.

[33] R. J. Chadwick, The constitution of the alloys of magnesium and zinc, Journal of the Institute of Metals, Vol. 449, 1928, pp. 285-299.

[34] G. Grube, A. Burkhardt, The electrical conductivity, thermal expansion and hardness of magnesium–zinc, Zeitschrift fur Elektrochemie und Angewandte Physikalische Chemie, Vol. 35, 1929, pp. 315-331.

[35] J. J. Park, L. L. Wyman, Phase relationship in Mg alloys, WADC Technical Report 1957, pp. 1-27.

[36] W. Hume-Rothery, E. D. Rounsefell, The system magnesium-zinc, Journal of the Institute of Metals, Vol. 41, 1929, pp. 119-138.

[37] S. Samson, The crystal structure of Mg_2Zn_{11}: Isomorphism between Mg_2Zn_{11} and $Mg_2Cu_6Al_5$, Acta Chemica Scandinavica, Vol. 3, 1949, pp. 835-843.

[38] T. Takei, The equilibrium diagram of the system magnesium-zinc, Kinzokuno Kenkyu, Japan Institute of Metals, Vol. 6, 1929, pp. 177-183.

[39] I. Higashi, N. Shotani, M. Uda, T. Mizoguchi, H. Katoh, The crystal structure of $Mg_{51}Zn_{20}$, Journal of Solid State Chemistry, Vol. 36, 1981, pp. 225-233.

[40] P. Ghosh, M. Mezbahul-Islam, M. Medraj, Critical assessment and thermodynamic modeling of Mg-Zn, Mg-Sn, Sn-Zn and Mg-Sn-Zn systems, CALPHAD: Computer Coupling of Phase Diagrams and Thermochemistry, Vol. 36, 2012, pp. 28-43.

[41] G. A. Mellor, The constitution of magnesium-rich alloys of magnesium and zirconium, Journal of Institute of Metals, Vol. 77, 1950, pp. 163-174.

[42] J. H. Schaum, H. C. Burnett, Magnesium-Rich Side of the Magnesium-Zirconium Constitution Diagram, Journal of Research of the National Bureau of Standards, Vol. 49, No. 3, 1952, pp. 155-162.

[43] A. A. Nayeb-Hashemi, J. B. Clark, The Mg-Zr (Magnesium-Zirconium) system, Bull Alloy Phase Diagrams, Vol. 6, No. 3, 1985, pp. 246-250.

[44] I. M. Vesey, H. J. Bray, An investigation of the magnesium-zirconium system, Institute of Metals, Vol. 92, 1964, pp. 383-384.

[45] E. F. Emley, P. Duncumb, The maximum solid solubility of zirconium in magnesium, Institute of Metals, Vol. 90, 1962, pp. 360-361.

[46] M. Hämäläinen, K. Zeng, Thermodynamic Evaluation of the Mg-Zr System, CALPHAD: Computer Coupling of Phase Diagrams and Thermochemistry, Vol. 22, No. 3, 1998, pp. 375-380.

[47] R. Arroyave, D. Shin, Z. K. Liu, Modification of the thermodynamic model for the Mg–Zr system, Computer Coupling of Phase Diagrams and Thermochemistry, Vol. 29, 2005, pp. 230-238.

[48] E. Gebbhardt, Partial systems of zinc with titanium and zirconium, E. Z Metallkd, Vol. 33, 1941, pp. 355-357.

[49] P. Chiotti, G. R. Kilp, Zinc-Zirconium System, Transactions of The Metallurgical Society of AIME, Vol. 215, 1959, pp. 892-900.

[50] X. Chen, W. Jeitschko, Preparation, properties, and crystal structure of Zr_5Zn_{39}, a vacancy variant of the Ce_5Mg_{41}-Type, and structure refinement of $ZrZn_{22}$, Journal of Solid State Chemistry, Vol. 121, 1996, pp. 95-104.

[51] P. Pietrokowsky, A Cursory Investigation of Intermediate Phases in the Systems Ti-Zr, Ti-Hg, Zr-Zn, Zr-Cd and Zr-Hg by X-Ray Powder Diffraction Methods, Trans. AIME, Vol. 200, 1954, pp. 219-226.

[52] J. Dutkiewicz, The Zn-Zr (Zinc-Zirconium) System, Journal of Phase Equilibria, Vol. 13, No. 14, 1992, pp. 430-433.

[53] P. Villars, L. D. Calvert, Pearson's Handbook of Crystallographic Data for Intermetallic Phases, ASM International, Materials Park, OH, Vol. 4, 1991, pp. 53-65.

[54] W. Rossteutscher, I. C. Schubert, Titanium-Zinc and Titanium-Cadmium Alloys, Z. Metallkd, Vol. 56, No. 10, 1965, pp.730-734.

[55] D. R. Petersen, H. W. Rinn, A new phase in the zinc-zirconium system, Acta Crystallography, Vol. 14, 1961, pp. 328-337.

[56] M. E. Williams, W. J. Boettinger, U. R. Kattner, Contribution to the Zr-Rich Part of the Zn-Zr Phase Diagram, Journal of phase equilibria and diffusion, Vol. 25, No. 4, 2004, pp. 355-367.

[57] R. Arroyave, Z. K. Liu, Thermodynamic modeling of the Zn–Zr system, Computer Coupling of Phase Diagrams and Thermochemistry, Vol 30, 2006, pp. 1-13.

[58] R. Arroyave, A. van de Walle, Z. K. Liu, First-principles calculations of the Zn-Zr system, Acta Materialia, Vol. 54, 2006, pp. 473-482.

[59] N. E. Lashko, G. I. Morozova, E. S. Andreeva, V. V. Thonova, M. A. Gerasimova, Phase composition of cast magnesium-zinc-zirconium alloys, Izvestiya Akademii Nauk SSSR, Seriya Matematicheskaya, Vol. 2, 1969, pp. 159-163.

[60] V. M. Babkin, Solubility of zirconium in liquid magnesium and the ML5 alloy, Metallovedenie Termicheskaya Obrabotka Metallov, Vol. 10, 1968, pp. 221-223.

[61] K. Lohberg, G. Schmidt, Grain refuting effect of zirconium in magnesium alloys, Giessereiforschung, Vol. 27, No. 3, 1975, pp. 75-82.

[62] Y. P. Ren, Y. Guo, D. Chen, S. Li, W. L. Pei, G. W. Qin, Isothermal section of Mg-Zn-Zr ternary system at 345°C, CALPHAD: Computer Coupling of Phase Diagrams and Thermochemistry, Vol. 35, 2011, pp. 411-415.

[63] M. Dayananda, Y. Sohn, A new analysis for the determination of ternary inter-diffusion coefficients from a single diffusion couple, Metallurgical and Materials Transactions A, Vol. 30, No. 11, 1999, pp. 535-543.

[64] A. A. Kodentsov, G. F. Bastin, F. J. J. van Loo, The diffusion couple technique in phase diagram determination, Journal of Alloys and Compound, Vol. 320, 2001, pp. 207-217.
[65] http://en.wikipedia.org/wiki/Scanning_electron_microscope#mediaviewer/File:Schma_MEB_(en).svg.
[66] http://www.crystalimpact.com/pcd/.
[67] http://en.wikipedia.org/wiki/Atomic_radii_of_the_elements_(data_page).